HYSTERETIC CHARACTERISTICS OF WOOD-FRAME STRUCTURES UNDER SEISMIC MOTIONS

Thesis by

Daniel Sutoyo

In Partial Fulfillment of the Requirements for the

degree of

Doctor of Philosophy

CALIFORNIA INSTITUTE OF TECHNOLOGY

Pasadena, California

2009

(Defended January 27, 2009)

Acknowledgements

I would like to thank my advisor, John Hall, for his guidance. He has demonstrated to me how to think critically as an engineer and taught me how to be an independent researcher. I am grateful to have his support.

Special thanks to Professor James Beck for his teachings and introductions to MODE-ID and the Bayesian probabilistic framework, both of which have transformed the way I view system identification problems. Much thanks to Professor Tom Heaton for his informative discussions on dealing with field data. He has always made himself available to listen to me during my graduate life.

Special gratitude to my undergraduate advisor, Ziyad Duron, for his years of mentoring. I am appreciative for the foundation he established in me during my undergraduate studies.

I would also like to thank my colleague Sai Hung (Joseph) Cheung for being an excellent TA and assisting me in numerical methods. His patience and clarity in explaining concepts has enabled me to learn a great extent.

I am indebted to my brother David and sister-in-law Chanlee for being my proofreaders and opening their apartment for extended stay. Special thanks to my girlfriend Angel who has been confident in my ability to do great things. Her encouragement and support have helped ease my graduate study.

I thank God for blessing me with my parents who have shown their unconditional love and provision throughout my life. I would not have accomplished anything without their continual care.

I am grateful for having the opportunity to pursue a graduate degree.

Abstract

In order to develop seismic codes that can effectively mitigate damage to wood-frame construction under seismic activity, the dynamic characteristics of wood-frame buildings must be well understood. Funding of full-scale structure experimental tests can be costly and may not be a true replica of real life scenarios. Therefore, data interpretation projects focusing on dynamic behavior of low-rise wooden shearwall buildings under large seismic motions have become increasingly important. Procedures include determining the modal parameters and extracting hysteretic characteristics from the available records. The results help extend the understanding of wood-frame structures and update building codes. Furthermore, the amount of information extracted can help evaluate the effectiveness of the current instrumentation program.

This work focuses on the seismic records from wood-frame structures during the 2004 Parkfield Earthquake. Studies involve verifying the amplitude dependence of modal parameters and retrieving pinching hysteresis curves that are common in wood-frame structures. Modal parameters are identified with a robust routine called MODE-ID. Equivalent viscous damping estimates in wood-frame buildings can range from 5% - 10% in largely linear behavior and 10% - 20% in significant nonlinear behavior. The discrepancies of damping estimates reported in the past are a result of inappropriate comparisons without understanding 1) the degree of nonlinear response and 2) the system identification methods used for the studies. By studying the hysteretic curves, insights can

be obtained to reveal and to resolve the damping estimate discrepancies. Since displacement time histories of structures are not typically measured, the hysteretic curves are extracted from acceleration time histories. The proposed process accounts for inherent double integration errors and phase delay through filtering. It is still being debated that if the double integration can provide meaningful structural relative displacement time histories. In a laboratory setting with unilateral ground motion, the extraction process provides accurate hysteretic curves. However, this dissertation demonstrates that if the building experiences bi-directional ground motions, the nonlinear behavior of the diaphragm tampers with this process.

The results from modal identification and hysteresis curves serve as a basis for creating numerical models. Direct and gradient search methods were used for model updating. Bayesian updating and model selection provided the best results for dealing with hysteretic structural models. This probabilistic framework demonstrates potential benefits in a seamless integration with a seismic database. The selected hysteretic model showed great resemblance to the measured responses and had evidence of pinching hysteresis. Insights on the structure's deformations and dissipation of energy can be inferred from the model.

Contents

List of Figures

List of Tables

CHAPTER 1

Introduction

In recent years, much of the focus and resources in earthquake engineering have shifted

towards a preemptive approach aimed at minimizing life and economic losses. In order to

effectively mitigate the damage caused by seismic activity, the dynamic characteristics of

buildings must be well understood. This knowledge provides the basis for building code

updates for new construction, identifies old structures that need retrofitting, and enhances

numerical modeling for building collapse predictions. This process seems straightforward,

yet it requires gathering data from buildings stirred by large seismic motion (magnitude 6.0

and greater) – which on average occurs only about 150 times annually around the world

(USGS 2008). To further complicate matters, recording instruments are not always readily

available as they become increasingly expensive to deploy and maintain. As a result, many

of the existing building codes rely primarily on laboratory tests, engineering judgment, and

experience.

One case in particular is the design of wood-frame structures. It has been observed

that wood-frame construction performs well during earthquakes as it is flexible, light-

weight, and stiff considering its density. Large amplitudes of motion are absorbed by the

ductility of the structure and dissipated by the friction of connections. Confidence in these structural properties led many to believe that the existing building code was sufficient (Diekmann 1994). However, the 1994 Northridge Earthquake exposed the engineers' lack of understanding of wood-frame structures. Damages and property loss in the amount of $20 billion raised doubts over the reliability of wood-frame construction (Reitherman 1998). While 99% of all residences in California are constructed of wood (Malik 1995), engineers understand less about the behavior of these wood-frame structures compared to those of their concrete and steel counterparts (Cobeen, Russel and Dolan 2004). Therefore, testing of wood-frame structures has attracted a lot of government and research attention in the past decade. Advancement in wood-frame research has been made through the collaboration of agencies such as the Federal Emergency Management Agency (FEMA) and the Consortium of Universities for Research in Earthquake Engineering (CUREE). The CUREE wood-frame project covered five main areas: testing and analysis, field investigations, building codes and standards, economic aspects, and education and outreach (CUREE 2008). The ultimate goal of such work is to make the basis of building codes more applicable and reliable.

1.1 Instrumentation Program

No matter how established are the theories in structural analysis, engineers are unable to improve building codes without proper instrumentation and records. A major contributor of these records is the California Strong Motion Instrumentation Program (CSMIP), which was established by California legislators to obtain vital earthquake data for the engineering

and scientific communities through a statewide network of strong motion instruments (CSMIP 2006). In 2003 and 2004, CSMIP was able to measure some key records on one-story wood-frame structures during the San Simeon and Parkfield earthquakes.

Despite the availability of data and records, a recurrent problem in the instrumentation program is how to assess the inherent value of current instrumentation (Sutoyo and Hall 2006). If the current data are limited in the amount of information they provide for structures, what necessary improvements must take place? What resources must be committed in order to establish and maintain an instrumentation network that obtains meaningful data? Another way to approach this question is to determine the extent to which the records are being used. What exactly can be extracted and learned from the data records? Is the amount of data sufficient to make conclusions on the design of wood-frame construction?

1.2 Overview of the Thesis

This dissertation extends the work in *Dynamic Characteristics of Wood-frame Structures* (Camelo, Beck and Hall 2002) by investigating wood-frame records at higher shaking levels and explaining many of the discrepancies raised in reported modal parameters. A proposed methodology to process the CSMIP records is presented to help maximize the value of information gained. The analyses and numerical models presented in the dissertation will also assist in evaluating the CSMIP instrumentation program and in updating the wood-frame construction building codes. The dissertation is divided into the following chapters to address each facet of this data interpretation project.

Chapter 2 highlights many of the advances in understanding of wood-frame construction from the CUREE Wood-Frame Project. This literature review will focus specifically on the dynamic characteristics of wood-frame construction on a full-scale test specimen. The chapter will also identify any unresolved issues, such as high damping estimates.

Chapter 3 presents the time histories used in this investigation and explains the significance of each record. Chapter 4 presents the results of the system identification on these data sets. Results will reaffirm the amplitude dependence of frequency and damping estimates. Chapter 5 connects the quantitative analysis in Chapter 4 to the physical characteristics in wood-frame construction. The chapter will also dispel some of the confusion in the overestimation of damping by explaining hysteretic behavior in wood-frame structures.

Chapter 6 introduces the finite element models that will simulate the measured responses. The models will validate the hysteresis extraction procedures and the component identification process. It will also discuss common model updating routines used in selecting parameters for the models and offer a Bayesian framework for simulation and model selection as a better alternative for this type of data interpretation. Finally, Chapter 7 presents conclusions for the data interpretation project and reviews the methodology, analyses and models presented in this dissertation.

CHAPTER 2

Literature Review of Wood-frame Structure Tests

This dissertation focuses on the investigative process of extracting dynamic characteristics of wood-frame structures from measured seismic response. Although there has been some research measuring modal parameters in an experimental setting, most tests have been conducted on a structural component level (Fischer, et al. 2001). Many of the tests on full-scale wood-frame housing since the 1950s have been summarized in W*ood-frame Project Testing and Analysis Literature Review* (Filiatrault 2001). Instead of replicating the entire literature review, accomplishments pertaining to the modal parameters and dynamic characteristics of full-scale wood-frame housing are highlighted in this chapter. An overall summary at the end of the chapter will present notable findings and identify areas of further research.

2.1 Significant Case Studies

Yokel, His and Somes (1973) tested a full-scale two-story house representative of housing in the United States. The experiment tested whether existing drift limitations for medium-rise and high-rise structures can be applied to low-rise housing, and measured dynamic

response characteristics of conventional housing. The wood-frame structure was 47 ft (14.3 m) long by 26 ft (7.9 m) wide.

Results from four static tests designed to measure stiffness of the structure under simulated wind loads in the transverse direction showed that the walls behaved elastically. Results also showed that the roof diaphragm behaved like a flexible diaphragm, whereas the second floor diaphragm behaved more like a rigid body.

A dynamic test measured the natural frequency to be around 9 Hz, and the percentage of critical damping to be between 4-9%, with an average of 6%. Due to resolution limits in the recording equipment, the test was inconclusive.

Sugiyama et al. (1988) subjected a full-scale house to lateral loads. The researchers examined the influence of wall sheathing above and below door and window openings on the racking resistance of the wall, as well as the effect of shear frames placed perpendicular to the direction of lateral loading. The test structure was a full-size, Japanese style two-story house measuring 7.28m (24 ft) wide by 10.01 m (33 ft) long, and was subjected to loading at various stages during construction. Each shear wall frame was loaded individually on the second floor during test Stages 1 through 5; during Stage 6, the entire structure was loaded at once.

The researchers found that the total stiffness of the first floor walls were almost equal during Stages 1 and 2, and lateral stiffness was similar between Stages 3 and 4. However, the total stiffness in Stage 3 was about 50% greater than that of Stages 1 and 2 due to the sheathing of shear walls. Total stiffness in Stage 5 was about 10-15% greater

than that of Stage 4 with the installation of exterior wall siding. Local failure of the house occurred during test Stage 6. The researchers concluded that differences in floor diaphragm openings had little effect on wall stiffness, whereas the addition of calcium silicate sidings to walls parallel to loading increased lateral stiffness in that direction. They also concluded that sidings installed perpendicular to loading had little effect on lateral stiffness, but conceded that more testing was needed.

Yasamura et al. (1988) examined the safety of a wood-frame three-story house when subjected to lateral loads. The researchers tested three different sheathing configurations and compared the shear resistance of each story to theoretical calculations. In Specimen A, the load was applied monotonically at three loading points, while increasing cyclic loads were applied at each of the three shear walls in Specimens B and C. Furthermore, interior shear walls in Specimens B and C received one and a half times the load compared to exterior shear walls.

The researchers found that the shear resistance of the north longitudinal wall was one and a half times the shear resistance of the south longitudinal wall. The discrepancy, possibly caused by more openings in the south wall, had little effect on the torsional deformation. Forced vibration tests on Specimens B and C revealed that damage caused by horizontal loads decreased the natural frequency from 5.8 Hz to 3.1 Hz. On the other hand, the addition of sheathing to transverse walls increased the torsional natural frequency from 4.8 Hz to 8.8 Hz.

Carydis and Vougioukas (1989) subjected a two-story timber frame construction house to 40 repetitions of the 1986 Kalamata Earthquake, measuring 6.2 on the Richter scale. The structure was 3.6 m (11.8 ft) both in width and length. The measured natural periods of the structure slowly increased throughout the shocks – starting from 0.18 seconds in the longitudinal and transverse directions and 0.16 seconds in the vertical direction after the 1st repetition, to 0.22 seconds in the longitudinal and transverse directions and 0.17 seconds in the vertical direction after the last repetition. The damping varied across repetitions – with the damping at 17% after the 15th repetition.

Phillip, Itani and McLean (1993) studied the effect of a horizontal diaphragm on the distribution of load into shear wall elements, as well as the stiffness of the wooden shear walls with different sheathing materials. The full-scale, single story wood-frame structure was 16 ft (4.9 m) wide and 32 ft (9.8 m) long. The structure was subjected to loading at four stages during construction. In Stage I, sheathing was added on one side of the shear walls, whereas in Stage II sheathing was added on both sides. Test results showed that shear wall stiffness was additive with more sheathing. The roof diaphragm was not present in Stage III to transfer applied loads to unloaded walls, but was installed for Stage IV. During Stage IV, the longitudinal walls carried up to 23% of the load distribution, but decreased at higher loads. Results demonstrated that the roof diaphragm behaved more like rigid diaphragm as opposed to a flexible diaphragm.

Kohara and Miyazawa (1998) tested six two-story wood-frame houses using a shake table generating a sine-wave sweeping frequency motion, as well as a Japan Meteorological Agency (JMA) 1995 Kobe Earthquake record, and the 1940 El Centro Earthquake record with a scale factor of 1.5. The tests aimed to assess damage from ground motions and to examine the dynamic behavior of the structures. Results for two of the structures – Type B and Type F – were discussed in the paper. Both structures were 11.83 m (33.8 ft) long by 7.28 m (23.9 ft) wide. Both were tested during five different phases with varying amounts of diagonal braces, plywood sheathing, and gypsum wallboards. Gypsum wallboards were installed for the interior wall surfaces for both structures. The exterior wall surfaces for structures Type B and F were mortar stucco and siding boards, respectively.

Initial natural frequencies for structures Type B and F were 6.49 Hz and 6.05 Hz, respectively. The natural frequencies decreased as a result of sheathing and wallboard removal as well as cumulative damage effects. Damage occurred to exterior wall surfaces and the gypsum wallboard when the natural frequency was 4-5 Hz. Furthermore, damage occurred to the structural frame when the natural frequency was 3 Hz. Diagonal braces resisted 7-17% and 29-54% of total base shear for structures Type B and F, respectively. In structure Type B, mortar stucco resisted between 21% and 47% of the base shear. The researchers concluded that the walls in Type B covered with mortar stucco had higher stiffness than those in Type F, which were sheathed with siding.

Using a shake table, Tanaka, Ohasi and Sakamoto (1998) tested a full-scale, two-story wood-frame house against the 1995 Kobe Earthquake record by the Japan Meteorological

9

Agency (JMA) at the Kobe station, and the 1940 El Centro Earthquake record with an amplitude scale factor of 1.5. The goal of the experiment was to test the safety of wood-frame houses, and to determine the effect of nonstructural sheathing materials on the dynamic response of the structure. The structure measured 7.28 m (23.9 ft) wide by 7.28 m (23.9 ft) long, and was designed using a seismic shear coefficient of 0.28. The interior wall surfaces were covered with gypsum wallboard, while the exterior was sheathed with siding. The structure was tested during three phases of construction. Various amounts of sheathing were removed after each phase. Analysis of frame damage revealed that the nonstructural finish materials resisted a significant portion of the lateral forces in the structure. Drift results also showed that these materials added considerable stiffness to the structure.

Seo, Choi and Lee (1999) used a shake table to test two single-story one-quarter-scale wood-frame house models. The researchers measured the natural frequency and damping in the test models while determining the maximum peak ground acceleration these models can withstand without collapsing. The models were 1.8 m (5.9 ft) long by 0.9 m (3.0 ft) wide by 0.7 m (2.4 ft) high. The first model was tested with the 1985 Nahanni Earthquake recorded at a rock site, while the second model was tested with the 1979 Imperial Valley Earthquake recorded at a soft soil site. Random white noise tests showed that the natural frequencies of Model 1 were 3.32 Hz and 3.52 Hz in the longitudinal and transverse directions, respectively; natural frequencies of Model 2 were 3.32 Hz and 4.29 Hz in the longitudinal and transverse directions, respectively. The natural frequencies of an actual

prototype would then be expected to be one-half of the frequencies in the models. The modal damping ratio of both models was 7% in both directions.

Yamaguchi and Minowa (1998) tested timber shear walls with a shake table, and compared dynamic hysteresis loops of these shear walls with static hysteresis loops previously developed. They also performed a collapse analysis using conservation of energy. The shear walls tested were 3.64 m (12 ft) long by 2.94 (9.6 ft) high with a 1.82 m (6 ft) wide opening at the center. Three specimens, with seismic shear coefficients 0.3, 0.4, and 0.5, were excited with the Japan Meteorological Agency (JMA) Kobe North-South ground motion record. The dynamic hysteresis of the specimen with a 0.3 seismic shear coefficient matched well with the static hysteresis. However, the tilting angle of the static hysteresis increased rapidly after a tilting angle of about 1/120 rad. Maximum strength of the shear wall during the dynamic test was 114% of the maximum strength during the static test. The researchers concluded that shear walls, when subjected to dynamic loads, have more strength but less ductility compared to when they are subjected to static loads.

Polensek and Schimel (1991) found that damping in wood subsystems increases with increasing amplitude of vibration. After reaching a certain threshold, damping and stiffness decrease due to reduced interface friction caused by prior damage. They also observed that the behavior was independent of lumber grade, and more dependent on nailed joints.

Seo, Choi and Lee (1999) observed viscous damping ratios between 13% and 27% while performing static and cyclic lateral load tests on wooden frames with tenon beam-column joints. Stiffness was also reduced with increased amplitude of displacement.

Hirashima (1988) performed static loading tests on a two-story building, and found that it oscillated mainly in its fundamental mode of vibration in each direction. The corresponding frequency was mostly constant, at 4 Hz and 4.5 Hz in the transverse and longitudinal directions, respectively. Damping ratios were 2.4% and 1.4% in the transverse and longitudinal directions, respectively, from a free vibration test with initial peak-to-peak displacements of about 0.5 mm.

Fischer et al. (2001) conducted a shake table test on a two-story single family wood-frame house. The 16×20 structure was tested in ten different phases. Each of the ten phases differed in their structural configurations, ranging from sheathed shear walls, symmetrical and unsymmetrical openings, and the presence of non-structural wall finish materials. Results showed that the building exhibited a fundamental frequency that ranged from 3.96 Hz to 6.49 Hz dependent on the presence of non-structural wall finish materials. There were also significant variations in the equivalent viscous damping. The measured mean damping was 7.6% of critical.

Camelo, Beck and Hall (2002) performed a series of forced vibration tests on multi-storied wood-frame housing. These studies identified transverse and longitudinal fundamental

frequencies of 5.5 Hz and 5.7 Hz which were lower than the ones identified from ambient survey (6.5 Hz and 7.8 Hz). Damping ratios range from 4% to 6% of critical. Camelo also performed a data analysis of the shake table test done by Fischer et al. (Camelo 2003). The most apparent finding was the discrepancy of damping estimates. Camelo's analysis showed 15%-20% of critical damping compared to Fischer's average damping value of 7.6%.

2.2 Informative Findings

Results from full-scale testing of wood-frame housing support many findings that are documented at the subsystem level. For one, nonstructural wall-finish elements add substantial lateral stiffness to the overall structure. Experimental results show that the nonlinear behavior of the structure depends more on the connection joints and nailing as opposed to the grade of lumber used. Observations made solely from full-scale testing include the effects of symmetric and asymmetric openings on torsional modes and the role the diaphragm plays in distributing loads on walls.

Table 2-1 provides a summary of the observed dynamic characteristics of the test structures from the preceding reports. A trend apparent from the results is the increase in stiffness when additional sheathing to the shear wall is applied. When there is a decrease in stiffness, either the amplitude of the loading has increased or the test specimen has been damaged. The trend for damping ratios seems less conclusive. Although some investigators have observed its dependence on amplitude, reported ratios have ranged from as low as 2% to as high as 27%. The discrepancies can be a result of several factors such as resolution of

recording equipment, the method used to calculate ratios, amplitude of loading, and the presence of nailing and connection joints. Substantial differences in damping ratios can cause some uncertainties when selecting an appropriate value for numerical models. This dissertation will attempt to remove any confusion and uncover apparent trends in modal damping estimates.

Table 2-1: Summary of observed dynamic characteristics of full-scale wood-frame tests

Author	Test Specimen	Frequency (Hz)	Damping (%)	Notes
(Yokel, Hsi and Somes 1973)	2 story house 47x 26	9	6 (4-9)	Roof (flexible), 2nd floor (rigid)
(Sugiyama, et al. 1988)	2 story house 33 x 24	N/A	N/A	Diaphragm opening little effect on wall stiffness; wall siding parallel to loading increased later stiffness
(Yasamura, et al. 1988)	3 story	5.8 → 3.1 (damaged) 4.8→8.8 (sheathing)	N/A	Stiffness changes
(Carydis and Vougioukas 1989)	2 story 11.8 x 11.8	5.8 → 4.5 6.25 →5.88	17	High damping ratios
(Phillips, Itani and McLean 1993)	32 x 16	N/A	N/A	Roof(rigid), distribute to unloaded walls
(Kohara and Miyazawa 1998)	2 story house 33.8 x 23.9	6.5, 6.05 → 4-5	N/A	Damages lower stiffness
(Tanaka, Ohasi and Sakamoto 1998)	2 story	N/A	N/A	Nonstructural elements provide significant lateral force resistance
(Seo, Choi and Lee 1999)	1 story (1/4 scale)	3.32, 3.52 3.32, 4.29	7 7	Low frequencies
(Polensek and Schimel 1991)	Wood Subsystems	Decrease with amplitude	Increase with amplitude	Independent of lumber grade; dependent on nail joint
(Seo, Choi and Lee 1999)	Wooden frames (tenon joints)	Decrease with amplitude	13-27	High damping ratios
(Hirashima 1988)	Free vibration test (.5 mm peak to peak)	4 to 4.5	1.4 – 2.4	Low damping ratios
(Fischer, et al. 2001)	2 story (16x20)	3.96 to 6.49	7.6 (5-11)	Nonstructural wall finishes played significant role
(Camelo 2003)	Multi-story houses	5.5 and 5.7 (shaking) 6.5 and 7.8 (ambient)	4-6 (shaking) 15-20 (analysis)	Discrepancies between analysis and experimental results

15

CHAPTER 3

Seismic Records from Wood-frame Structures

Many of the full-scale shake tests used recorded ground motions for excitation. Seismic records provide intense ground motions to structures and can cause serious damage and possibly structural failure. With proper seismic instrumentation, engineers can also characterize structural behavior of wood-frame buildings during strong seismic motion. The California Strong Motion Instrumentation Program (CSMIP) is one of the pioneers in providing seismic records for the engineering and scientific communities over the last few decades. Aside from data processing and delivery, CSMIP also seeks to gain understanding in earthquake ground-shaking and its effect on structures. This chapter will introduce the records that CSMIP has provided for investigation along with additional data sets from other sources. These records are used to reinforce hypotheses and support conclusions presented in this dissertation.

3.1 Parkfield and San Simeon Earthquake Records

The primary data set used in this dissertation is the 2004 Parkfield Earthquake, also coined the Best Recorded Quake in History by the USGS (Michael 2006). Prior to the most recent major quake in 2004, moderately-sized earthquakes of about magnitude 6 have occurred on the Parkfield section of the San Andreas fault at fairly regular intervals – in 1857, 1881,

1901, 1922, 1934, and 1966. This observation has led to the Parkfield Experiment – a long term research project analyzing the San Andreas Fault (USGS 2008). Seismograms were installed at over 100 near-field sites in the area, making the 2004 Parkfield earthquake one of the best recorded earthquakes for seismic engineering purposes (Bakun, et al. 2004).

Instrumented wood-frame construction sites are typically fewer in number than concrete and steel construction sites. The large number of available records in the 2004 Parkfield Earthquake also meant that available wood-frame records were more numerous than average (Figure 3.1 shows an instrumental intensity map; Figure 3.2 shows a contour of near-fault ground accelerations; Figure 3.3 shows particle displacement motions). The 2003 San Simeon Earthquake, on the other hand, provided as its distinguishing mark, the record exhibiting the highest peak structural acceleration for wood-frame structures ever recorded. Previous recorded highs were approximately 60% g, whereas those recorded in 2003 were as high as 125% g. Due to the high dependence of wood-frame structures on the amplitude of motion, these data sets are invaluable to understanding the non-linear behavior and peak amplitudes of these types of construction. CSMIP was particularly interested in two of its wood-frame instrumented sites, one of which was studied by Camelo for the 1993 and 1994 Parkfield Earthquake (Camelo 2003). Comparing the results from these two sites will also be a point of interest of this paper.

CISN Rapid Instrumental Intensity Map for Parkfield Earthquake
Tue Sep 28, 2004 10:15:24 AM PDT   M 6.0   N35.81 W120.37   Depth: 7.9km   ID:51147892

Processed: Mon May 9, 2005 11:20:54 AM PDT,
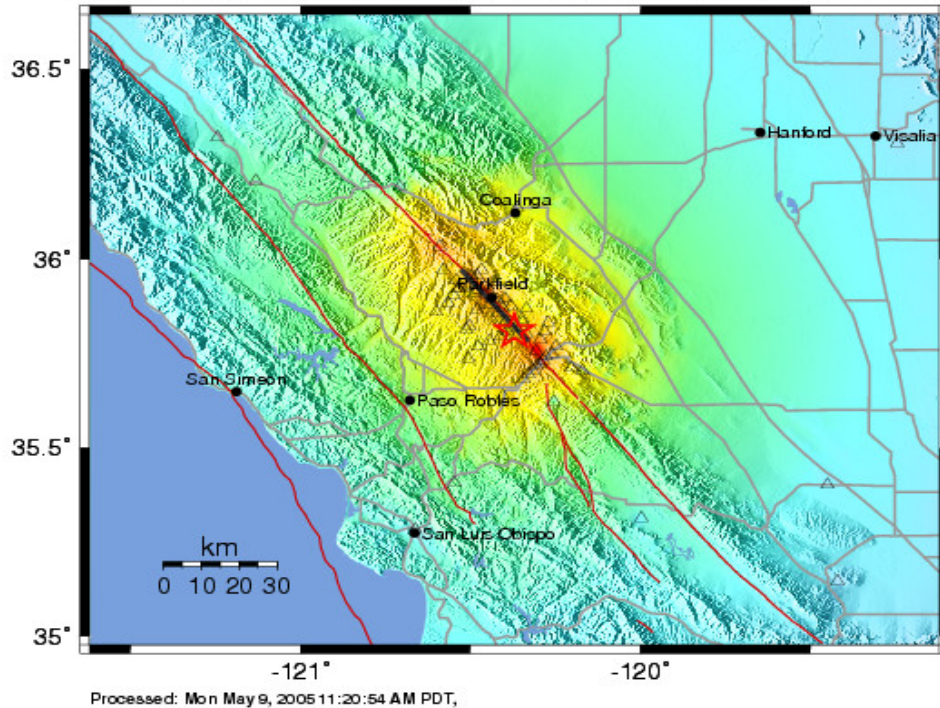
PERCEIVED SHAKING	Not felt	Weak	Light	Moderate	Strong	Very strong	Severe	Violent	Extreme
POTENTIAL DAMAGE	none	none	none	Very light	Light	Moderate	Moderate/Heavy	Heavy	Very Heavy
PEAK ACC.(%g)	<.17	.17-1.4	1.4-3.9	3.9-9.2	9.2-18	18-34	34-65	65-124	>124
PEAK VEL.(cm/s)	<0.1	0.1-1.1	1.1-3.4	3.4-8.1	8.1-16	16-31	31-60	60-116	>116
INSTRUMENTAL INTENSITY	I	II-III	IV	V	VI	VII	VIII	IX	X+

Figure 3.1: Rapid instrumental intensity map for the Parkfield earthquake (CSMIP 2006).
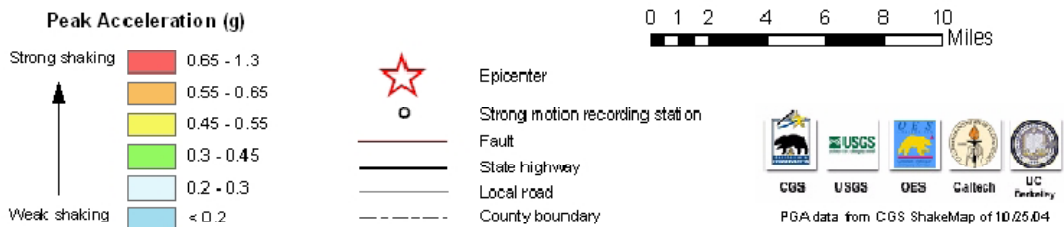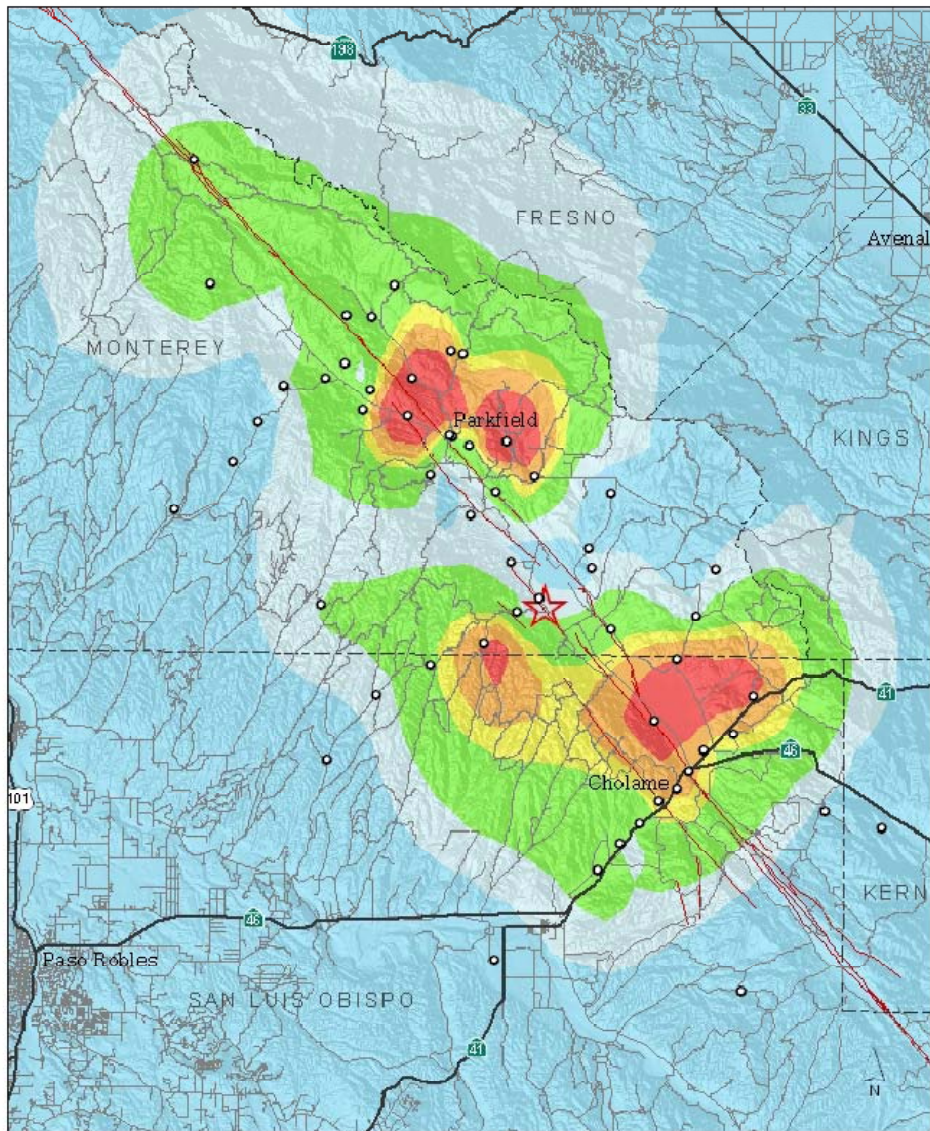
Figure 3.2: Contour map of near-fault peak ground accelerations (CSMIP; Shakal, et al. 2005; Graphic generated by Pete Roffers at CSMIP).
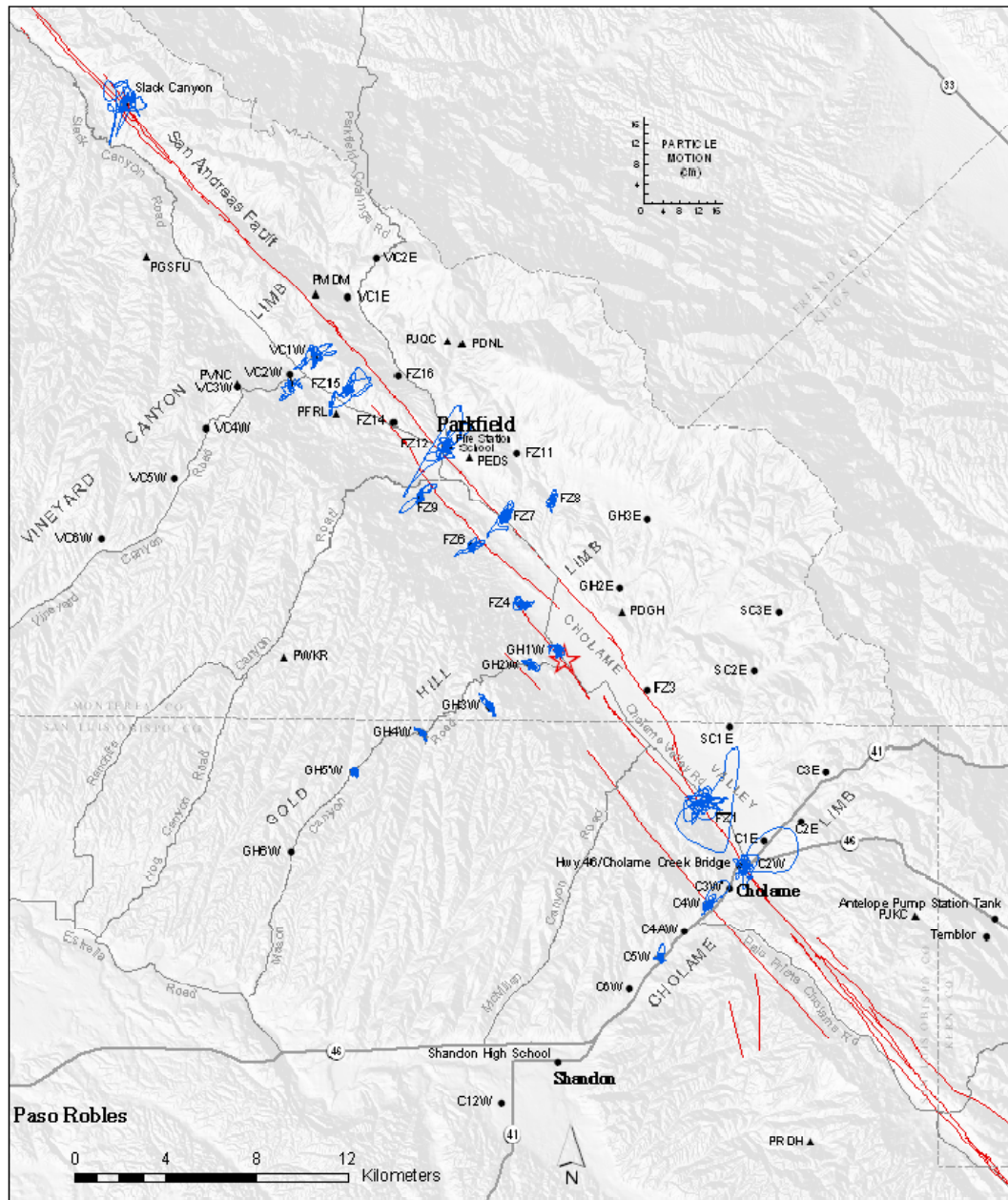
Figure 3.3: Particle displacement motions of Parkfield Earthquake of 28 Sep 2004 (CSMIP 2006).

3.1.1 Parkfield School Building

The Parkfield school building is a one-story rectangular building built in 1949, with plywood shear walls installed in the longitudinal direction. The base dimensions are 48' × 30'. Figure 3.4 shows the location and photograph of the station. The instrumentation was installed in 1987 with a total of 6 accelerometers in place. There were three channels in the N-S (transverse) direction and three in the E-W (longitudinal) direction. The hypocenter of the 2004 earthquake was 13 km away (CISN 2006).
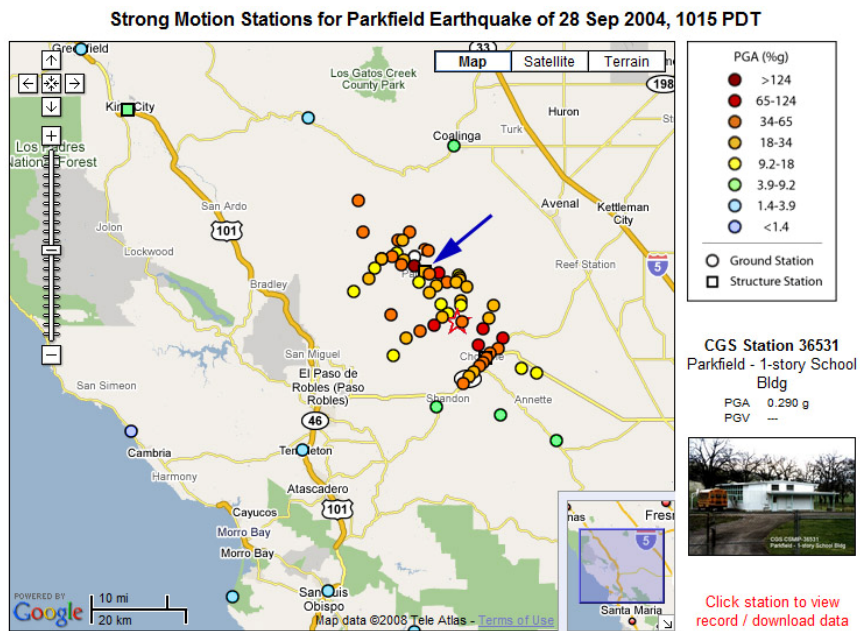
Figure 3.4: Location and photograph of the Parkfield school building strong motion station.
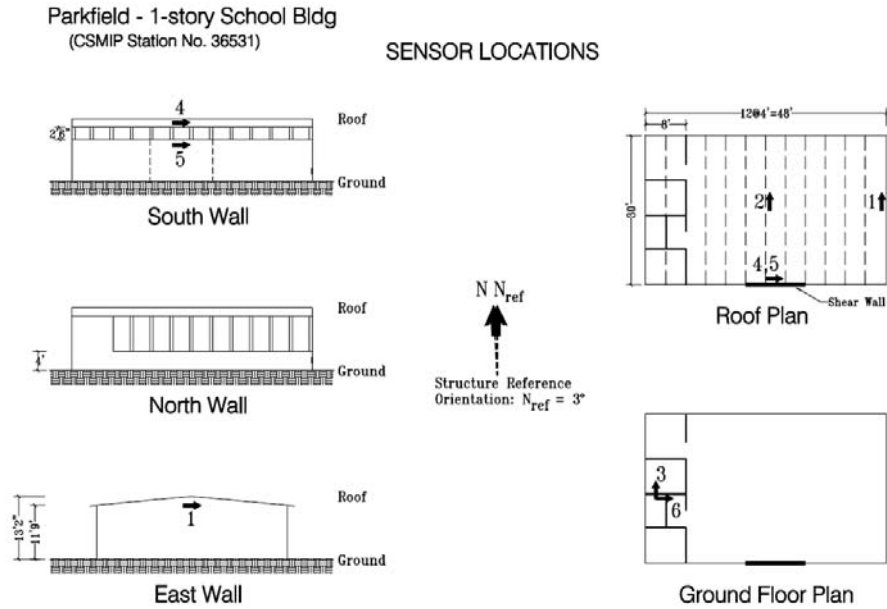
Figure 3.5: Instrumentation layout of the Parkfield school building.

The instrumentation schematic layout is shown in Figure 3.5. Two channels (3 and 6) are situated on the first floor, and three (1, 2, and 4) are located on the roof. Channel 5 sits on the main lateral force resisting system which is a shear wall (12' long) in the long direction on the south wall. Recording with only four channels may seem limited compared to the numbers used in a shake table test in a laboratory setting. However, the symmetry in the building's rectangular structural plan simplifies many of the analyses. For example, it is safe to assume that the motion on the west of the building will be similar to the motion experienced on the east side of the building. However, it is important that symmetry be used with care. From the structural sketches (Figure 3.6) one can notice that the north wall and the south wall differ greatly in their equivalent stiffness. Most of the surface area of the north wall is comprised of windows, and the gaps in these window frames will greatly lower the lateral force resistance on the north side of the wall.
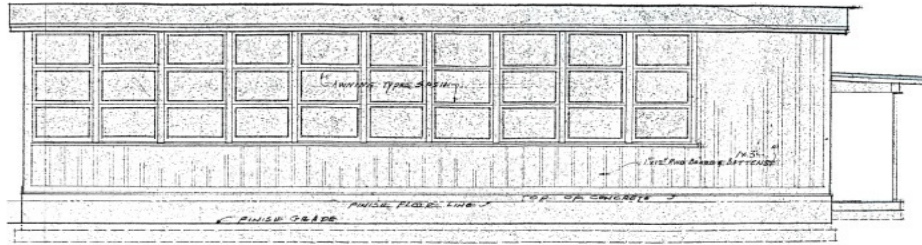
North Wall
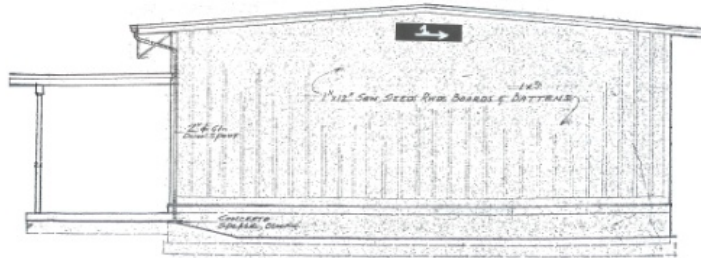
East Wall
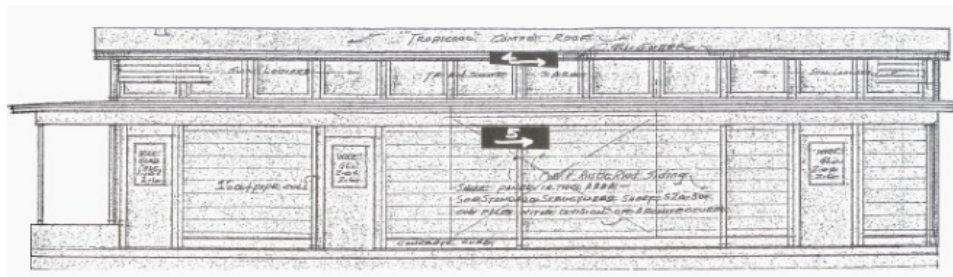
South Wall
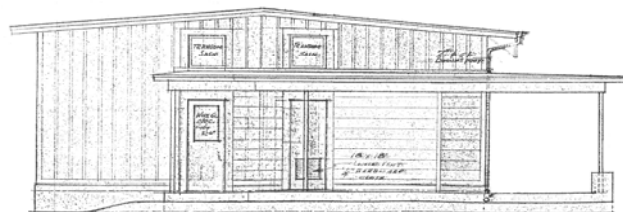
West Wall

Figure 3.6: Elevation views of the Parkfield school building (CSMIP).

Figure 3.7 and Figure 3.8 plot the acceleration time histories from the Parkfield school building. Peak structural acceleration is approximately 35% g. The records in 2004, along with data from 1993 and 1994, can be downloaded from the CSMIP website (http://www.strongmotioncenter.org). Included are raw time histories, calculated velocities and displacement time histories, and response spectrum analyses.
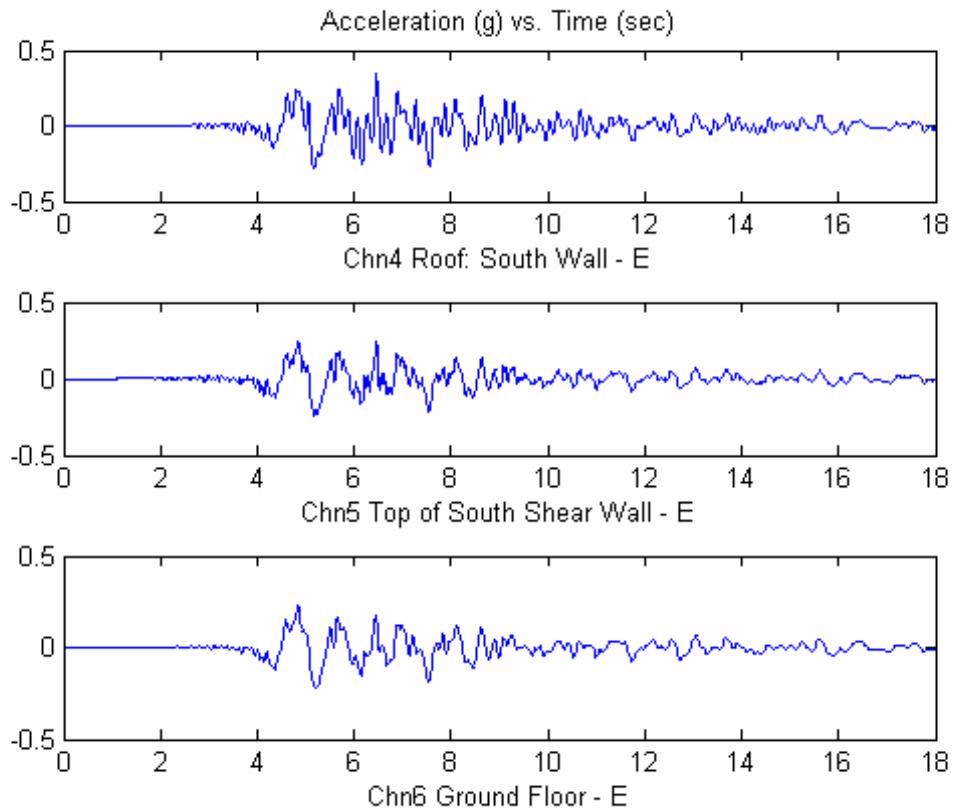
Figure 3.7: Acceleration strong motion time histories (East/West direction) of the Parkfield school building.
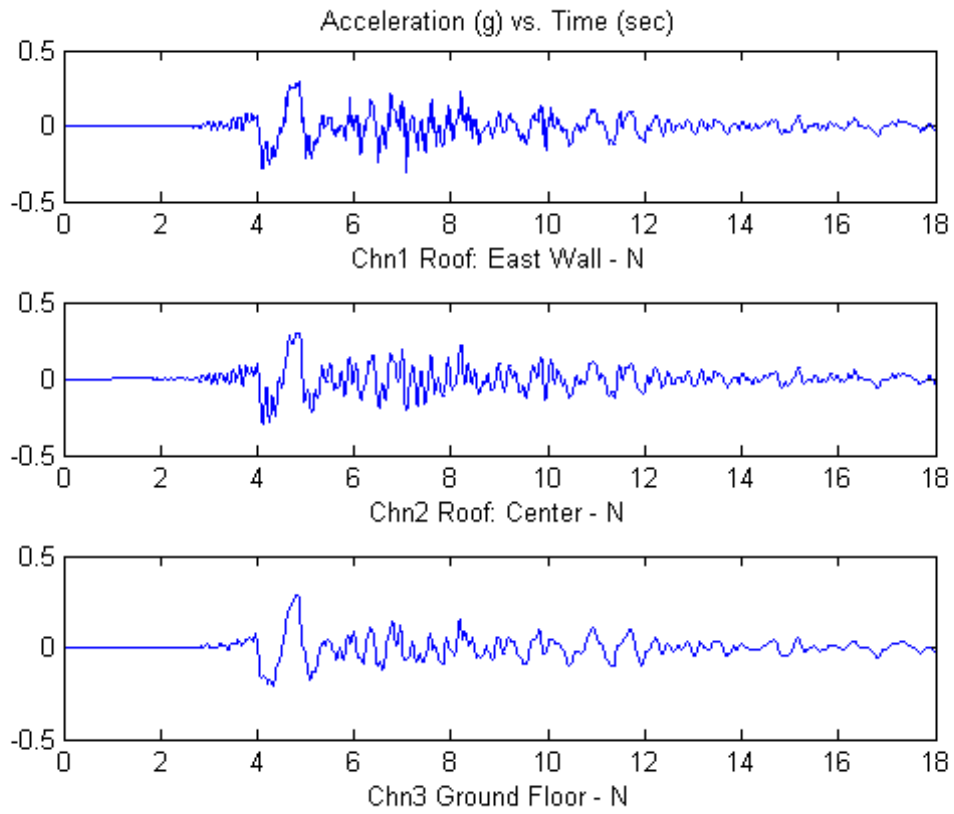
Figure 3.8: Acceleration strong motion time histories (North/South direction) of the Parkfield school building.

3.1.2 Templeton Hospital

The Templeton Hospital, built in 1975, has an irregular plan shape and measures 336' × 277'. Figure 3.9 shows the location and photograph of the station. In 1994 nine accelerometers were installed in the building. Plywood sheathed shear walls are installed in both directions. The hypocenter of the 2003 earthquake was 40 km away (CESMD 2006).
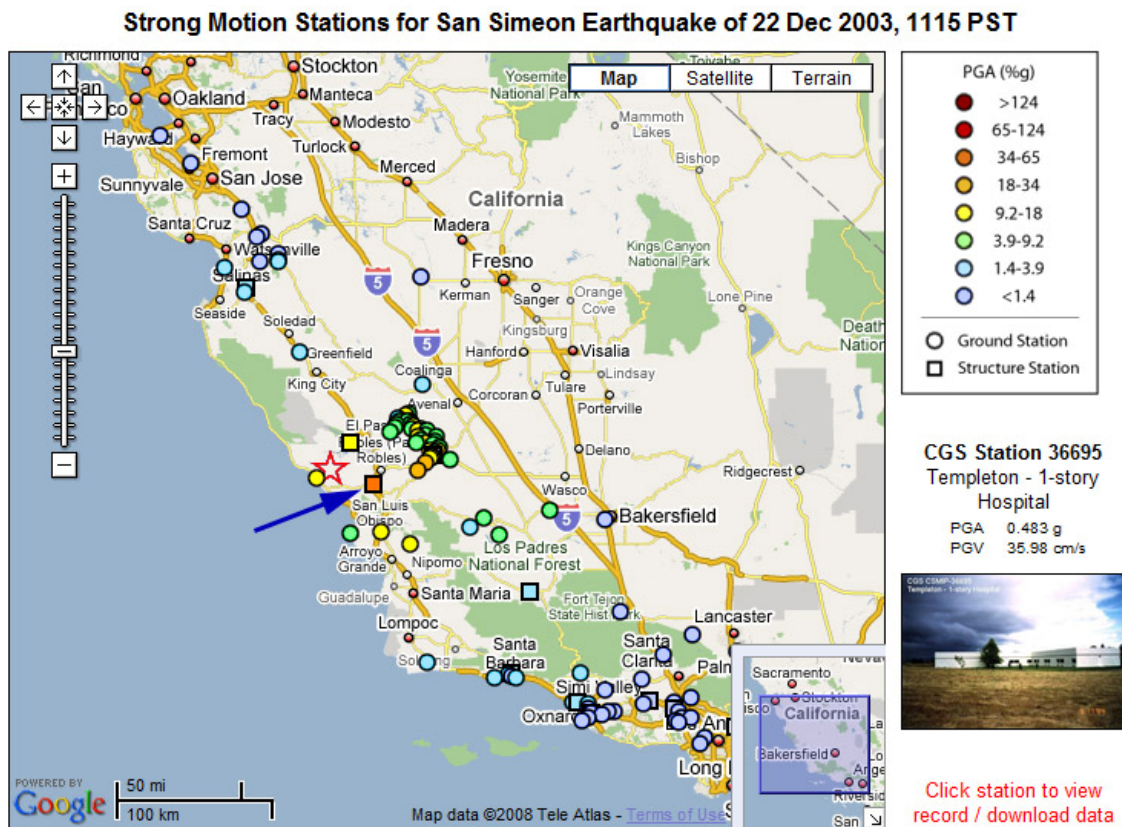
Figure 3.9: Location and photograph of the Templeton hospital.
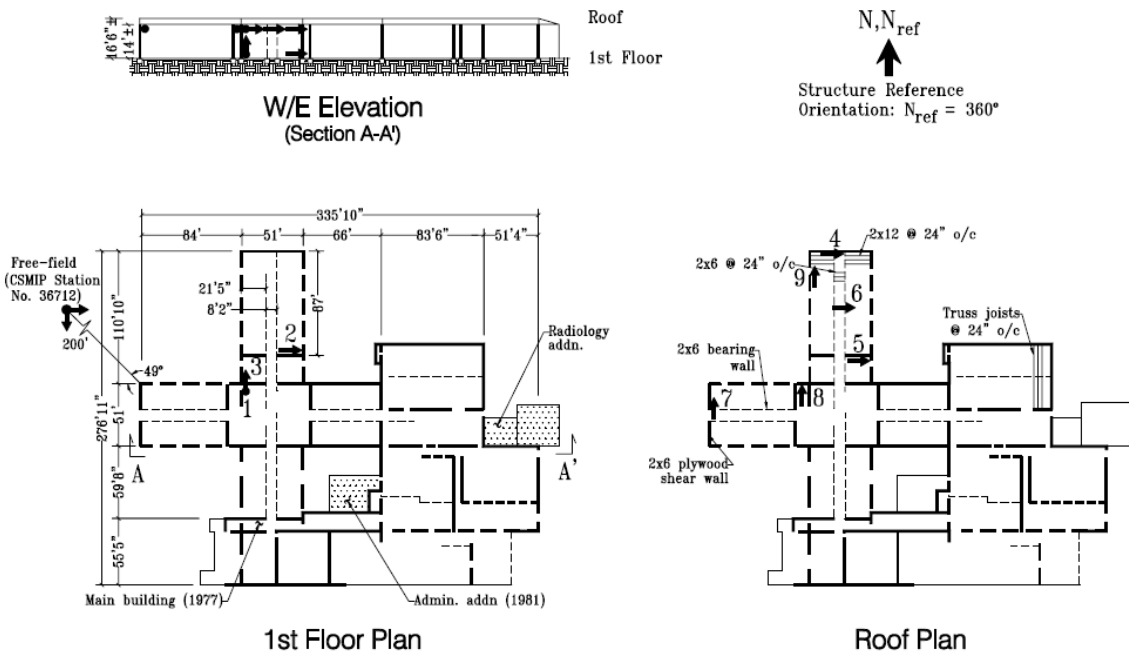
Figure 3.10: Instrumentation layout of the Templeton hospital.

The instrumentation schematic layout is shown in Figure 3.10. Three channels (1, 2 and 3) are situated on the first floor. Channel 1 measures the vertical acceleration of the building, whereas Channels 2 and 3 measure the ground motions in the longitudinal and transverse directions, respectively. The remaining channels are located on the roofs of the North and West Wings. The irregular floor plan and concentration of sensors present a challenge to the modeling effort of the entire structure. There is not much information regarding the rest of the building aside from the North and West Wings. As an alternative, one can model just the North Wing and make some assumptions regarding the inertial force transmitted to this wing from the rest of the building. Therefore, this dissertation will present only the modeling efforts for the Parkfield school building and not for the Templeton hospital.

27

Figure 3.11 and Figure 3.12 depict some of the channels having more than 100% g for its peak structural acceleration. Prior to this record, it was unknown if low-rise wood-frame structures could reach such peak structural accelerations.
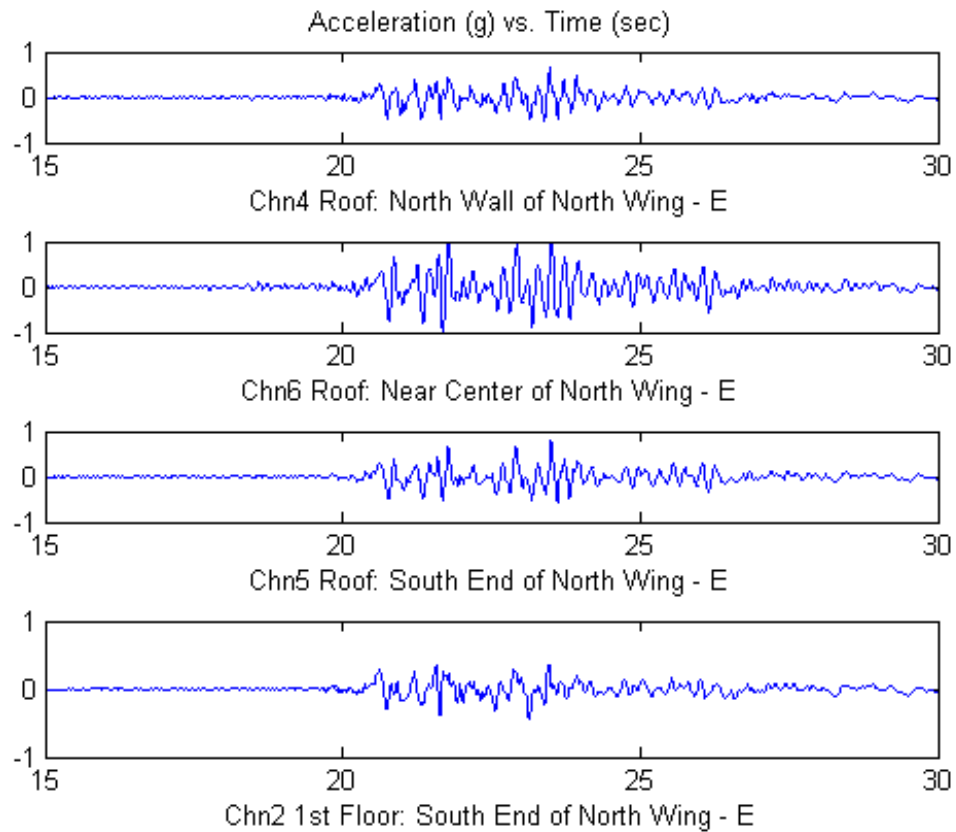
Figure 3.11: Acceleration strong motion time histories (East/West direction) of the Templeton hospital during the 2003 San Simeon Earthquake.
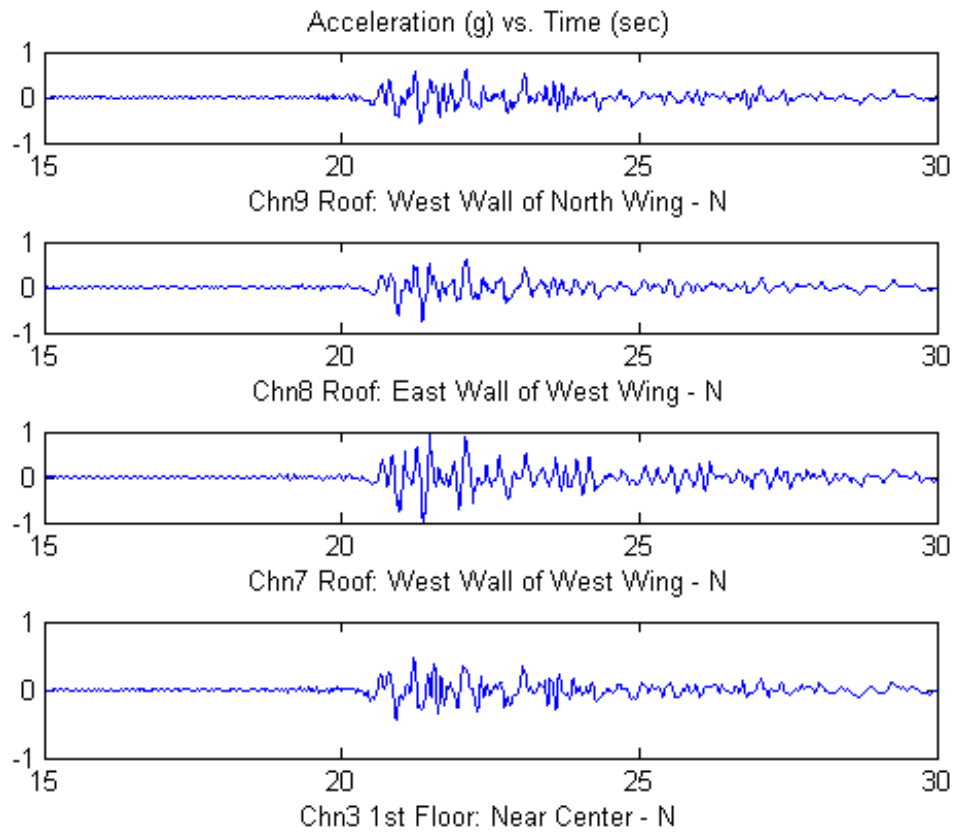
Figure 3.12: Acceleration strong motion time histories (North/South direction) of the Templeton hospital during the 2003 San Simeon Earthquake.

3.2 Experimental Records

Although this dissertation focuses on the interpretation of seismic response records, it was necessary to employ some experimental records for comparison. The advantage of using experimental records is the abundance and variety of available instrumentation on the test specimen, as well as the ability to control environmental and structural settings.

3.2.1 Shake Table Tests – University of California, San Diego (UCSD)

The UCSD shake table tests were part of Task 1.1.1 of the CUREE-Caltech Wood-frame Project. The test structure was a simplified full-scale two-story house. The testing occurred in several phases, each with different structural configurations. Quantifying the dynamic response during these tests will lead to a better understanding of the behavior of full-scale structural wood-frame systems.

The test structure has a 16' × 20' floor plan and is situated on the UCSD uniaxial shake table. The structural components of the test structure are full-scale, but plan dimensions are smaller due to restrictions of the shake table (Fischer, et al. 2001). The test structure was instrumented with nearly 300 displacement, acceleration, and force measuring devices. Since there have been so few full-scale shake table tests, the experimental results from this task will be a benchmark for interpreting field records. Having both acceleration and displacement histories, double integration on acceleration records used for field records is not necessary.

3.2.2 Forced Vibration Tests – Vanessa Camelo

The forced vibration tests included in this dissertation were part of Task 1.3.3 of the CUREE-Caltech Wood-frame Project. Multiple tests were performed on a three-story and

two-story wood-frame buildings, which were all owned by the California Institute of Technology.

These tests measured harmonic vibrations induced by a shaking machine. The shaking machine generates forces through the centrifugal acceleration of spinning weights. Sensors are mounted on the building to measure the building response at each driving frequency, and will in turn map out the frequency response of the building. These forced vibration tests provide an alternative method in calculating the system's frequency and damping estimates, and are invaluable for comparing with results from shake table tests and field records.

3.3 Remarks

Several records were mentioned in this chapter. Data were obtained in full-scale whole buildings for both field records and lab experiments. These data sets help formulate an understanding of the structure as a whole. In the next two chapters, system identification and hysteretic analyses are performed on the data set to fully extract all the information available in the record.

CHAPTER 4

System Identification

The process of system identification in structural engineering can be understood as identifying parameters for a numerical model that best represents the measured response of an instrumented structure (Eykhoff 1974). However, solving for these parameters is often an ill-conditioned inverse problem, making it extremely challenging in its application. Other complications in system identification include the choice of numerical algorithms and models, the amount of available instrumentation, the variability in construction methods and material strength, and any other environmental factors. Typically, system identification employs a least-squares metric to quantify the data fit between the measured response and the model. Specifics vary depending on the construction of the objective function, but one aims to find the minimum of the objective function and thus minimize the least-squares-error.

Lower least-squares-errors mean a better data fit. However, this does not always translate to better model predictions for future responses, since the method may over-fit the measured response. For example, observe a high-degree polynomial data fit that is present in any curve fitting toolbox. A ten-degree polynomial will result in a smaller error compared to a linear fit of the empirical data, but it does not necessarily lead to a better

predictive model, especially when the data demonstrate a roughly linear relationship between the two parameters. This over-fitting of what is likely just noise can easily happen when the chosen model has significantly more parameters relative to the information in the data set.

The over- and under-fitting of data complicate the fidelity of resulting models. To minimize these effects, engineers strive to uncover the underlying structural mechanics that produce these data. Since physical behaviors of structures are difficult to extract from time records alone, experimental setups are needed to complete the picture. However, selecting the right model is open to interpretation; models only perform as well as how an engineer thinks the physical system behaves. Therefore, predictions of responses are only as good as the predictive capability of the model, regardless of the accuracy of previous data fits.

The byproduct of leaving the model selection to an engineer's interpretation is that there is often a number of models developed for the same purpose. In modeling wood-frame structures and subassemblies, each researcher often proposes a proprietary element that mimics the hysteretic behavior of wood-frame construction (Foliente 1994). The objective of this dissertation is not to assess which custom hysteretic element works best (as each has its own advantage), but to provide a methodology to evaluate the results. Chapter 6 will discuss in detail the non-linear numerical model used to model the responses. The remainder of this chapter will focus on linear analysis and identify key modal parameters for the records.

4.1 Linear Analysis

Although it seems counterintuitive to use linear analysis in dealing with responses that can be nonlinear, there are many benefits from using this approach (Beck and Jennings 1980).

When a system is linearized, several fundamental properties can be utilized, such as the principle of superposition, linear elasticity, homogeneity in materials, and conventional computational methods (Ma 1995). The analysis becomes less computationally intensive and easier to comprehend for presentation. Results can be summed up with a few numbers pertaining to the fundamental frequencies, modeshapes, and damping ratios.

Even though linear analysis has been extensively studied and applied, it is still necessary to spend extra effort in interpreting the results. A thorough understanding and application of linear analysis to a system does not equate to knowledge of the governing dynamics of the actual system. This does not mean that the results of linear analysis are not meaningful. Observations of the time-varying trends of the modal parameters can give insights to the nonlinear behavior of the system. These findings will be discussed later in the chapter after an introduction of the linear analysis used for system identification.

4.2 MODE-ID

There are numerous system identification algorithms available for structural analysis. However, not all of them are suitable for strong motion records and nonlinear responses. Many of these methods have severe limitations on signal-to-noise ratio, construction of mass and stiffness matrices (K.-Y. Chen 2003), and geometric information. They also make assumptions that are not suitable for high amplitude transient signals found in an earthquake (He et al. 2005). Some of the methods are ad-hoc, requiring special conditions not met in practice with real seismic response records (James, Carne and Lauffer 1993). Other methods require assumptions that require specific tailoring of the records. This dissertation does not attempt to determine the best method, as an extensive study of all the algorithms is out of the scope of the project (Jovanovie 1997; Asmussen 1997; Sain and

Spencer 2005; Shi 2007; Gang). For purposes of this dissertation, MODE-ID is the method

of choice which has its origins in Beck (1978). There are several reasons MODE-ID is used

for the system identification routine.

1) Previous results are calculated from MODE-ID (Camelo, Beck and Hall 2002).
   Using the same algorithm for new data analyses facilitates comparisons.

2) System identification can be performed in the time domain without the need to
   develop a structural model by constructing mass, stiffness and damping matrices
   (Beck 1978).

3) MODE-ID can handle linear and nonlinear, multiple input-output, and output-only
   responses (Beck and Jennings 1980; Werner, Beck and Levine 1987).

4) MODE-ID analysis can be applied on both full and windowed records.

5) Parameter values estimated by MODE-ID can be considered as *most probable
   values* based on the given data in a Bayesian probability framework (Beck 1990).

Inputs for MODE-ID include ground excitation records, measured structural

response histories, and initial modal estimates. The modal parameters estimated for each

mode are frequency, damping factor, normalized modeshape, participation factors, initial

displacement, and initial velocity. MODE-ID has been applied extensively to earthquake

and other dynamic data, demonstrating its robustness. The data fitting in MODE-ID is

based on a nonlinear least-squares output-error method. The measure of fit between

recorded and calculated responses is optimized by a modal minimization algorithm (Beck

and Beck 1985). Although the minimization is performed in the time domain, a frequency domain MODE-ID can be employed through Parseval's Inequality.

The specifics of the modal identification process are to minimize a measure-of-fit parameter J, defined as the ratio of the mean-square output error between measured and model motions to the mean-square output from the measured motions (Werner, Nisar and Beck 1992). This modal minimization routine first begins with modal decomposition, allowing the response of the structure to be expressed as a superposition of the responses of several single-degree-of-freedom (SDOF) oscillators. Given N measurements (N_{in}: base accelerations, N_{out}: floor accelerations) a modal model can be mathematically expressed as

$$\ddot{x}_i = \sum_{m=0}^{M} \ddot{x}_{im}(t), \qquad i = 1, 2, \dots, N_{out} \tag{4-1}$$

where M is the number modes considered for the model. The ith predicted acceleration time history $\ddot{x}_i$ can then be represented as a summation of modal mode responses $\ddot{x}_{im}$. The subscript refers to the contribution of the mth mode to the ith output channel. For each of the m modes, the governing equation is the following:

$$\ddot{x}_{im} + 2\xi_m \omega_m \dot{x}_{im} + \omega_m^2 x_{im} = \phi_{im} \sum_{k=1}^{N_{in}} P_{mk} f_k(t) \tag{4-2}$$

$$x_{im}(0) = \phi_{im} c_m, \qquad \dot{x}_{im}(0) = \phi_{im} d_m \tag{4-3}$$

ω_m : natural frequency of mth mode

36

ζ_m : critical damping ratio of mth mode

φ_{im} : modeshape component of mth mode at the ith location

P_{mk} : participation factor of the mth input channel for the mth mode

c_m : initial modal displacement of mth mode

d_m : initial modal velocity of mth mode

MODE-ID's modal identification routine can also account for a pseudo-static component by incorporating a pseudo-static matrix that directly relates the input and output channels. Completing the modal decomposition and establishing the time-stepping algorithm (Beck and Dowling 1988), modal minimization determines the combination of parameters $\underline{\theta}$ that minimizes the aforementioned measure of fit J. Given measurement records $\hat{y}_i$, the mean-squared fractional error J can be calculated as the following:

$$J(\underline{\theta}) = \sum_{i=1}^{N_{out}} \sum_{n=1}^{N} [\hat{y}_i(n) - \ddot{x}_i(n; \underline{\theta})]^2 \tag{4-4}$$

MODE-ID performs a series of sweeps in which optimization is performed one mode at a time. Optimization within each mode is calculated by the method of steepest descent with respect to the modal frequency and damping (Beck and Jennings 1980). This modal minimization routine has been proven to be superior to the transfer function approach in structural identification of linear models (Beck and Beck 1985). Additional background information regarding MODE-ID method can be found in EERL Reports 85-06 (Beck and Beck 1985) and 78-01 (Beck 1978). Information regarding the usage of MODE-ID can be found on the COMET website and a downloadable MODE-ID user manual (Beck and Mitrani 2003).

4.3 Results

The MODE-ID results shown here focus on the 2004 data obtained from the Parkfield school building and the Templeton hospital building. Older earthquake data will also be analyzed to ensure that changes in dynamic characteristics are not due to any discrepancies in MODE-ID settings. Previous results (Camelo, Beck and Hall 2002) will be used as reference to validate the results from older earthquakes.

4.3.1 Parkfield School Building

The Parkfield school building is only one story tall. It is expected that the dominant response will largely consist of the fundamental N-S, E-W modes and possibly one torsional mode. The frequency, damping and modeshape estimates are presented in Table 4-1 and Figure 4.1. In addition to the 2004 Parkfield Earthquake, records from two smaller earthquakes in 1993 and 1994 can be used to evaluate the change in dynamic characteristics over a range of ground motion amplitudes. Note from Figure 4.1 that the modes are coupled and therefore not purely N-S, E-W and torsional.

Table 4-1: The Parkfield school building frequency and damping estimates calculated from MODE-ID. The peak structural acceleration is provided for each earthquake.

Earthquake	Freq.(Hz) E-W	Damp. (%) E-W	Freq.(Hz) N-S	Damp. (%) N-S	Freq.(Hz) T	Damp. (%) T
4.2 M 0.123 g 04/04/1993	7.3	12	8.6	15	11	16
4.7 M 0.201 g 12/20/1994	6.5	11	8.2	15	11	23
6.0 M 0.30 g 09/28/2004	5.3	13	6.0	22	8.9	13

E-W Mode   **N-S Mode**

Roof Plan

South Wall

Torsional Mode

Roof Plan

South Wall
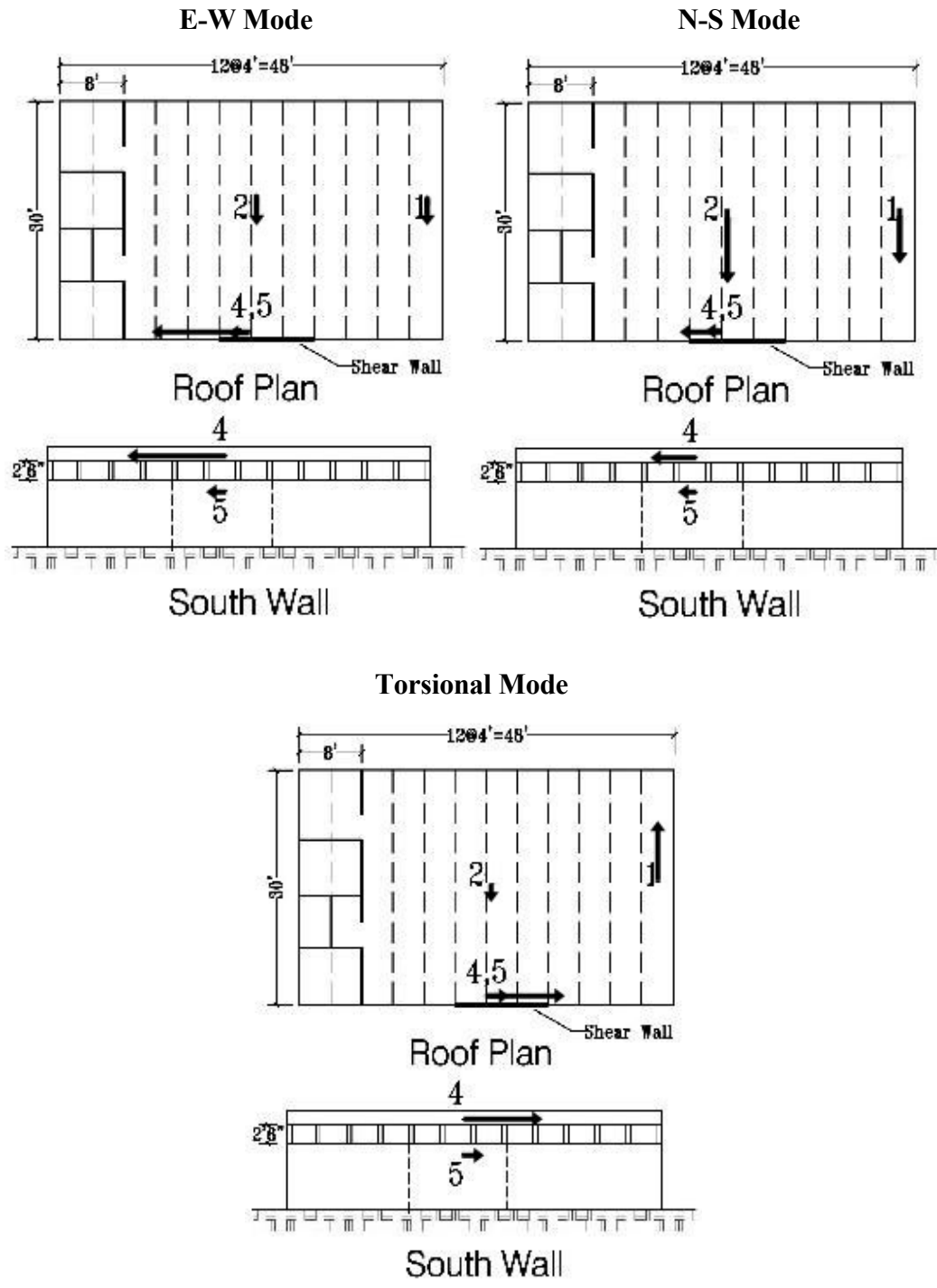
Figure 4.1: First three modeshapes of the Parkfield school building generated from the 2004 Parkfield Earthquake.

The 1993 and 1994 earthquakes have been re-analyzed and compared to the results in CUREE Task 1.3.3 (Camelo, Beck and Hall 2002). The values are found to be consistent. Since the magnitudes of the 1993 and 1994 earthquakes were similar, the reported modal frequency and damping estimates are comparable with the exception of the damping ratios of the torsional mode. The reason for this difference is not evident. It is likely the ground motion was not able to excite the torsional mode throughout the entire time record. In comparison with the records from 2004, amplitude dependence can be observed. The larger response amplitudes in 2004 are accompanied by lower frequencies and higher damping values.

Analysis of full-duration records produced high damping estimates as have been noted in previous studies. Damping is inherently difficult to estimate accurately with any method (Beck and Beck 1985). The credibility of a 20% damping ratio in wood-frame buildings needs to be investigated since steel or concrete buildings generally have values of 3 to 5%. For MODE-ID, a linear viscous damping is assumed. The meaning of a linear damping value that is fit under conditions of nonlinear response will be discussed in Chapter 5.

Table 4-1 also shows that the damping estimates in the N-S modes are generally greater than those of the E-W modes. This may be related to the fact that the north and south walls have less shear wall contribution due to a substantial area designated for windows, as shown in Figure 3.6.

Based on the identified modal parameters, MODE-ID can generate predicted responses for each of the measured channels. Table 4-2 displays the sum squared error between the measured and predicted responses from the different Parkfield school records.

It is evident that a two-mode MODE-ID model provides a drastic improvement compared to a single-mode MODE-ID model. This makes physical sense since it is anticipated that the fundamental frequencies in the longitudinal and transverse direction will be excited. The third mode, potentially a torsional mode, provides marginal improvement.

Figure 4.2 through Figure 4.10 present the predicted responses based on MODE-ID modal parameters for the measured earthquake records of the Parkfield school building in 1993, 1994, and 2004. Each earthquake record set has three MODE-ID models identified. Each model represents different number of modal modes used in the modal identification process. The red dotted lines are the measured responses and the blue lines are MODE-ID's predicted responses. The sum squared error is listed above each channel of record for comparisons between models. The two-mode model does a remarkable job in fitting the measured responses with the exception of the last channel, which sits on a shear wall.

Table 4-2: Sum squared error between the measured and predicted responses from different MODE-ID models. Measurements are from the 1993, 1994, and 2004 Parkfield school records.

Number of Modes	1993	1994	2004
One-Mode	0.4892	1.9049	4.5085
Two-Mode	0.1385	0.5383	1.8090
Three-Mode	0.1244	0.4599	1.5398
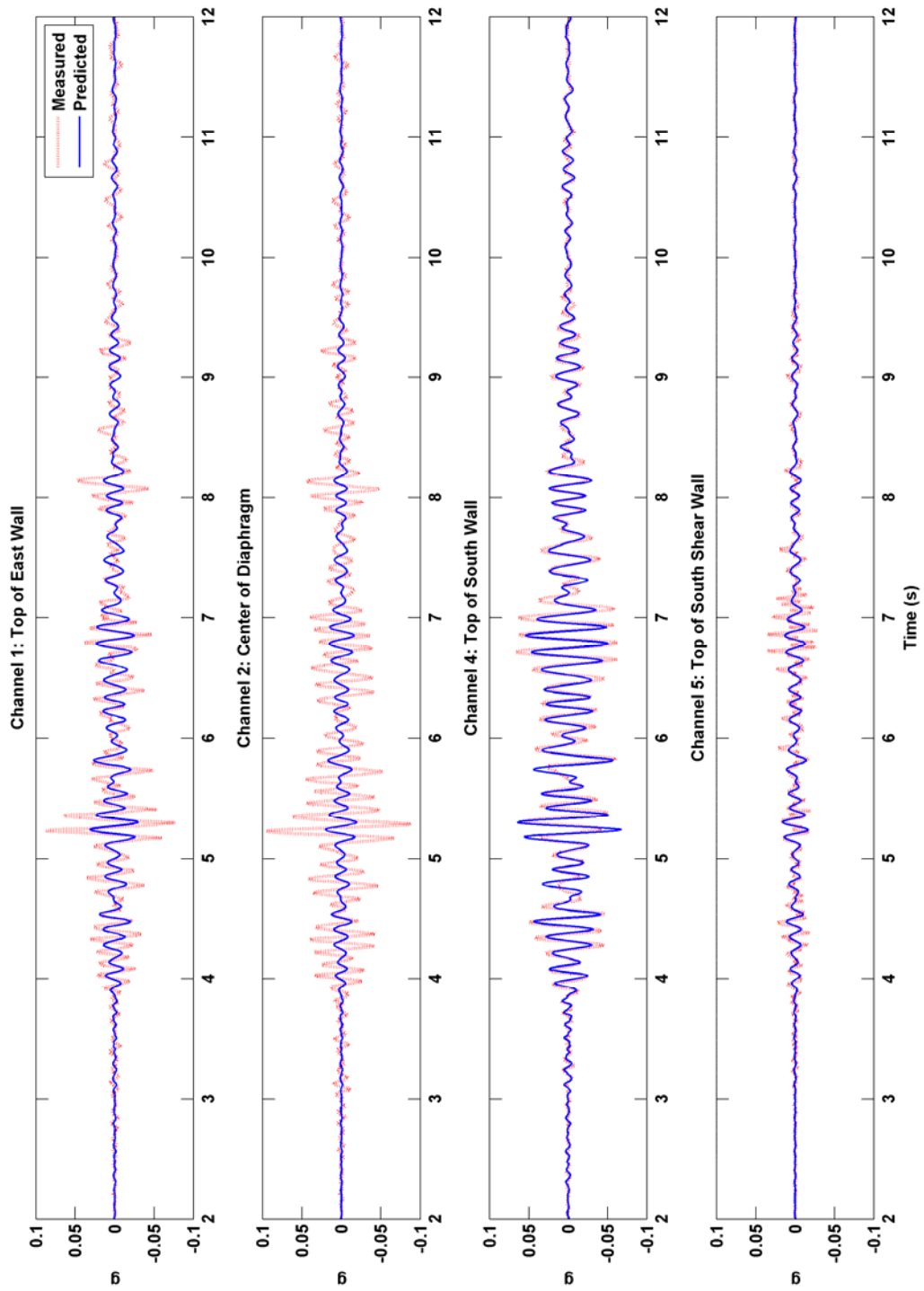
Figure 4.2: One-mode model for the 1993 Parkfield school records.
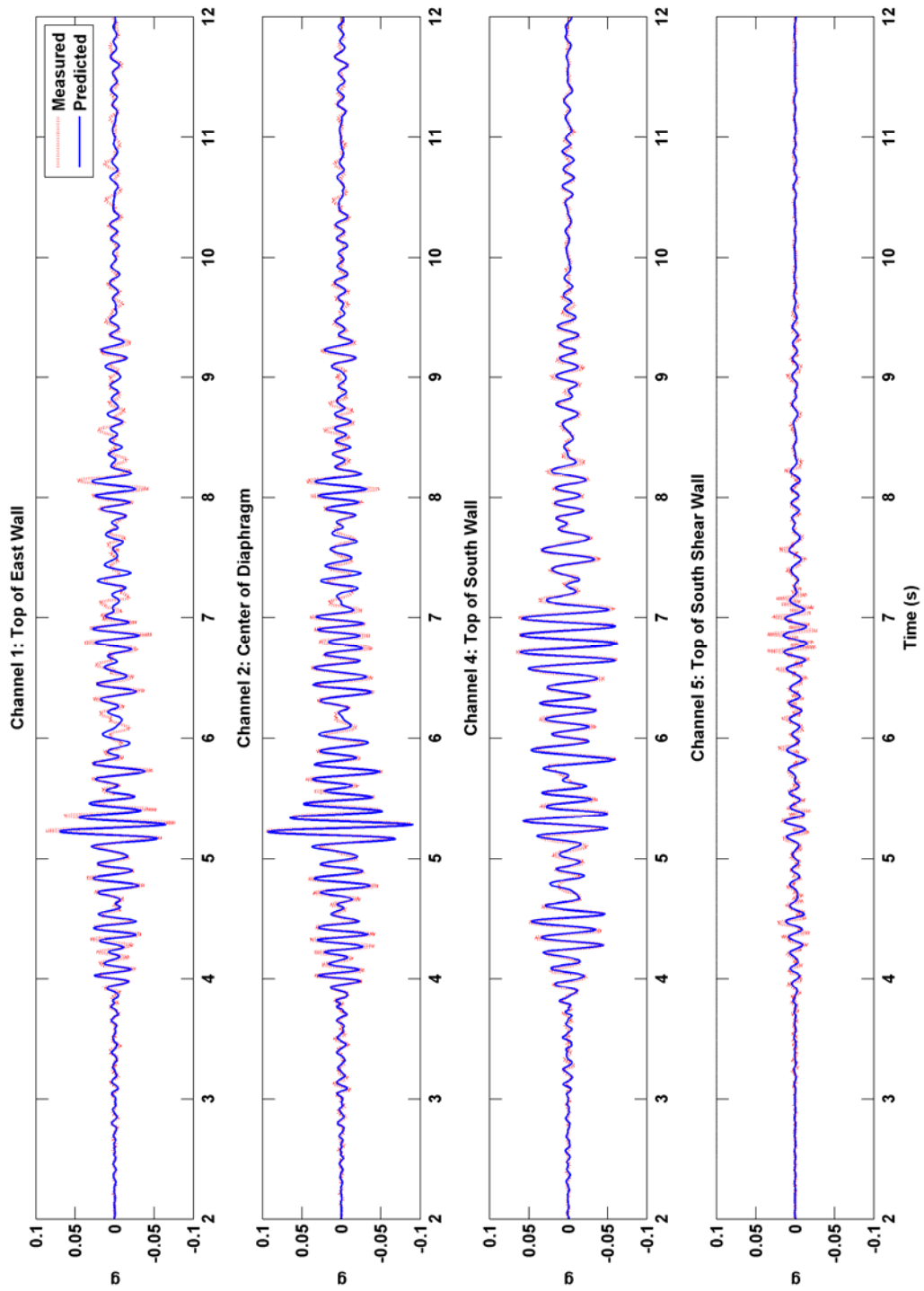
Figure 4.3: Two-mode model for the 1993 Parkfield school records.

44
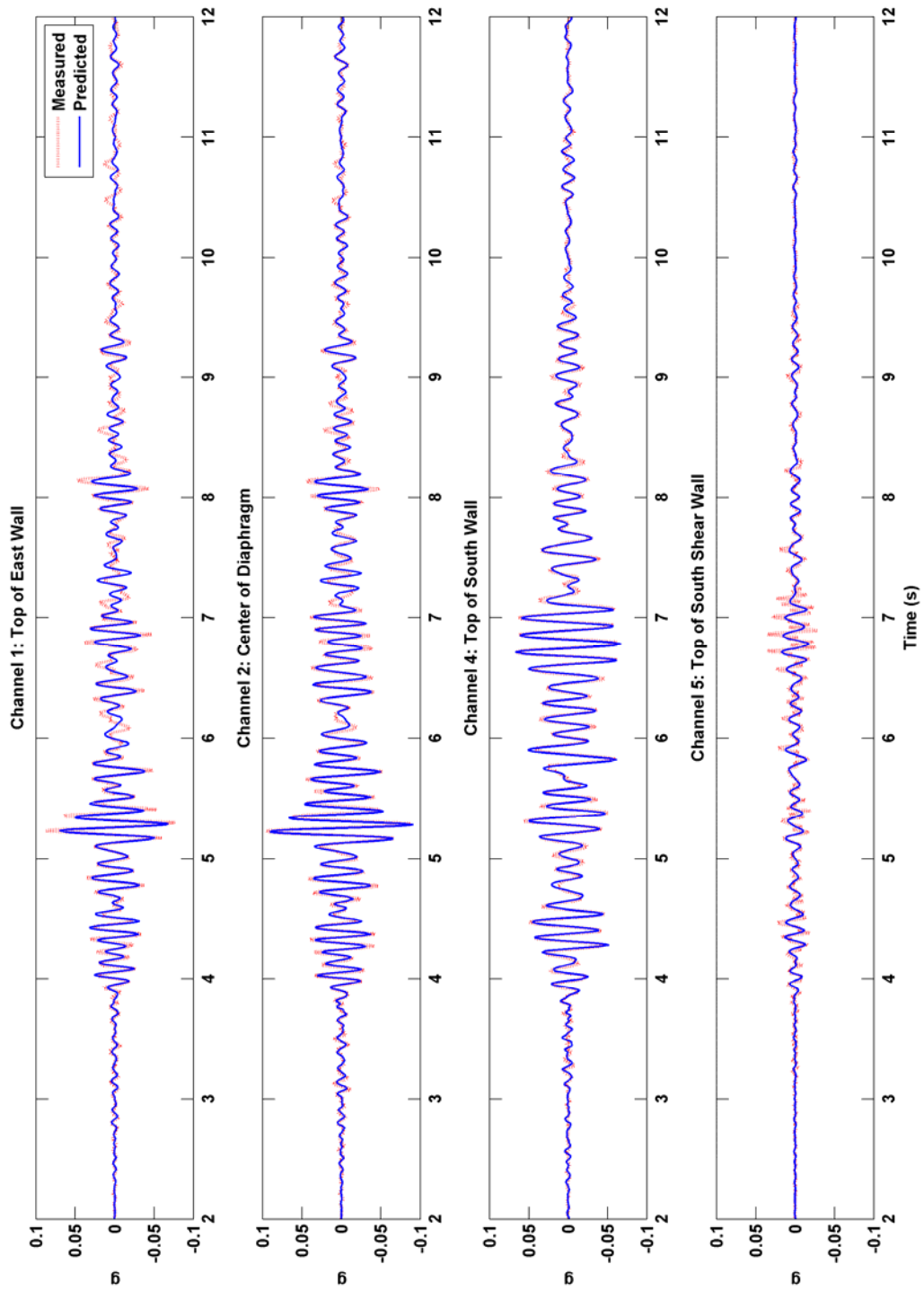
Figure 4.4: Three-mode model for the 1993 Parkfield school records.
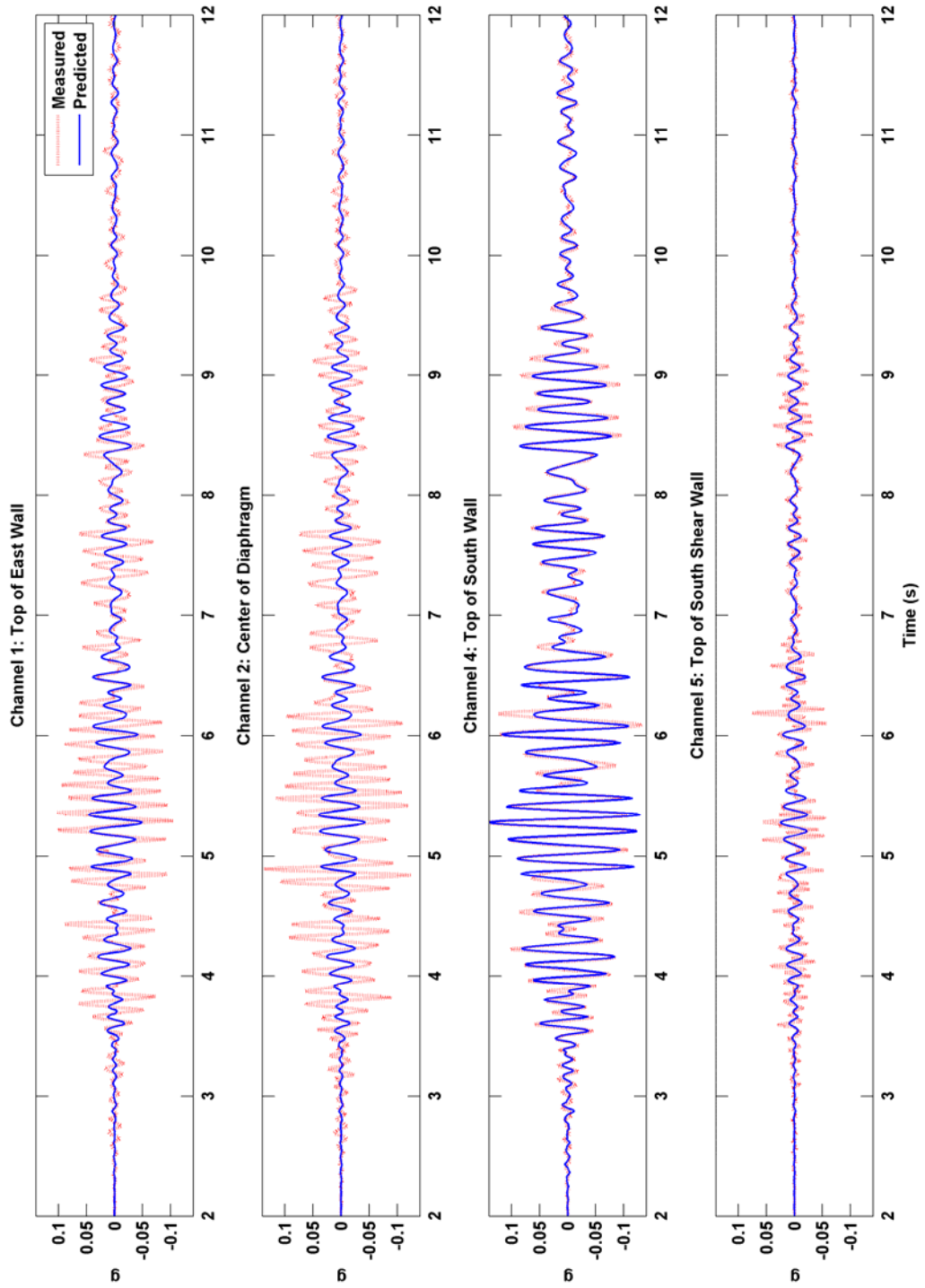
Figure 4.5: One-mode model for the 1994 Parkfield school records.
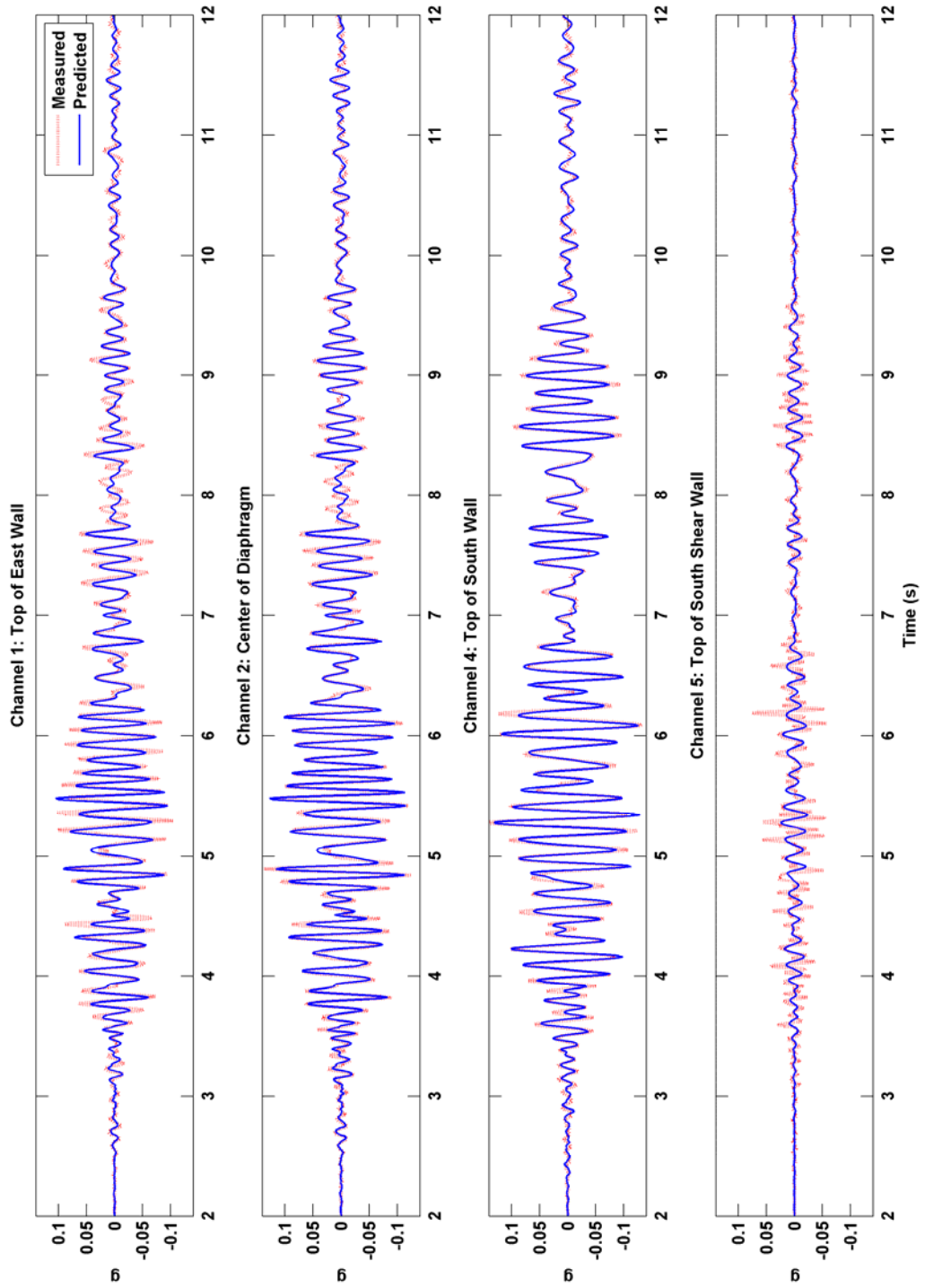
Figure 4.6: Two-mode model for the 1994 Parkfield school records.
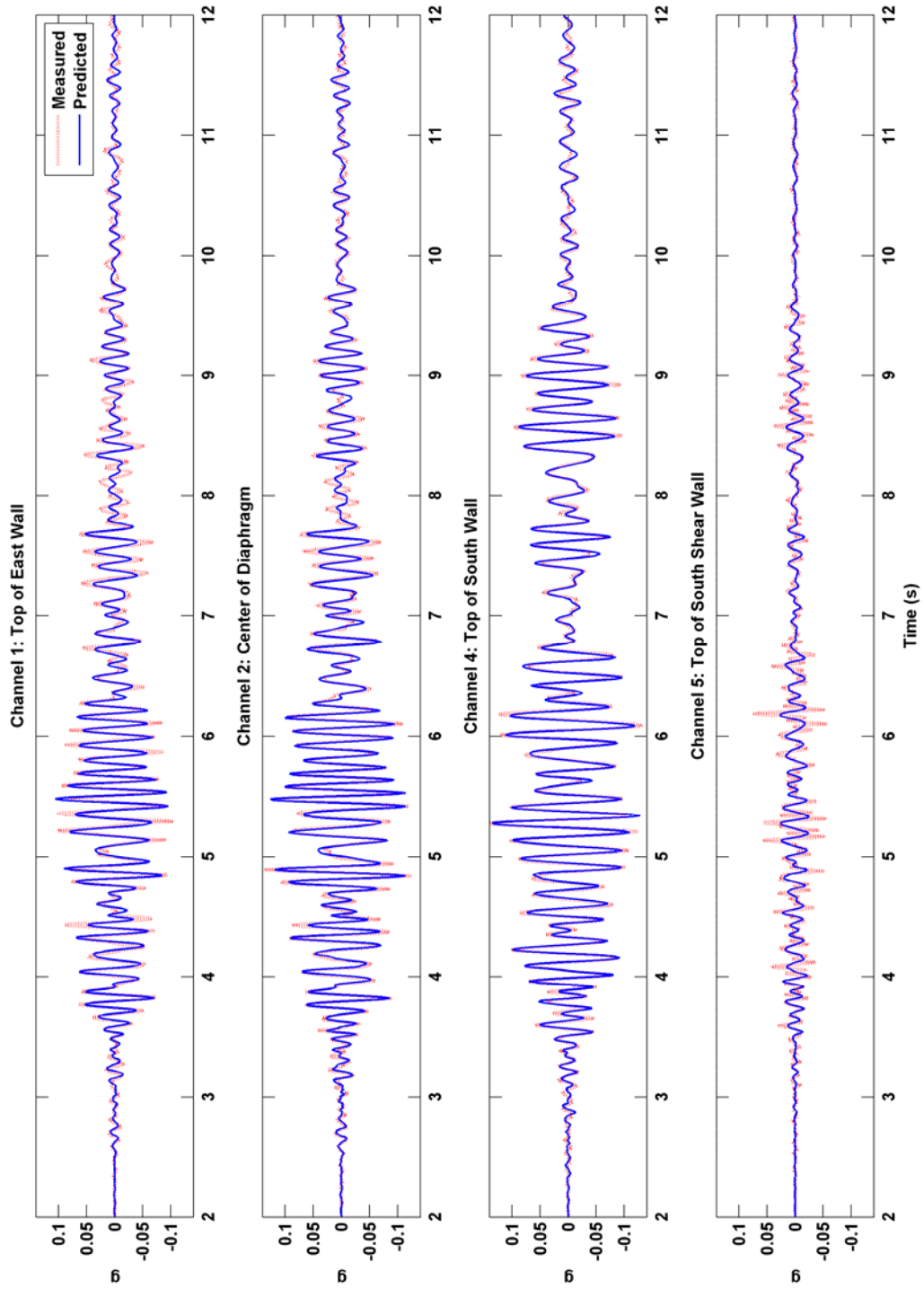
Figure 4.7: Three-mode model for the 1994 Parkfield school records.

48
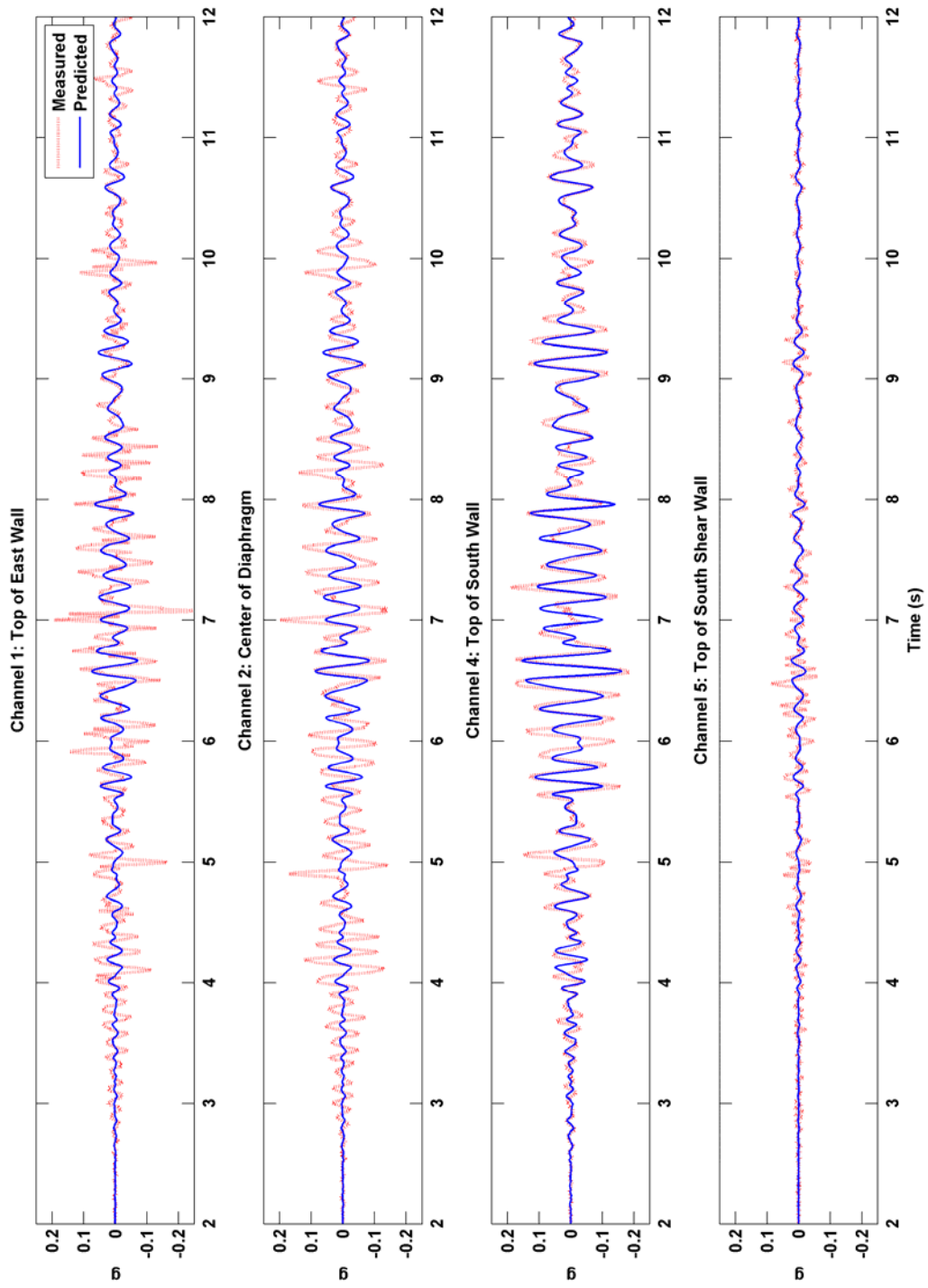
Figure 4.8: One-mode model for the 2004 Parkfield school records.

49
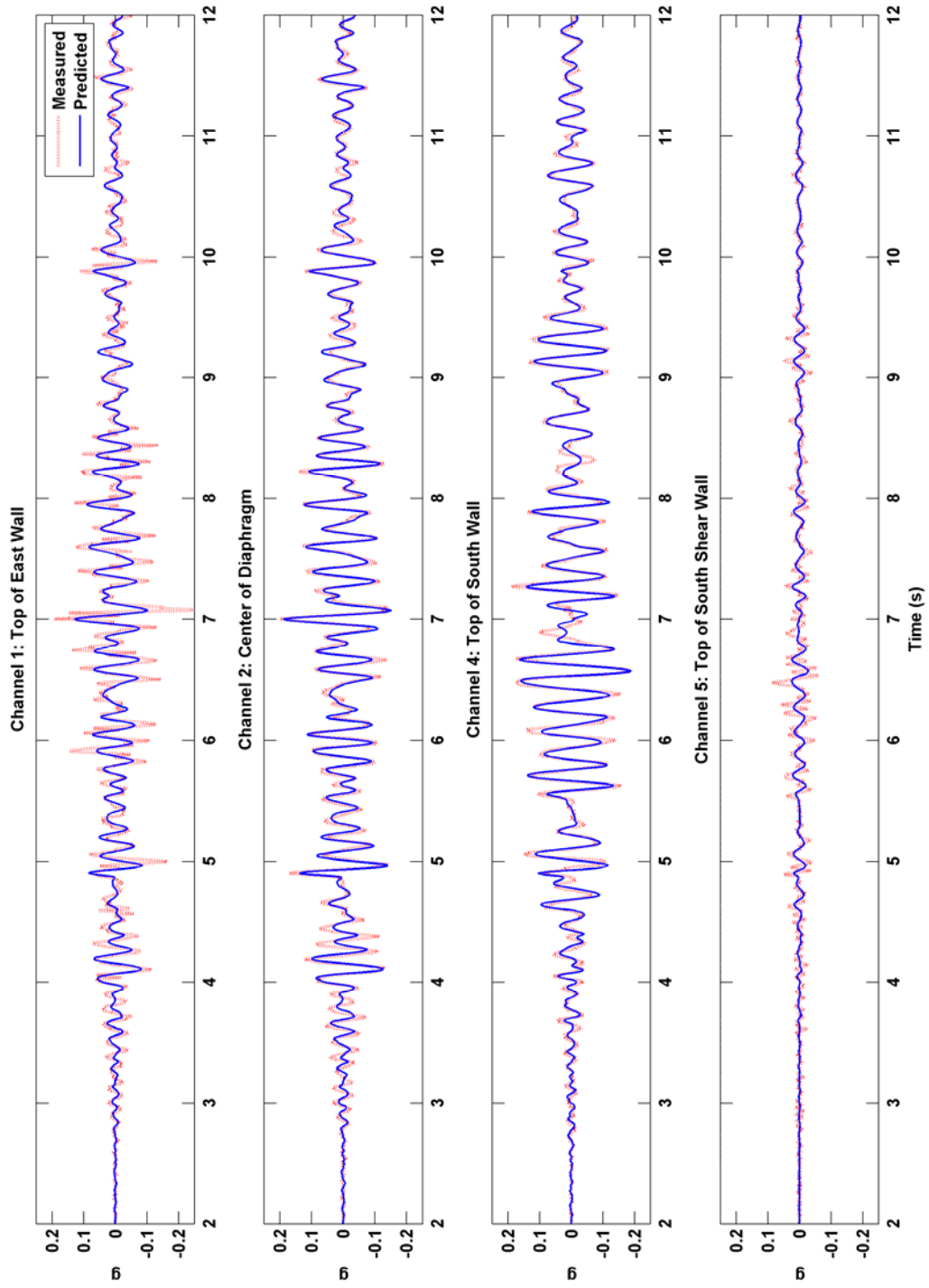
Figure 4.9: Two-mode model for the 2004 Parkfield school records.

50
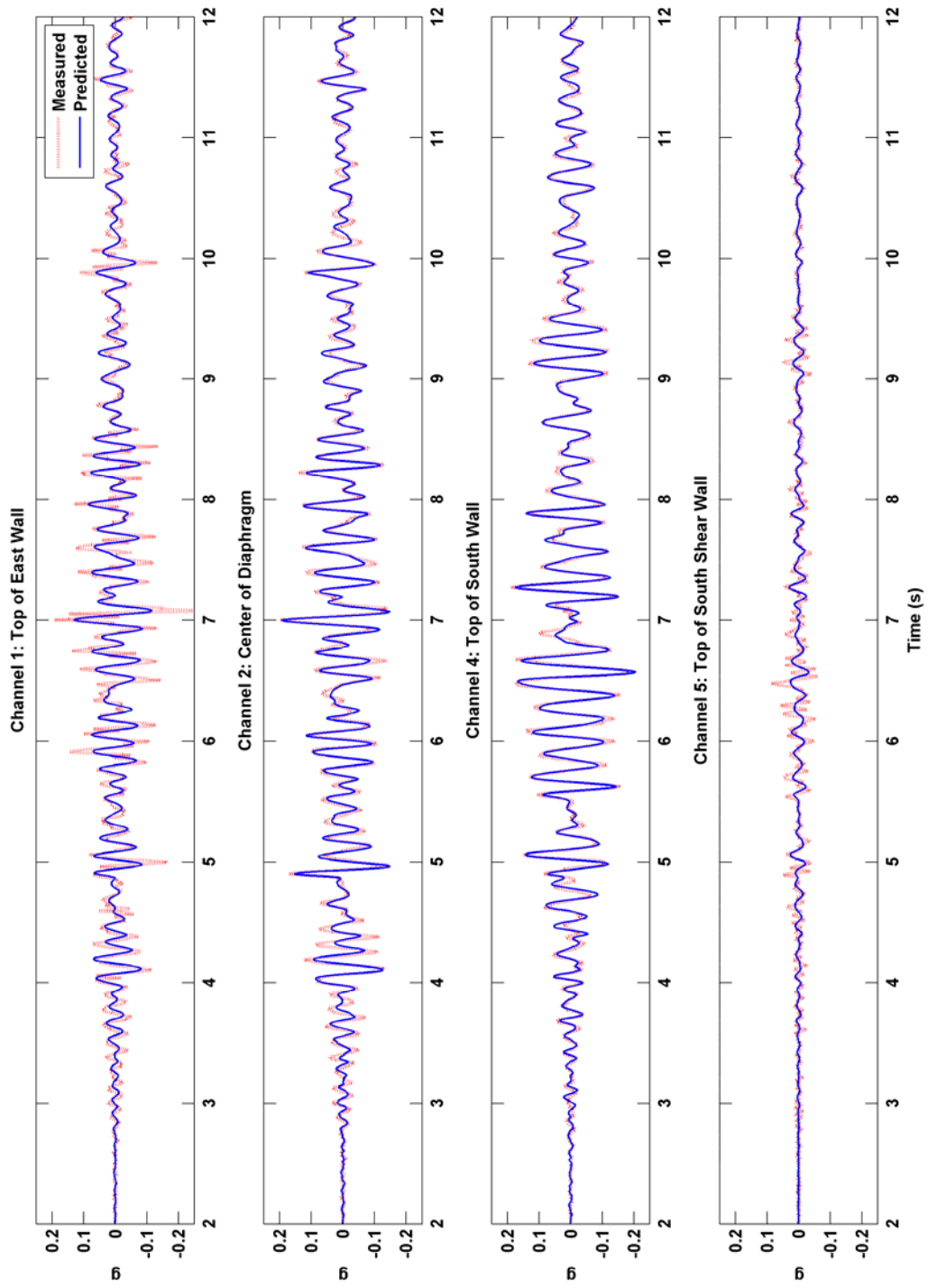
Figure 4.10: Three-mode model for the 2004 Parkfield school records.

A windowing analysis can be performed on the 2004 Parkfield records through MODE-ID. Results are presented in Figure 4.11 and Figure 4.12. A two-second window with 50% overlap was chosen because it is the smallest window that results in consistent convergence. Windowing analysis reveals the change in modal frequency and damping during the earthquake.

From Figure 4.11 it is apparent that the building did reach nonlinear motion because each fundamental frequency changed during the course of the response. Following the locus of the estimated fundamental frequencies of the building, the initial frequencies were around the 7 Hz range when the initial motion was recorded. The building's frequencies decrease to nearly 5 Hz as the magnitude of the ground response increases, reaching these significantly lower values during the time of the strongest ground shaking at around 5 seconds (Figure 3.7). As the ground motion subsides, the building's fundamental characteristics revert to initial frequencies. This suggests that the building sustained no significant damage.

The window analysis on damping estimates (Figure 4.12) shows that damping fluctuates greatly throughout the earthquake shaking. At lower ground motions, the damping ratio still displays values of 12-20%, which are high relative to steel and concrete buildings. These results are a fabrication of MODE-ID attributing high damping estimates to compensate for the high participation factors for low amplitude responses. There is a trend that the frequency estimates decrease and damping estimates increase before the largest amplitude of ground motion. How early the trend begins depend on the length of window used.

This should not be seen as an error, but a tradeoff between model resolution and accuracy. Additionally, as ground motion subsides, the reported damping estimates have high variance in a small window time frame. To illustrate this, longer time windows were used for records from 1993 and 1994 Earthquakes (Figure 4.13 to Figure 4.16). The fluctuations in damping estimates are no longer present at the expense of a coarser time resolution. The same observations can be made with regard to the amplitude dependence of frequency and damping estimates.
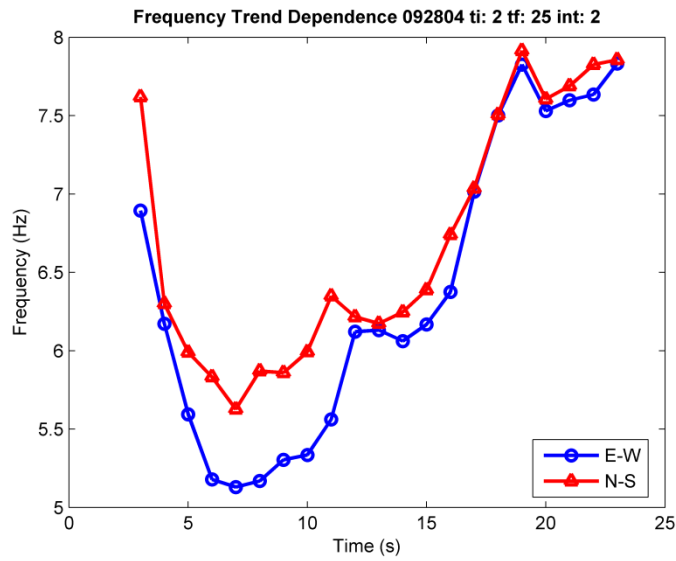
Figure 4.11: Amplitude dependence of the E-W and N-S mode frequency estimates for the Parkfield school building. The window analysis is performed on the 2004 Parkfield Earthquake.
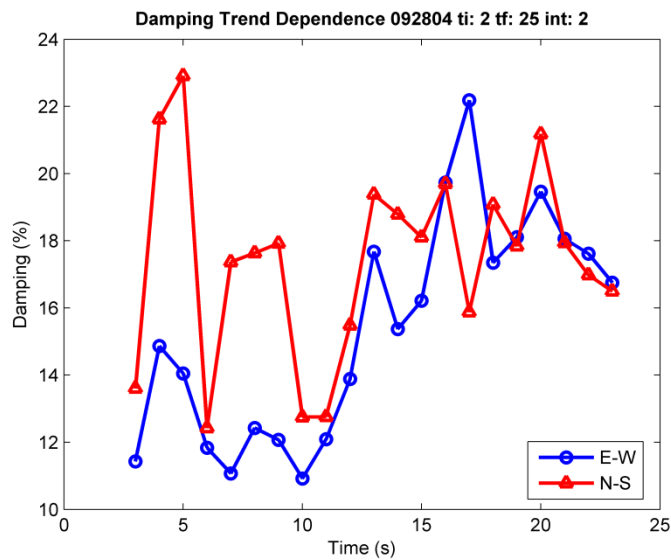
Figure 4.12: Amplitude dependence of the E-W and N-S mode damping estimates for the Parkfield school building. The window analysis is performed on the 2004 Parkfield Earthquake.
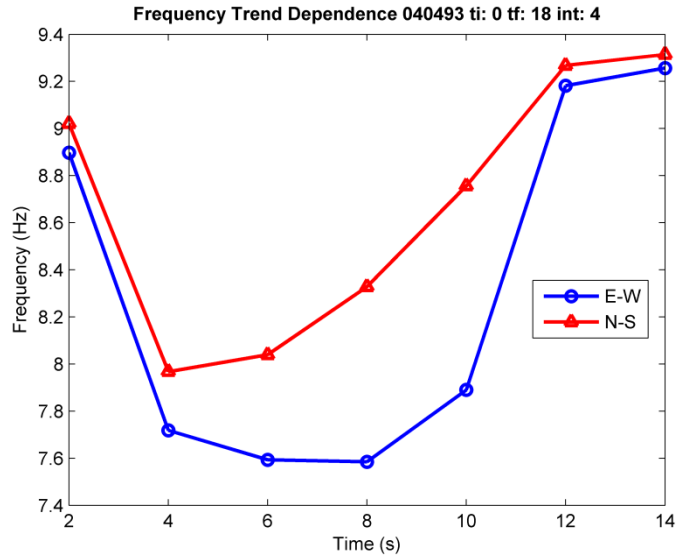
Figure 4.13: Amplitude dependence of the E-W and N-S mode frequency estimates for the Parkfield school building. The window analysis is performed on the 1993 Parkfield Earthquake.
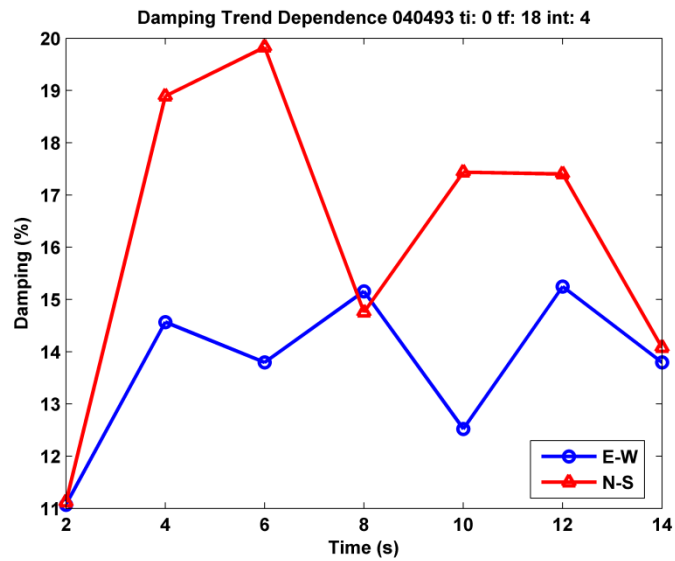
Figure 4.14: Amplitude dependence of the E-W and N-S mode damping estimates for the Parkfield school building. The window analysis is performed on the 1993 Parkfield Earthquake.
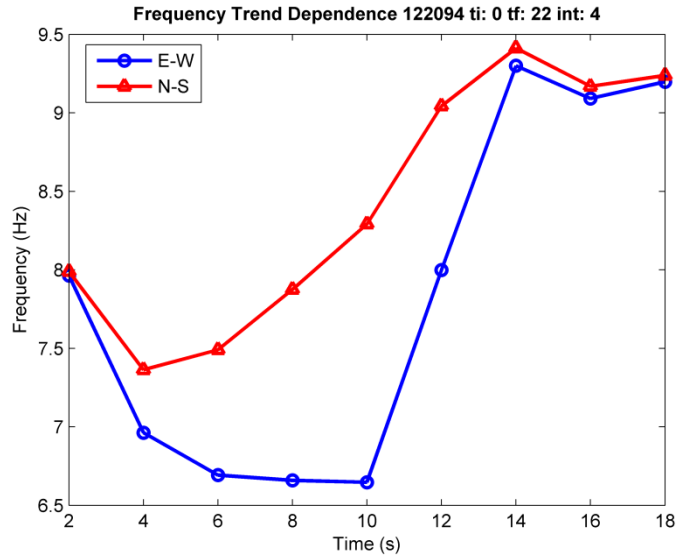
Figure 4.15: Amplitude dependence of the E-W and N-S mode frequency estimates for the Parkfield school building. The window analysis is performed on the 1994 Parkfield Earthquake.
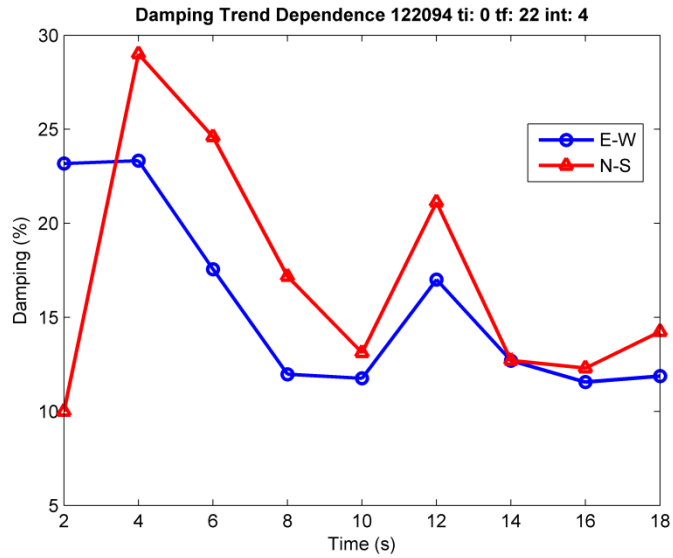
Figure 4.16: Amplitude dependence of the E-W and N-S mode damping estimates for the Parkfield school building. The window analysis is performed on the 1994 Parkfield Earthquake.

4.3.2 Templeton Hospital

Frequency, damping and modeshape estimates are presented in Table 4-3 and Figure 4.17. The first mode mostly involves transverse motions of the west wing, and the second mode is predominately north wing. Both wings contribute to the third mode. The instrumentation layout allows only the study of the northwestern wings of this very asymmetric building.

Table 4-3 contains the results for the M 6.5 earthquake in 2003, three of its aftershocks, and another smaller earthquake in 2005. Results seem to be consistent with the observations made from the analysis of the Parkfield school building. Reported frequencies are higher for the aftershock records and much lower for the 6.5 M San Simeon Earthquake. Damping estimates continue to be within the 15-20% range with the west wing exhibiting higher damping for all five records.

Figure 4.18 to Figure 4.20 are the predicted responses generated from MODE-ID for the 2003 Templeton hospital records. Again, the sum squared error is labeled above each channel. For the 2003 record, the one-mode model had a sum squared error of 61.584 compared to 28.4894 and 20.8913 for the two- and three-mode model. Larger discrepancies are seen in rows 1, 4, and 6, which correspond to measurement channels 4, 7, and 9 in the instrumentation layout. These channels sit along the outer shear walls.

Table 4-3: Templeton hospital building frequency and damping estimates calculated from MODE-ID. The peak structural acceleration is provided for each earthquake.

Earthquake	Freq. (Hz) W. Wing	Damp. (%) W. Wing	Freq. (Hz) N. Wing	Damp. (%) N. Wing	Freq. (Hz) Mode 3	Damp. (%) Mode 3
4.4 M .017 g 05/16/05	7.3	20	7.0	12	9.9	8.9
Aftershock .031g 02/09/04	7.4	22	7.3	15	9.7	21
Aftershock .073g 05/02/04	6.8	18	6.7	15	9.2	11
Aftershock .217 g 10/02/04	6.5	19	5.8	16	8.1	15
6.5 M 1.3 g 12/22/03	5.0	17	4.8	16	7.2	19

West Wing Mode

North Wing Mode
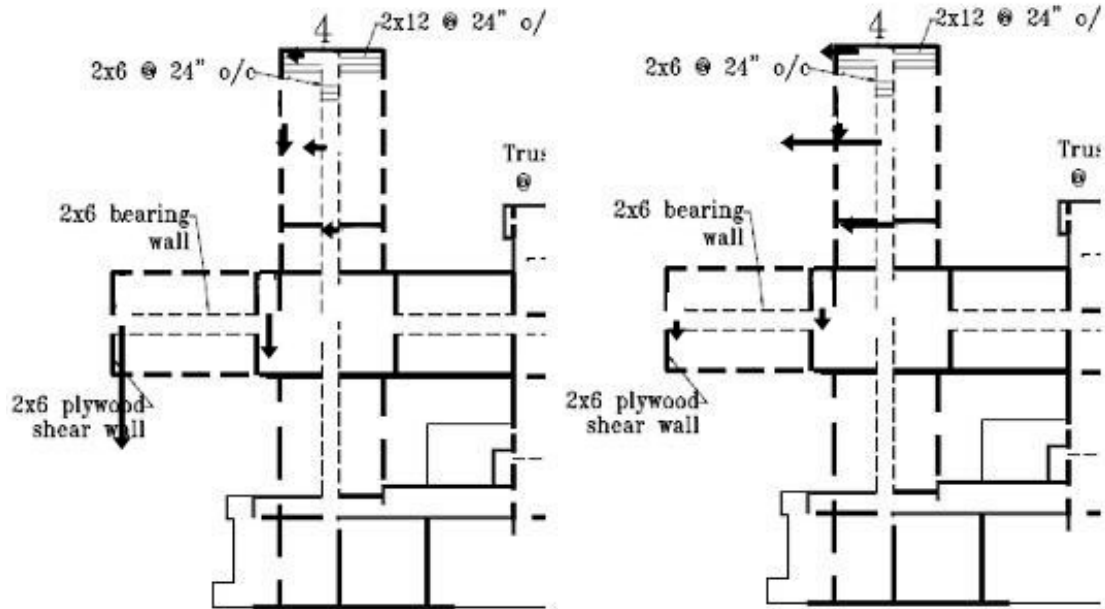
Mode 3
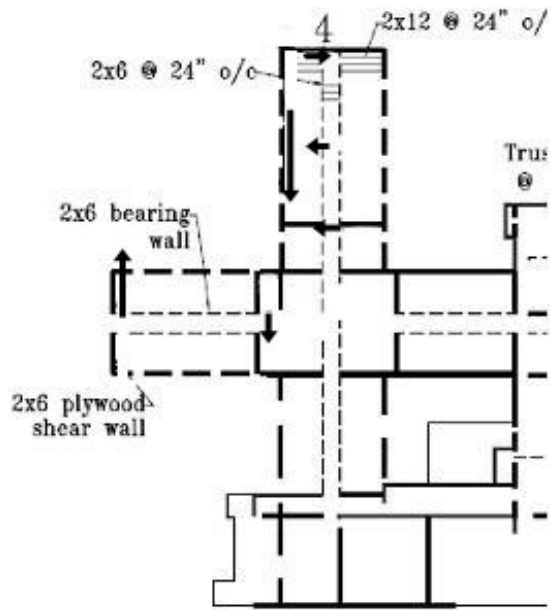
Figure 4.17: First three modeshapes of the Templeton hospital building generated from the 2003 San Simeon Earthquake.
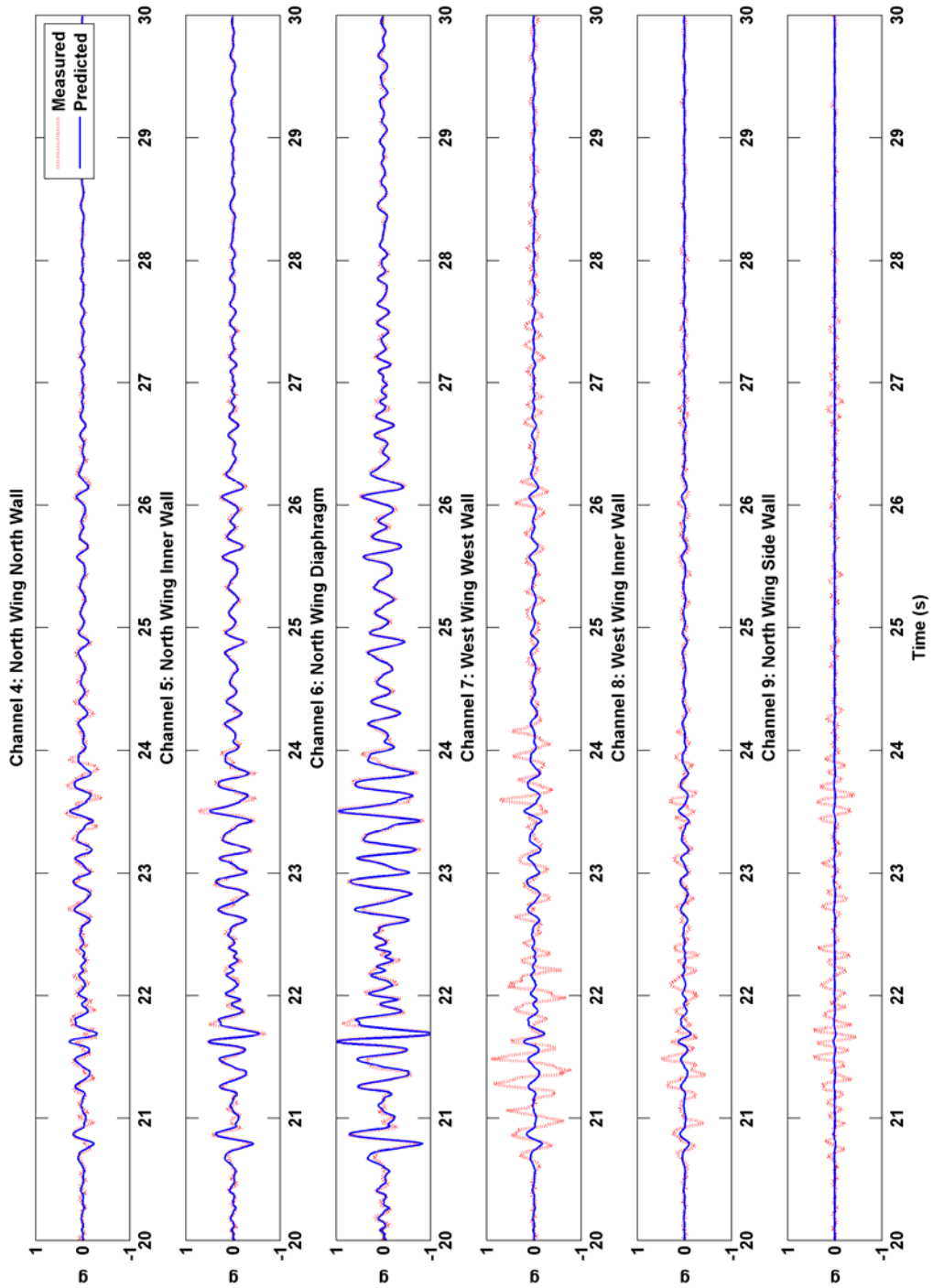
Figure 4.18: One-mode model for the 2003 Templeton hospital records.
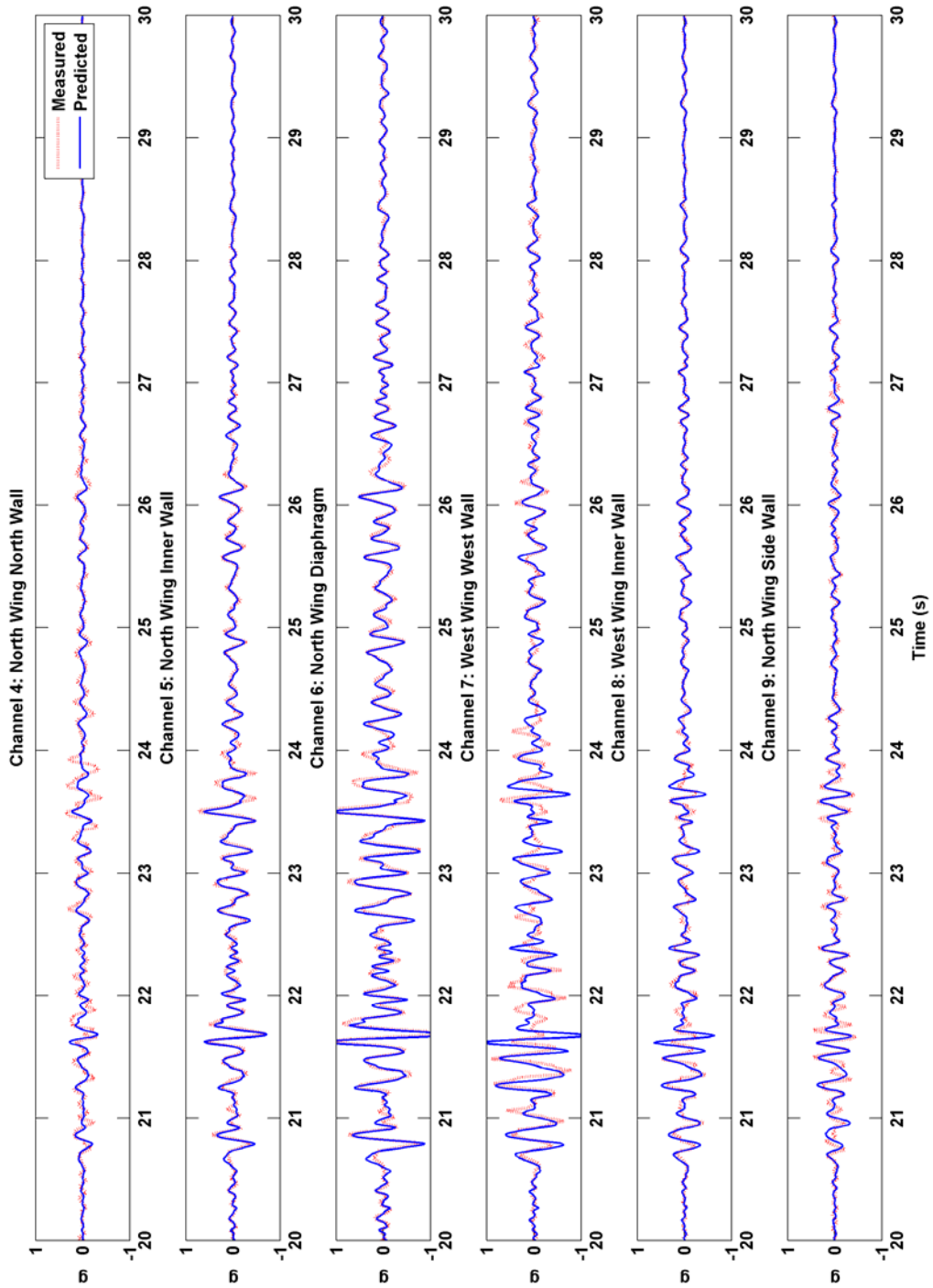
Figure 4.19: Two-mode model for the 2003 Templeton hospital records.
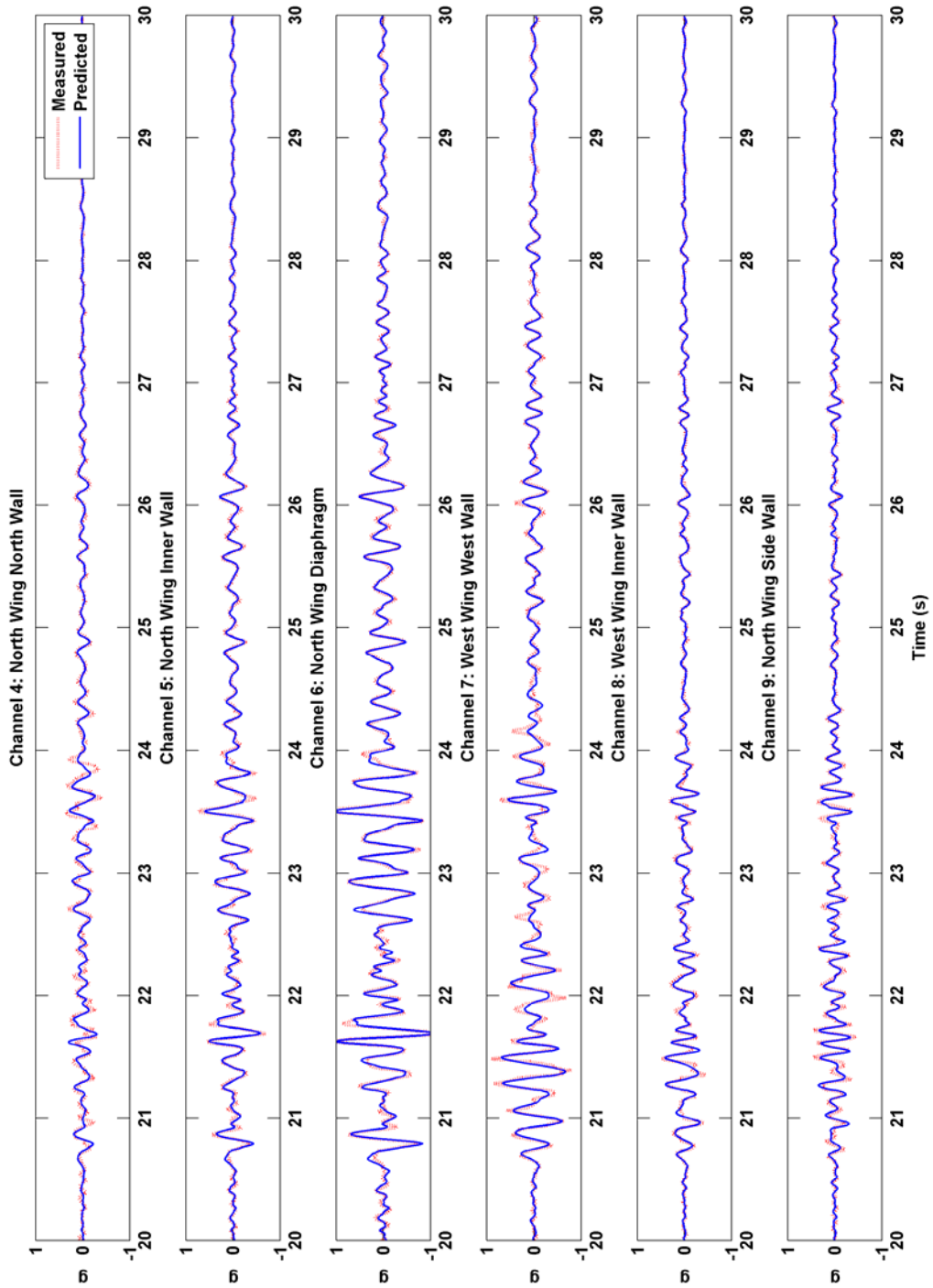
Figure 4.20: Three-mode model for the 2003 Templeton hospital records.

62

Window analysis was also performed on the Templeton hospital records. The amplitude dependence of the modal parameters is shown in Figure 4.21 through Figure 4.24. Refer to Figure 3.11 and Figure 3.12 for the acceleration time histories of the 2003 San Simeon Earthquake. The locus of frequency estimates in Figure 4.21 demonstrates the nonlinear response during the earthquake. The fundamental frequencies lost up to 50% of their initial values during the peak of the ground motion. These frequencies do return close to their initial values about 50 to 60 seconds into the record (not shown in figure).

The trend of high damping estimates at peak ground motion seen in the Parkfield school building is consistent with the Templeton hospital record (Figure 4.22). The high damping estimate is compensating for the dissipation of energy through nonlinear responses. Details of the energy dissipation are discussed in the next chapter. Figure 4.23 and Figure 4.24 show the windowed analysis for the 2004 San Simeon aftershock. Again the plots support many of the observations made in earlier sections.
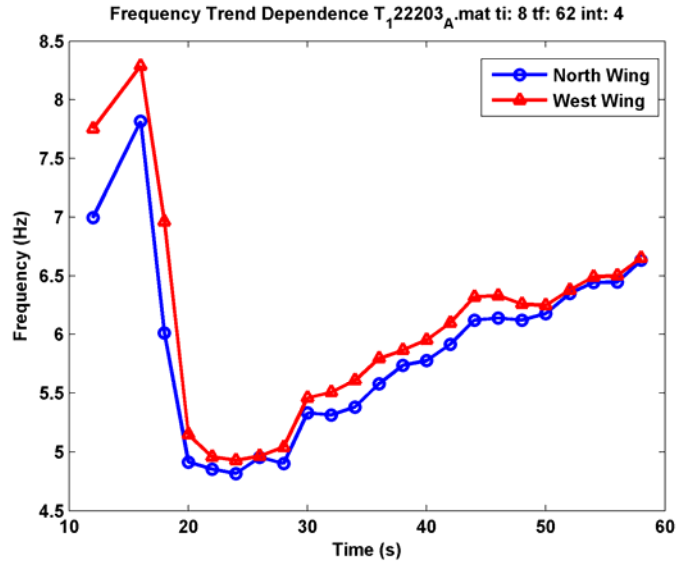
Figure 4.21: Amplitude dependence of the west wing and north wing frequency estimates for Templeton hospital building. The window analysis is performed on the 2003 San Simeon Earthquake.
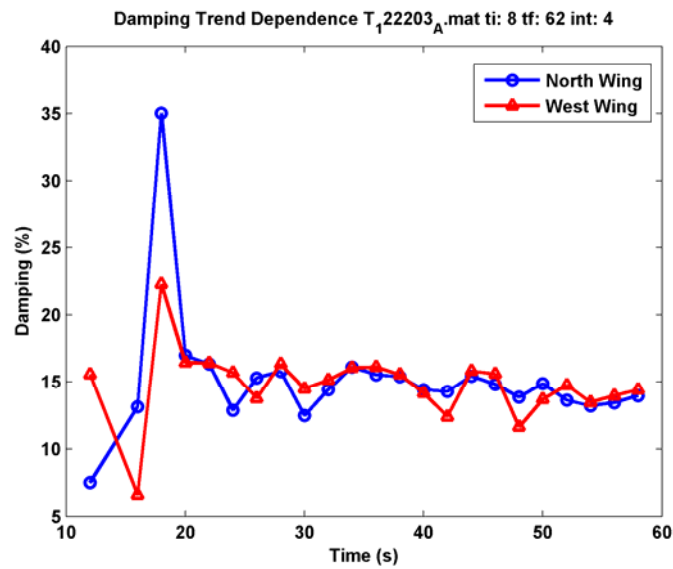
Figure 4.22: Amplitude dependence of the west wing and north wing mode damping estimates for Templeton hospital building. The window analysis is performed on the 2003 San Simeon Earthquake.

64
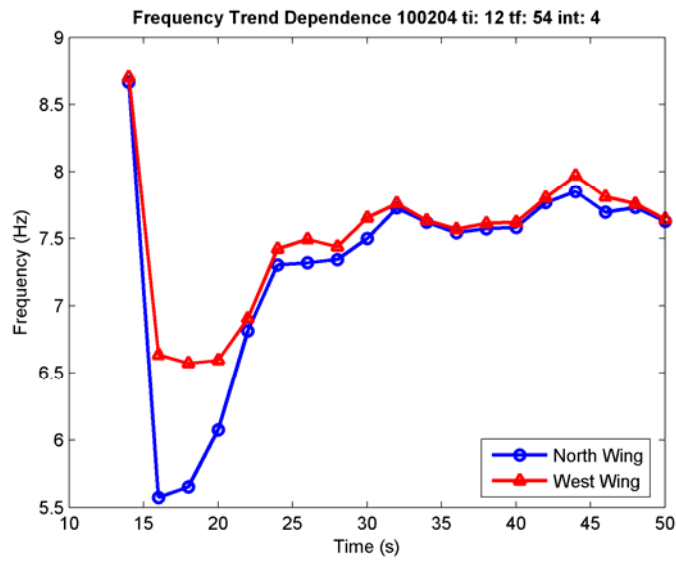
Figure 4.23: Amplitude dependence of the west wing and north wing frequency estimates for Templeton hospital building. The window analysis is performed on the 2004 San Simeon aftershock.
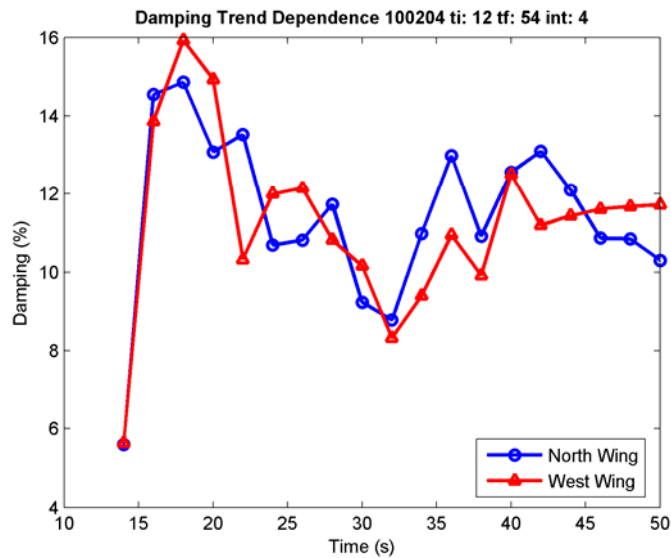
Figure 4.24: Amplitude dependence of the west wing and north wing mode damping estimates for Templeton hospital building. The window analysis is performed on the 2004 San Simeon aftershock.

65

4.4 Conclusions

Analyses of the 2004 Parkfield and 2003 San Simeon Earthquakes and some aftershocks reaffirm many of the claims of amplitude dependence of modal parameters. The 2-4 second time windows with 50% overlap offer greater insight into the progression of the estimates through time than previous studies. Predicted responses from MODE-ID greatly resembled the measured responses. The largest discrepancies are seen on measurement channels that are located on shear walls. The accelerations are smaller at these locations, and the differences are more pronounced with the magnified scale. The identified modal parameters in this chapter will be a basis in interpreting the physical behavior, primarily hysteretic responses, of the wood-frame structure in a later chapter.

CHAPTER 5

Hysteretic Characteristics in Wood-Frame Structures

One of the major characteristics of wood-frame buildings is their pinching hysteresis. In structural engineering, hysteresis refers to the path-dependence of the structure's restoring force versus deformation. The adjective *pinching* describes the shapes of hysteresis loops in wood-frame structures that appear to be pinched in the middle compared to the hysteresis loops of steel and concrete structures. The physical reasoning behind this behavior is the softening of connection joints. As loading increases in the structure and its connections become deformed, wood fibers are crushed and a nail may begin to yield. If the loading is reversed, the nail moves through the gap formed by the crushed wood fibers. Through each cycle of displacement, depending on the amplitude of the motion, the wood is increasingly indented by the nail. This creates extra spacing where the nail will displace with reduced opposing force (Judd and Fonseca 2005).

This chapter will describe a methodology to extract the hysteretic characteristics of a wood-frame structure from earthquake records. The discrepancies seen in the MODE-ID's predicted responses and the wide range of damping estimates reported in past literature will be discussed as a direct result of the presence of hysteretic response.

5.1 General Concepts

The hysteresis loops of a structure offer vital information about the forces that act upon it and the resulting deformations (Jayakumar 1987; Jayakumar and Beck 1988; Iwan and Peng 1988). It is imperative to accurately map hysteresis curves since they play a pivotal role in creating a better nonlinear model. Fortunately, many of the commercial products that provide nonlinear analyses have the option to input a hysteresis model. The hysteretic behavior of a structure plays a crucial role in many current approaches to seismic performance-based analysis and design. As a result, many experiments have been conducted to record hysteretic data for wood shear walls and other subassemblies. An example illustrating the pinching behavior is shown in Figure 5.1. Although this test was for a single-nail connection, similar behavior is observed for wall and diaphragm components and also for entire structures.
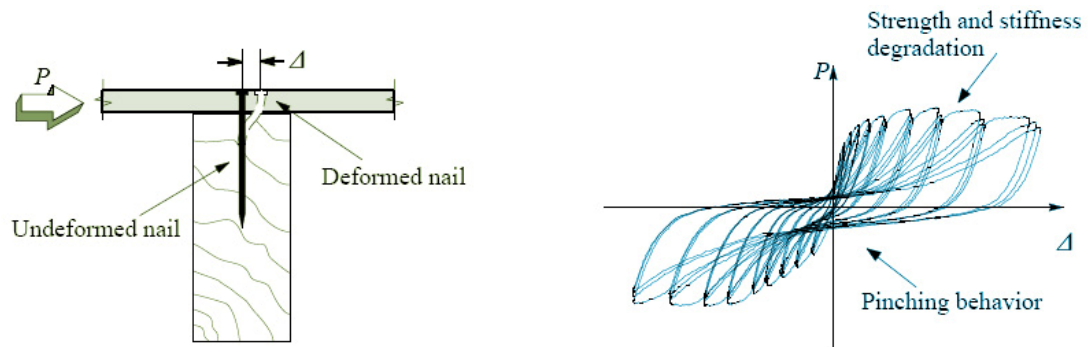
Figure 5.1: Illustration of the nailed sheathing connection and pinching hysteresis curve (Judd 2005).

Extraction of hysteretic characteristics of wood-frame building components can lead to an understanding of the structure's degradation and nonlinear response range. The process involves the construction of a hysteresis curve by plotting time history pairs of restoring force across the component (on the vertical axis), and relative displacement across the component (on the horizontal axis).

Hysteretic behavior has been observed and studied extensively in wooden shear walls. Fischer et al. (2001) conducted a full-scale test structure laboratory experiment and used a nonlinear dynamic time history analysis program RUAUMOKO (Carr 1998) and wood shearwalls program CASHEW (Folz and Filiatrault 2000) to create numerical models. Many hysteresis models have been developed to predict the seismic response of wood-frame structures. Some hysteretic models have produced relatively good results, but the data collected have usually been supported by displacement histories. Records from an instrumented site, such as California's strong motion stations, only have acceleration time histories. Extraction of hysteresis parameters becomes more challenging in the absence of displacement time histories.

5.2 Extraction Process

In theory, velocity and displacement time histories can be obtained directly from an acceleration time history by numerical integration (Iwan, Moser and Peng 1984). It is generally assumed that the calculated velocity and displacement time histories that come with the processed acceleration records contain identical information through numerical integration. However, in processing ground motion histories, additional corrections are

applied to the integrated records which are not reflected in the acceleration histories (Malhotra 2001). It is important to identify these changes if the provided displacement histories are used, as it can alter the results of the hysteresis loops.

After obtaining displacement records, the relative displacement time histories can be calculated by taking the difference between a pair of measurement locations. The relative displacement can be plotted with the restoring force to formulate a hysteresis loop. The restoring force time history can be obtained by scaling the acceleration record with a value representing mass. If the objective is to study the shape of the hysteresis loop, it is not imperative that the exact mass value is used. However, this means that the restoring forces are only as accurate as the mass estimate used. Also, this calculated restoring force is only all-inclusive if the point of interest does not experience other loads. Therefore, it is necessary to construct free body diagrams to correctly attribute all forces.

5.2.1 Free Body Diagrams

Consider the simple structure shown in Figure 5.2a as an example, consisting of north, south, east and west walls (N, S, E and W) and a diaphragm (D) with earthquake acceleration records obtained at locations *a*, *b* and *c* in the N-S direction. We wish to plot the hysteretic curve for the east wall. To obtain the restoring (shear) force time history, a free-body diagram (FBD) is needed as shown in Figure 5.2b. The east wall is cut at mid-height and the diaphragm at mid-span as shown, with the cuts extending through the north and south walls. In the N-S direction, the restoring force at the diaphragm cut is set to zero based on an assumption of symmetric response, and the forces on the north and south walls

are taken as zero because they would be out of plane, leaving only the restoring force F_E on the east wall. The N-S equation of motion is shown in Equation 5-1:

$$F_E(t) = m_a \ddot{x}_a + m_c \ddot{x}_c \qquad (5\text{-}1)$$

where m_a and m_c are tributary masses for the free body at a and c and $\ddot{x}_a$ and $\ddot{x}_c$ are the recorded accelerations at a and c, giving $F_E(t)$ directly. The relative displacement $x_{a\text{-}b}(t)$ across the north wall is obtained by subtracting the doubly integrated acceleration records at a and b. Pairs of $F_E(t)$ and $x_{a\text{-}b}(t)$ are then plotted.

The situation for the diaphragm is different because the shear force varies substantially along the diaphragm, with the maxima at the ends. The procedure employed here extracts the restoring (shear) force $F_D(t)$ at the quarter point and uses a free body consisting of one quarter of the diaphragm and adjacent pieces of the north and south walls cut at mid-height, as shown in Figure 5.2c. With similar assumptions as those made previously, only $F_D(t)$ is present and is determined from Equation 5-2:

$$F_D(t) = m_c \ddot{x}_c \qquad (5\text{-}2)$$

The relative displacement in this case is $x_{c\text{-}a}(t)$, obtained by subtracting the doubly integrated acceleration records at c and a.

71

a)

b)

c)
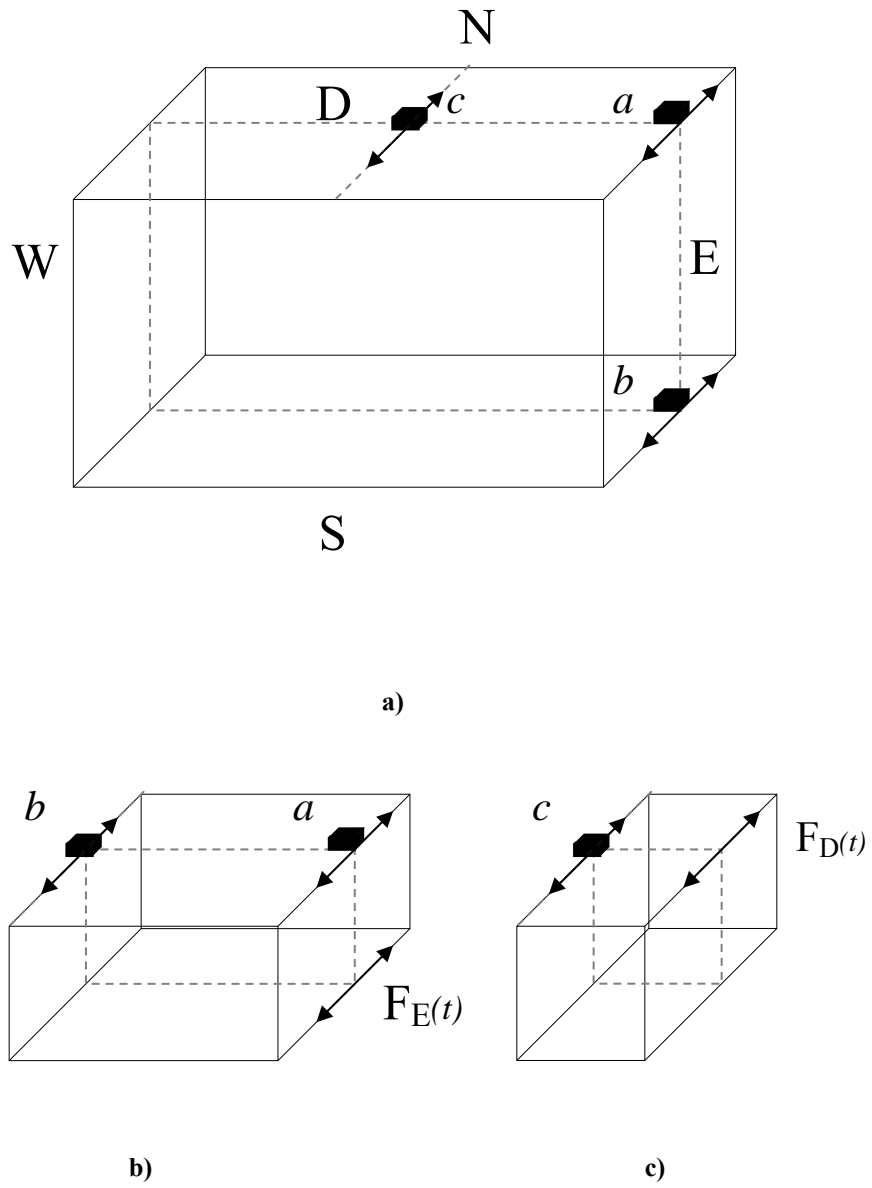
Figure 5.2: Illustrative example of the free body diagram concept to calculate a hystersis curve.

72

Using the free body concept described in the previous section, attempts are made to retrieve the hysteretic characteristics of the Parkfield school building. Results are shown in Figure 5.3 (east wall), Figure 5.4 (diaphragm), Figure 5.5 (south wall), and Figure 5.6 (only the shear wall portion of south wall). For example, calculations performed for the hysteresis curve in Figure 5.3 are based on Equation 5-1, with the east wall in Figure 5.2a representing the east wall of the Parkfield school. Channels *a*, *b* and *c* in Figure 5.2 represent channels 1, 3 and 2, respectively (see Figure 3.5). Since the ground motion is assumed to be uniform, it does not matter that channel 3 is not located directly under the Parkfield school's east wall. For the masses m_c and m_a in Equation 5-1, artificial values in the ratio of 1.3 to 1.0 are employed. The use of artificial values means that the force scale in Figure 5.3 is meaningless, but the overall shape of the hysteresis curve is not affected, since it depends only on the ratio of m_c to m_a.

The computed hysteresis curves (doubly integrated from acceleration time histories without any processing) in Figure 5.3 and Figure 5.4 show evidence of pinching in the larger excursions, but not nearly as pronounced as that in Figure 5.1, which was obtained from a controlled laboratory experiment. Results for the south wall in Figure 5.5 can be described similarly. Figure 5.6 may need some baseline correction and filtering of the displacement histories to remove long-period errors (Boore 2005).
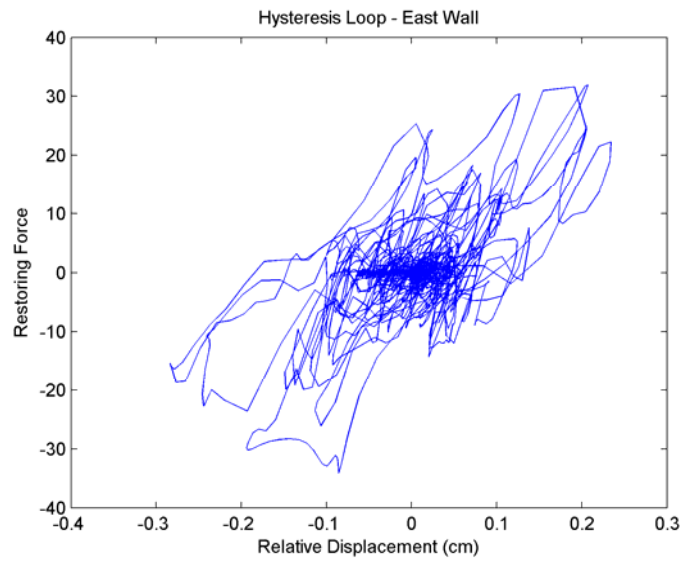
Figure 5.3: Hysteresis curves of the east wall.
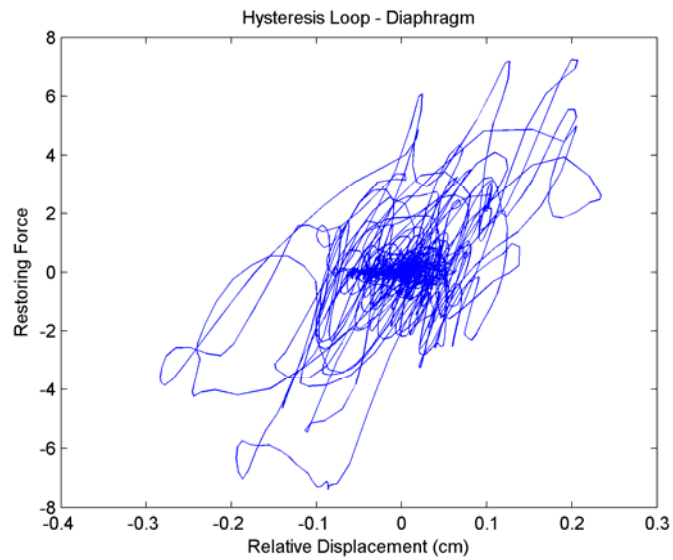
Figure 5.4: Hysteresis curves of the diaphragm.

74
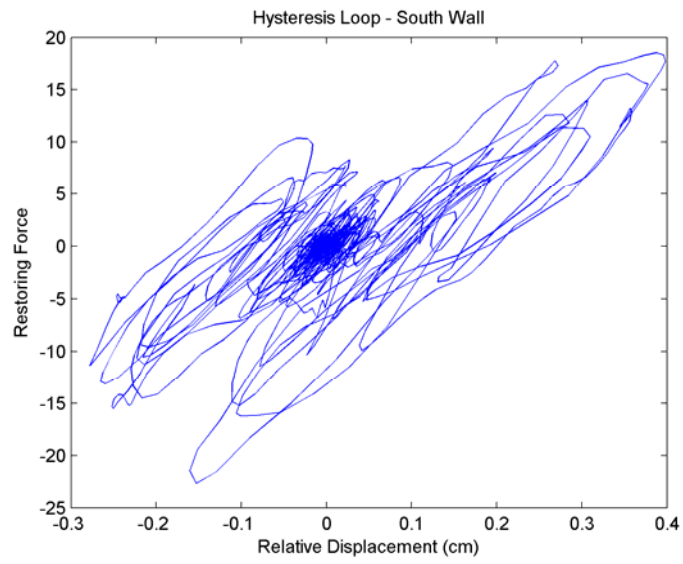
Figure 5.5: Hysteresis curves of the south wall.
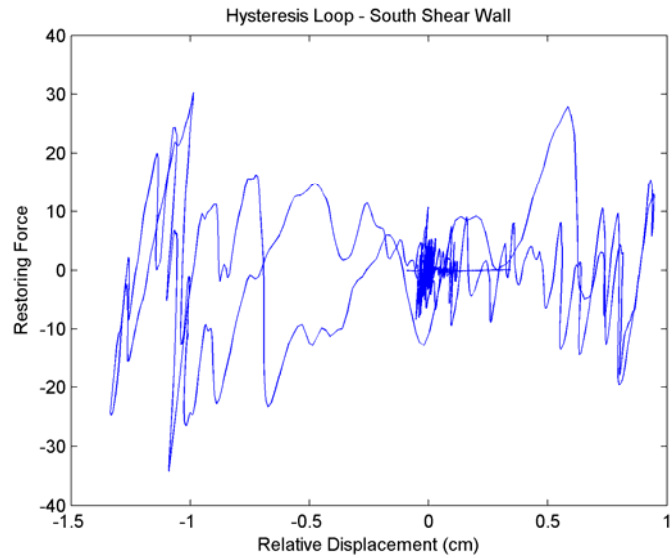
Figure 5.6: Hysteresis curves of the south shear wall.

75

Compared to hysteresis curves from measured displacement records, the double-integrated hysteresis loops seem chaotic in nature and less meaningful. Laboratory-generated hysteresis loops have experimental setups installed with various sensors. It is evident that obtaining these hysteresis curves would be the most ideal (Graves 2004). When sufficient instrumentation is not available, the practice of the double-integrated acceleration record becomes necessary. The application has served in various capacities such as nonlinear system identification of structures (Cifuentes and Iwan 1989), system identification of degrading structures (Iwan and Cifuentes 1986), and identification for hysteretic structures (Peng and Iwan 1992). However, all of its applications have either been involved with steel or concrete buildings (Cifuentes 1984), integrated from simulated response records from hysteretic models (Peng 1987), or supported by measured displacement time histories. In its application to steel and concrete structures, hysteresis curves are relatively well behaved. As shown in Figure 5.7, the hysteresis loops are slanted in an evident slope. Elastic responses are depicted through the dense slanted lines through the origin. The rotation and expansion of the curves with respect to the origin signify the stiffness reduction and degradation of the structure. This can be a result of yielding, cracking or other forms of failure in structural members (Cifuentes 1984).
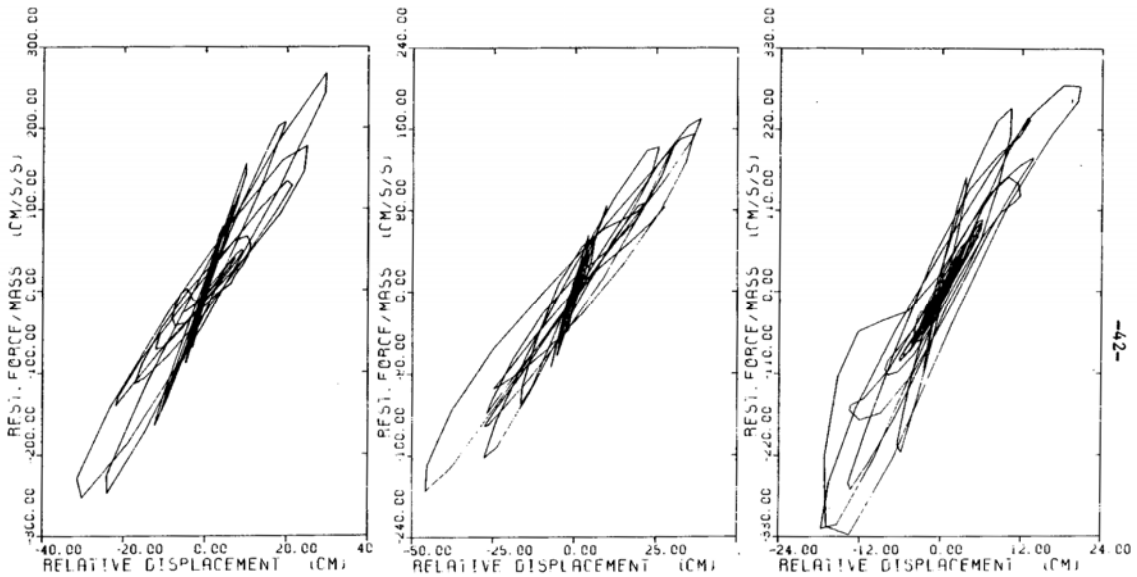
Figure 5.7: Corrected hysteresis curves of non wood-frame structures (Cifuentes 1984).

The same observations cannot be drawn for wood-frame structures. The pinching hysteresis alters the generally elliptical hysteresis loops. With the addition of the high dissipation of energy inherent in wood-frame structures, the area inside the curve fluctuates greatly. Stiffness reduction, unlike steel and concrete buildings, is more apparent in wood-frame structures due to the crushing of wood fibers and may not have a direct correlation to significant structural damages. Therefore, it is important to investigate the applicability of double integrating acceleration records from wood-frame structures, where the pinching hysteresis and high dissipation of energy must be captured. A lot of the complications in accurately mapping a hysteresis curve stem from the lack of measured displacement records. Double-integration errors may be more significant in wood-frame structures.

77

5.2.2 Double-Integration Errors

The effects of double-integration errors are widely studied in the strong motion instrumentation community. Subtle effects such as tilting or random noise in measurements can cause long period drifts in the recorded time history (Graizer 1979; Trifunac and Lee 1973). The magnitude of these effects is debatable, as some question the robustness of correction schemes. While some claim to successfully calibrate for the displacement errors (Thong et al. 2004) and apply the double-integrated acceleration for soil-structure interaction analysis (Yang, Li and Lin 2006), others adamantly believe these errors are unacceptable when the purpose of the measurement is to verify the integrity of engineering structures (Ribeiro, Freire and Castro 1997).

The correction schemes come in a variety of forms. The most typical approach to resolve the long period response is to apply a baseline correction. The adjustment can take the form of a polynomial (Graizer 1979), leveling out the displacement time history, and bandpass filtering (Trifunac and Lee 1973). However, another problem arises -- it eliminates any permanent displacement and simultaneously reduces the magnitude of the dynamic displacement (Iwan, Moser and Peng 1984). To preserve some of these displacement characteristics, a segmented polynomial baseline fit applied to the raw velocity is proposed (Iwan, Moser and Peng 1985). Since the ground velocity physically begins and ends at zero, the polynomial fit applies these constraints to the initial and final segment of the raw velocity. Integrating and differentiating the corrected velocity time history yields the adjusted displacement and acceleration time history (Wang 1996).

The resulting ground motions from the methods previously mentioned are heavily dependent on the choice of processing parameters. Without any independent constraints, these processing techniques are non-unique (Graves 2004), leaving much room for improvement. Suggestions for better techniques include tailoring procedures based on the specific instrumentation used (Chen 1995), using six-component recording measurements (three linear and three rotational) to eliminate drifts from tilting of sensors (Graizer 2005), and employing geodetic measurements of residual displacement to constrain the processing of the recorded motions (Clinton and Heaton 2004). Other measures are taken at a broader level, such as replacing older analog instruments with digital sensors (Boore 2005) or exploring a strong-motion velocity meter over the current strong-motion accelerometer network (Clinton and Heaton 2002).

Given the variety of methods mentioned above, several improvements are made for the hysteresis loops calculated earlier. Prior to any processing, the integrated time histories from CSMIP are nearly identical to self-integrated acceleration records. Figure 5.8 through Figure 5.11 show the changes in hysteresis loops by using processed records. In each figure, the left hysteresis loop is calculated without any processing. The middle hysteresis loop, labeled as Processed 1, uses baseline correction and minimum phase filtering (i.e. butterworth). The right hysteresis loop, labeled as Processed 2, is same as Processed 1 but uses zero-phase filtering. Zero-phase filtering can be accomplished by passing the record through the same minimum phase filter for the second time, but the record is first reversed in the time domain. Reversing the record again achieves zero-phase filtering on the record. The improvements are apparent in comparison to hysteresis curves using Processed 1. This

demonstrates that processing hysteresis curves are very susceptible to phase delays in filtering. Simple bandpass filtering as suggested by Cifuentes (1984) is not sufficient -- the zero-phase filtered hysteresis curves provide much better results.
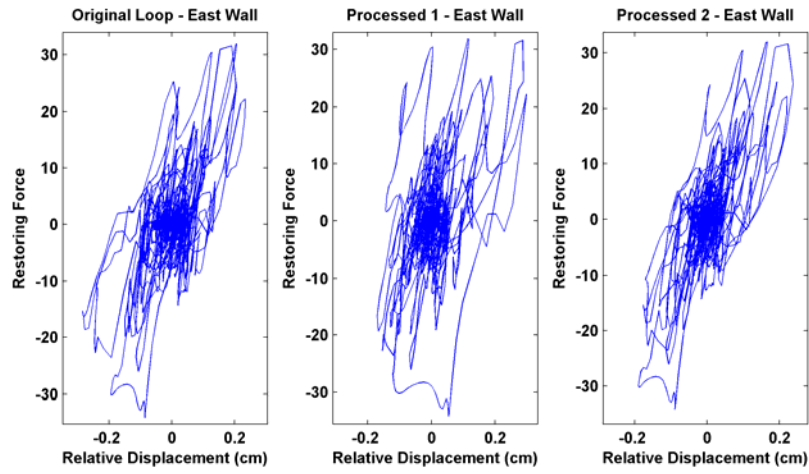
Figure 5.8: Comparison of the pre- and post-processed hysteresis curves from the east wall.
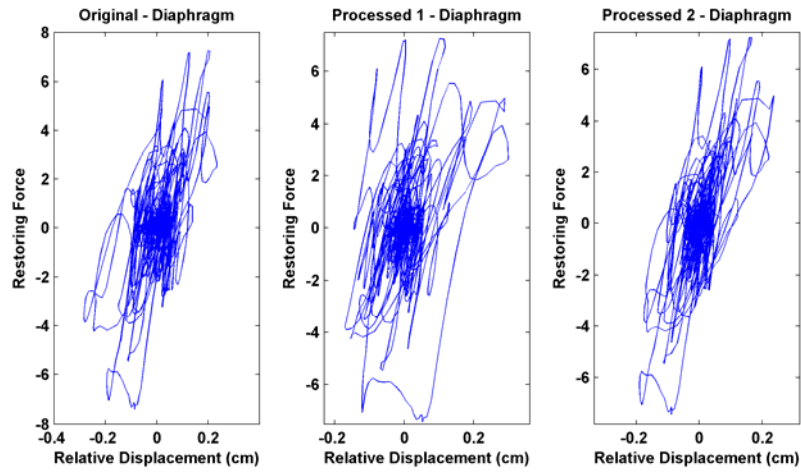
Figure 5.9: Comparison of the pre- and post-processed hysteresis curves from the diaphragm.
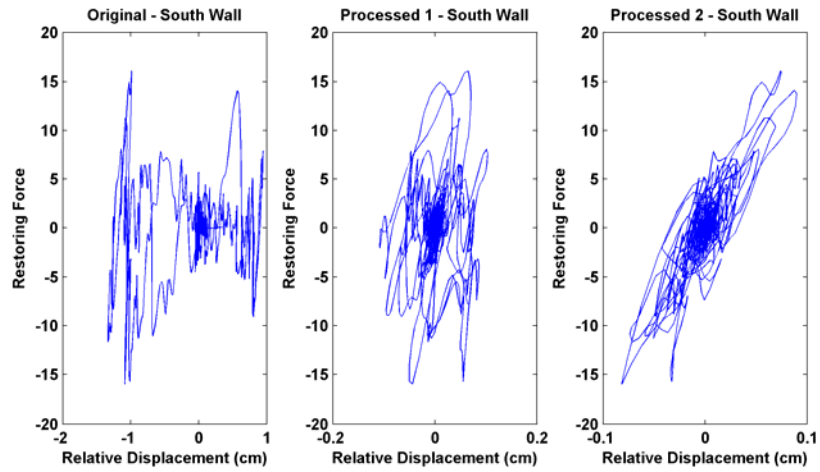
Figure 5.10: Comparison of the pre- and post-processed hysteresis curves from the south wall.
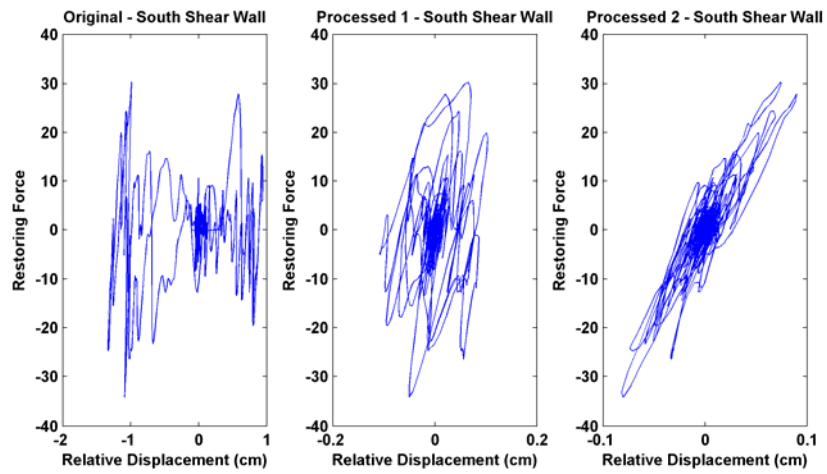
Figure 5.11: Comparison of the pre- and post-processed hysteresis curves from the south shear wall.

81

The drifts in Figure 5.8 and Figure 5.9 are eliminated and there are signs of slight pinching in each hysteresis loop. Figure 5.10 and Figure 5.11 received the most improvement and suggest mostly linear behavior with slight degradation in stiffness. The use of filters eliminated some of the non-physical behaviors but also tampered with the magnitude of drifts that dictate the shape of the loop. It is hard to verify if some of the pre-processed relative displacement time histories are reasonable. Baseline-fitting corrections are independent for each channel and may complicate the validity of relative displacement time histories. Despite these drawbacks, the extraction of the hysteresis loops have greatly benefitted from the processing. However, an ideal extraction is limited by the instrumentation on site during the event. Therefore, in order to further explore the applicability of double-integrated acceleration in wood-frame structures, the process should first be performed in controlled settings.

5.3 CUREE Task 1.1.1: Shake Table Test - USCD

The shake table tests at UCSD are well instrumented with accelerometers and displacement sensors. Since the tests are performed in a controlled setting, the data recorded are suited for testing the extraction of hysteresis loops through double-integrated accelerations. Figure 5.12 through Figure 5.16 compare hysteresis loops using measured displacements (left) and double-integrated acceleration (right) with different seismic levels. The extracted hysteresis curves from acceleration time histories are good representations of the hysteretic behavior of the structure at all seismic levels. Minor discrepancies are seen on the outskirts of the hysteresis loops at higher seismic levels.
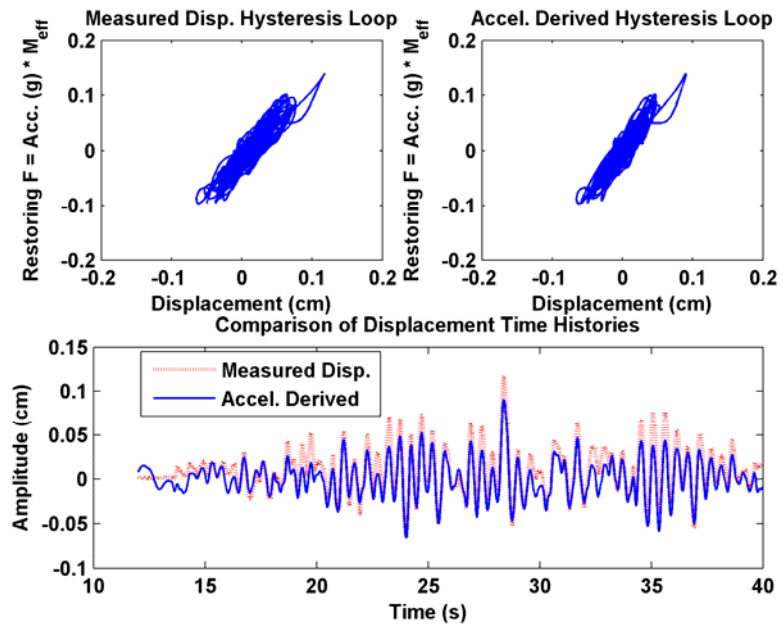
Figure 5.12: Comparison between hysteresis loops derived from measured displacements and double-integrated accelerations. Seismic Level 1 (5% g).
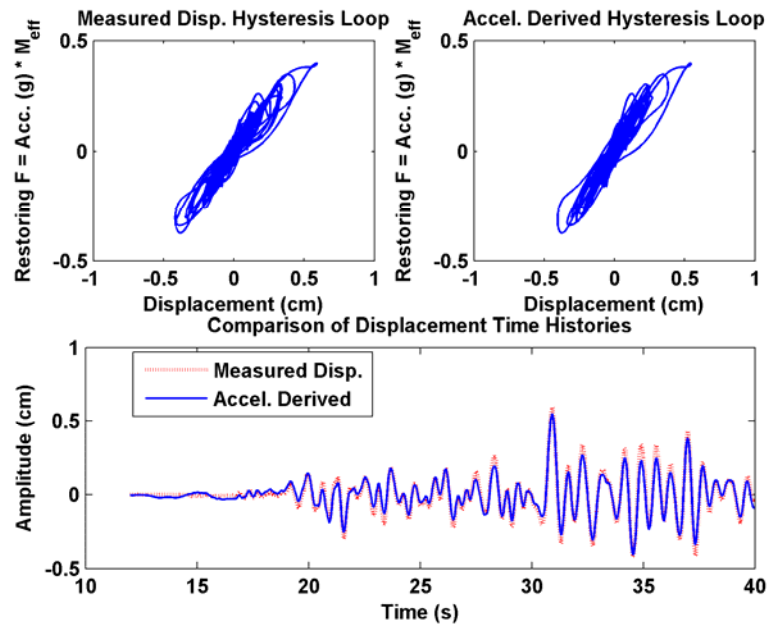
Figure 5.13: Comparison between hysteresis loops derived from measured displacements and double-integrated accelerations. Seismic Level 2 (20% g).
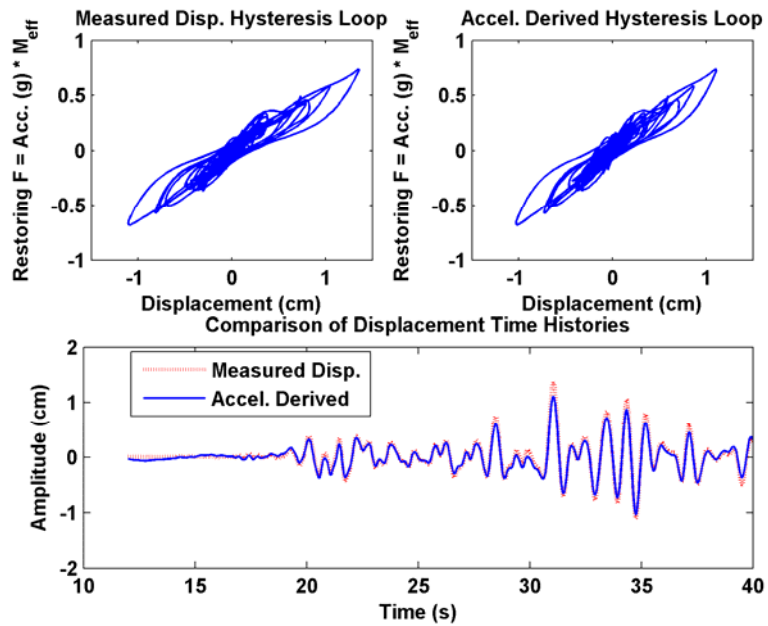
Figure 5.14: Comparison between hysteresis loops derived from measured displacements and double-integrated accelerations. Seismic Level 3 (50% g).
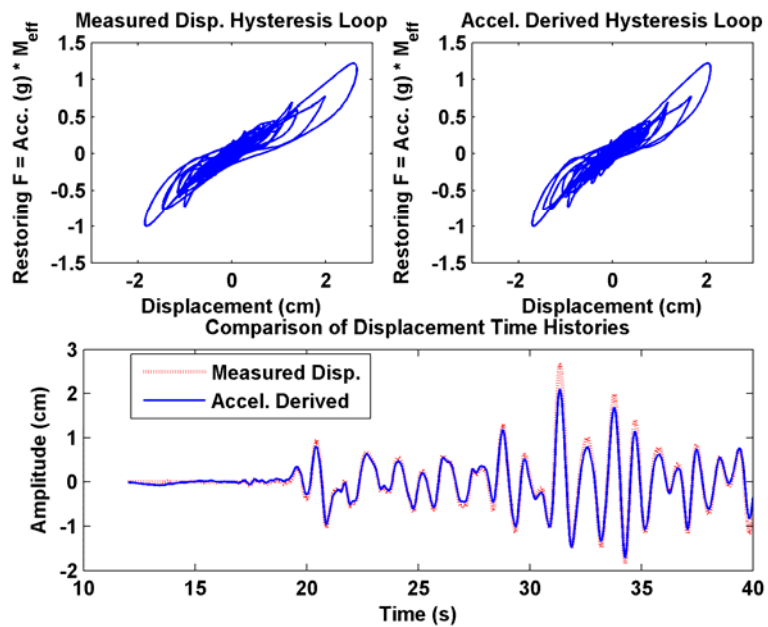
Figure 5.15: Comparison between hysteresis loops derived from measured displacements and double-integrated accelerations. Seismic Level 4 (80% g).

84
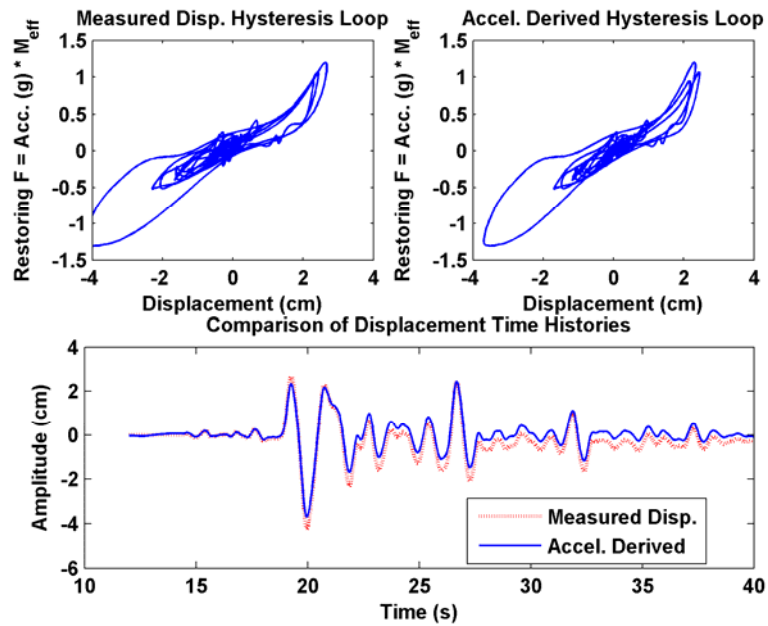
Figure 5.16: Comparison between hysteresis loops derived from measured displacements and double-integrated accelerations. Seismic Level 5 (100% g).

Regardless of these differences, the pinching behavior of the hysteresis loop is clearly represented and captured.

It is interesting that there is such a dramatic difference between hysteretic curves from experimentally obtained data and field records despite applications of the same extraction method. The two records share several common factors: use of a wood-frame structure, same building construction, recording with digitized accelerometers, and similar magnitude of earthquake loading. However, one important note about the experimental test is that the shake table is driven by a uniaxial seismic system. As a result, the building is subjected to forces from a single direction of loading. Unlike in a real earthquake scenario with multi-directional and rotational ground motions, loads perpendicular to the sensors

85

can cause rotations and tilts that can contaminate the integration process. The ramifications are well described in Graizer (2005).

The contamination is further magnified through the nonlinear behavior of the diaphragm. The multi-directional ground motions can cause nonlinear shearing and therefore introduce forces on the walls that cannot be accurately captured by an uniaxial accelerometer. More importantly, all the behaviors are hysteretic, complicating the extraction process when limited measurements are available.

5.4 Damping

Damping values have always been hard to estimate, the difficulty being that there is no instrument to measure the amount of energy being dissipated. Estimates must be inferred from response data in time or frequency domains. Oftentimes, a linear viscous damping model such as in MODE-ID is assumed for its simplicity and convenience in analysis. This assumption presents two recurring issues in its application to wood-frame buildings:

1) Damping estimates are reported to be much higher than that of steel and concrete structures. Although it is believed that wood-frame buildings dissipate more energy through the friction of joints, it is hard to justify the damping values being several-folds higher.

2) Damping estimates are reported over a wide range of 5% - 20% in wood-frame buildings. These large differences seen among different modal identification

methods and sources of data (seismic response records in the field and dynamic tests in the laboratory) raise questions as to the validity of the reported values.

5.4.1 Compensation for Hysteretic Damping

Many physical systems dissipate energy differently to from viscous damping. Although linear viscous damping is inherent in materials, it may or may not play a significant role in the overall energy dissipation. In wood-frame structures, friction between joints, heat generated from crushing of wood fibers, and nonlinear hysteretic behaviors of structural components, all play an additional role in dissipating energy. It is expected that a linear viscous damping model would have to compensate for these other forms of damping.

Evidence for this compensation can be inferred from both the time and frequency domains. In Chapter 4 it was clear from the windowed analyses that there is a strong amplitude dependence for fundamental frequencies and damping estimates. The variations of the modal parameters in time-segmented records demonstrate the presence of some nonlinear hysteretic response. However, if the analysis is done on a full record, these time-invariant modal parameters, shown in Table 4-1 and Table 4-3, encompass the nonlinearity into single modal parameters that best represent the response.

Another representation can be seen in the frequency domain through the Fourier transform (Brigham 1988; Chopra 2001). Figure 5.17 and Figure 5.18 are the frequency spectrums of the structure with the rigid body motions removed. Losing all time representation, the spectrum shows the signal predominantly in the range of 5 Hz to 8 Hz.

Given the results and conclusions in Chapter 4, we know this multi-peaked frequency band is a result of the shifting of the fundamental frequencies during the seismic ground motion. If a two-mode linear model is meant to characterize this response, the bandwidths of fundamental frequencies must cover the range of 5 Hz to 8 Hz. The nonlinear response inevitably broadens each of the model's resonant peaks. A rough estimate of the damping values can be obtained by the half-power bandwidth (Paz 1997). Estimates can be seen in the 15-20% due to the broadening of the spectrum.

The discussion thus far has been reliant on MODE-ID's time-segmented results that demonstrate the amplitude dependence of modal parameters. The same observations can be made by utilizing other time-frequency representations. A short-time Fourier transform (STFT) can be used to display the frequency content of the signal as it changes over time. The transformation is identical to that of Fourier transform, but a windowing function which slides along the time axis allows for a two-dimensional representation of the signal. Figure 5.19 shows the results of a STFT. A 4-second window is applied to all measurement channels obtained from the Parkfield school building. Each column represents a measurement channel with the changes of the frequency spectrum through time. Starting from the 20-second time interval to the end of record, the vertical axis is adjusted to show the smaller amplitude spectrum. At the first time interval, most of the frequency content is concentrated in the 8 Hz range. During the 4 to 12 second period, which is also when the largest ground motions occur, the spectrum broadens to as low as 5 Hz. The broader spectrum also reaffirms the higher damping estimate seen in the peak of the ground motion.

One drawback of the STFT is the tradeoff between time and frequency resolution. Other time-frequency representations of non-stationary signals such as wavelet transforms (Kijewski and Kareem 2003) and Wigner-Ville (W-V) Distribution (Bradford 2006) are alternatives that yield better temporal and frequency resolutions. Figure 5.20 and Figure 5.21 are W-V spectrums of the Parkfield records. In each figure, the top spectrum is the W-V distribution for the entire record. The bottom spectrum is the W-V distribution with normalized time-segmented records. The reason for the additional time segmentation is that the W-V distribution of the full record is dominated by the largest transient signal in the

ground motion. The analysis will only offer better resolution for the 5 to 10 second period. By applying the W-V distribution in various time segments, the changes in the fundamental frequencies can be better seen. The W-V spectrum has drawbacks such as the introduction of artifacts and negative values (Bradford 2006). Despite these shortcomings, the amplitude dependence of the fundamental frequencies is reaffirmed.
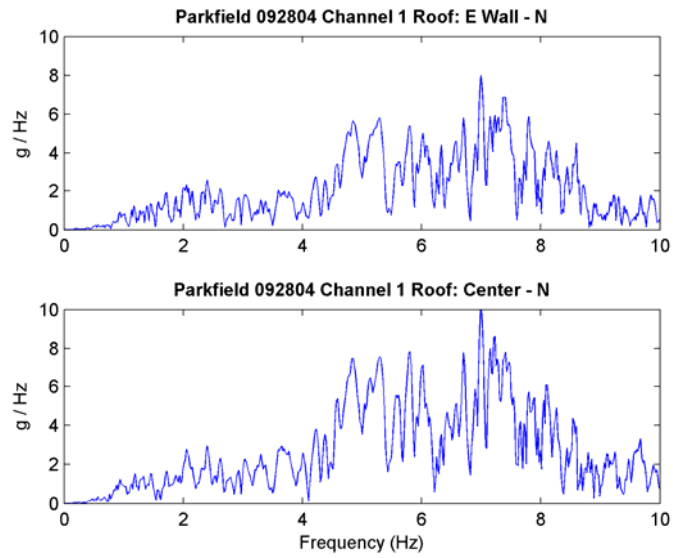
Figure 5.17: Fourier transform of the acceleration time histories from the east wall and diaphragm.
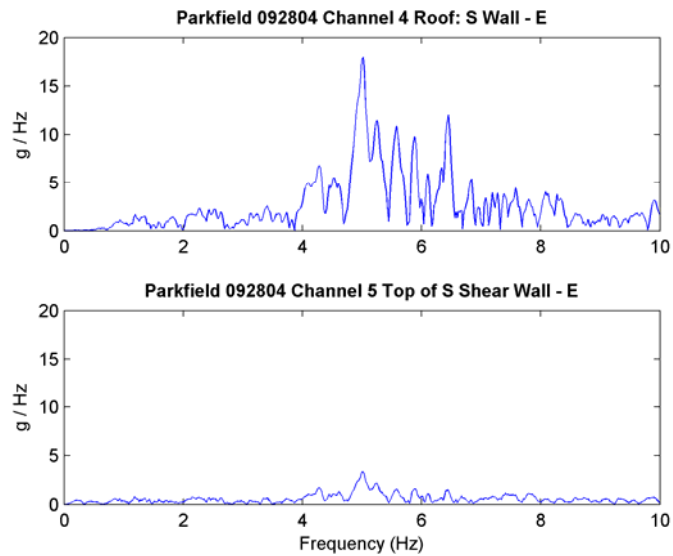
Figure 5.18: Fourier transform of the acceleration time histories from the south wall and south shear wall.
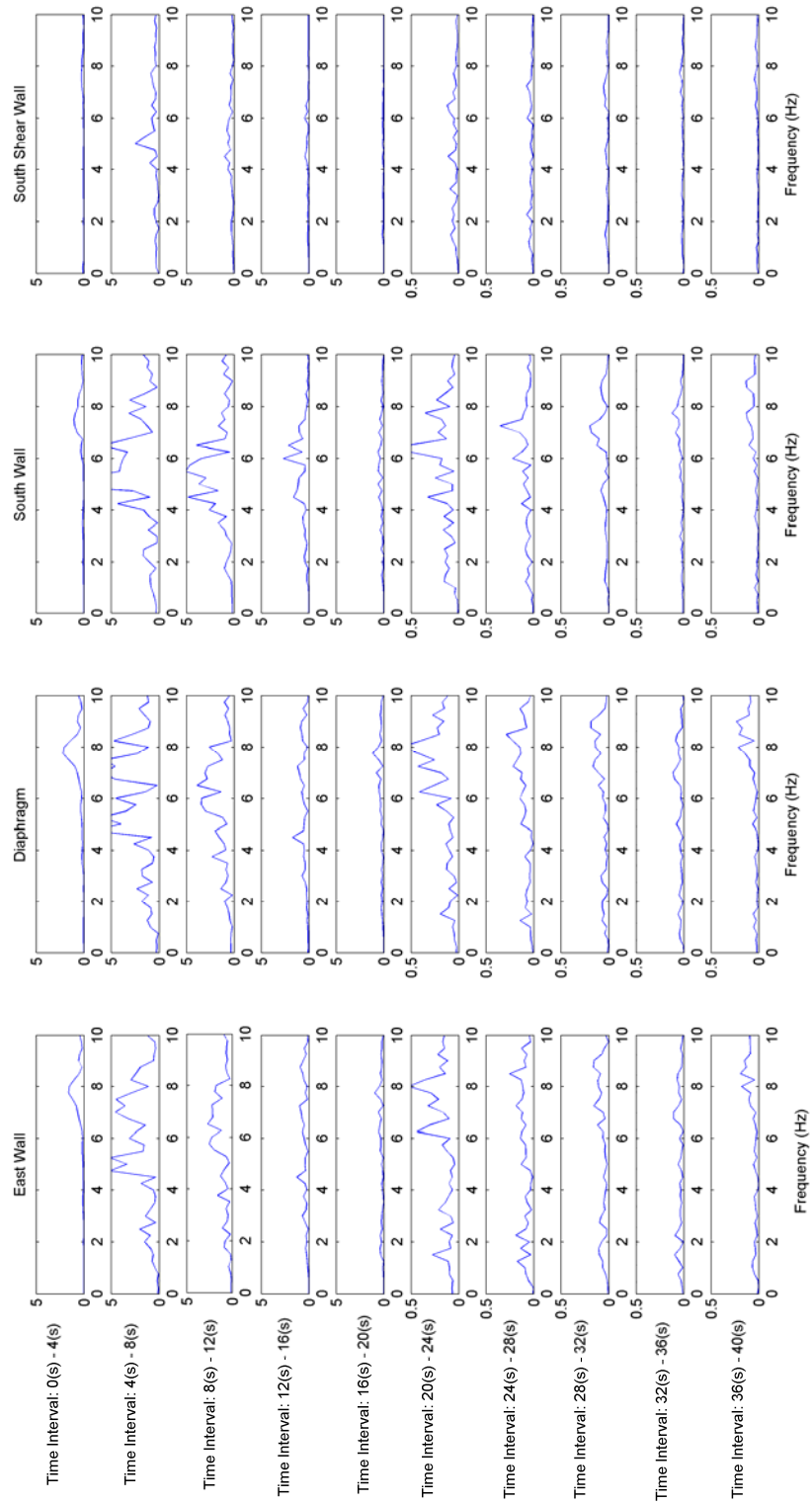
Figure 5.19: STFT of the Parkfield school building with 4 second time intervals.
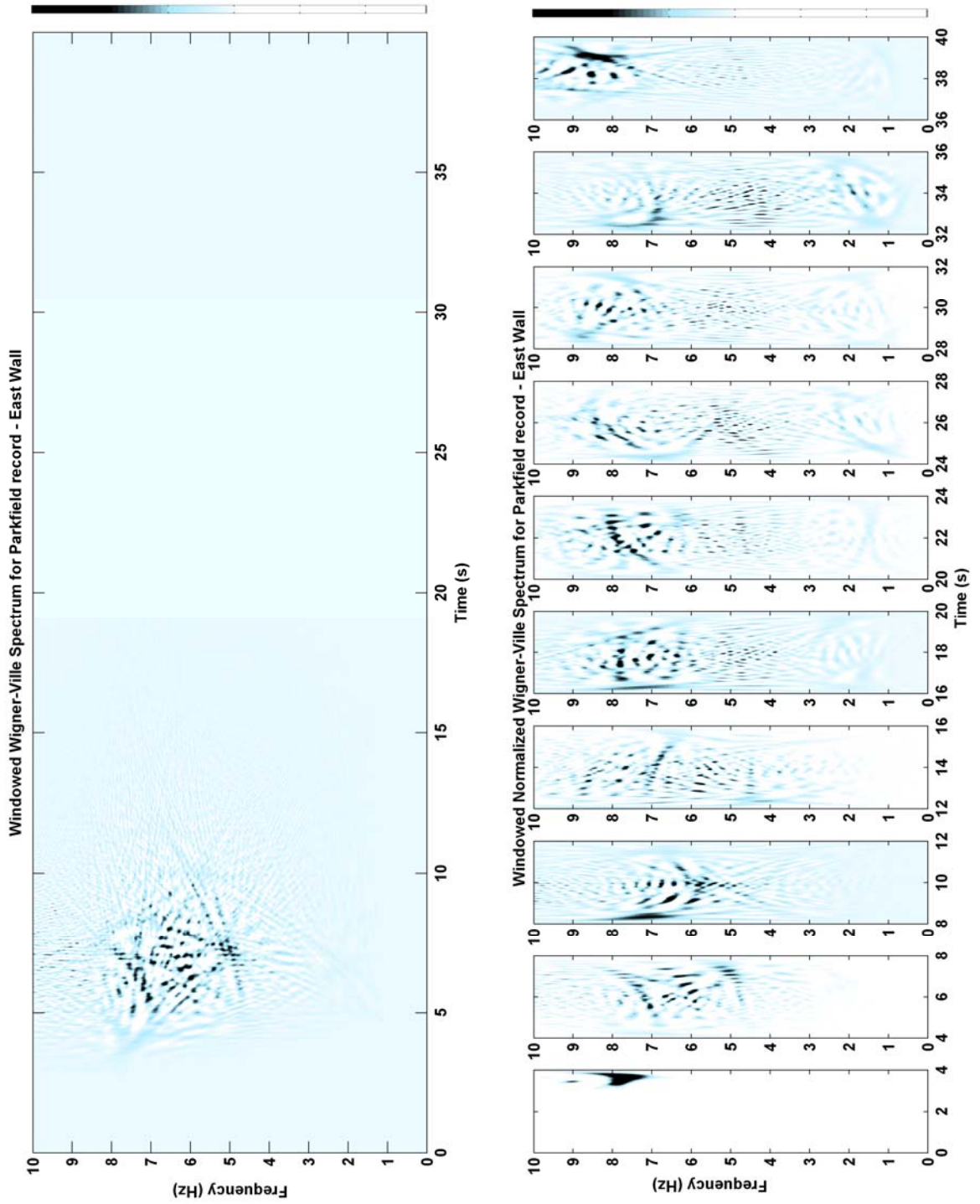
Figure 5.20: Wigner-Ville spectrums of the east wall.

93
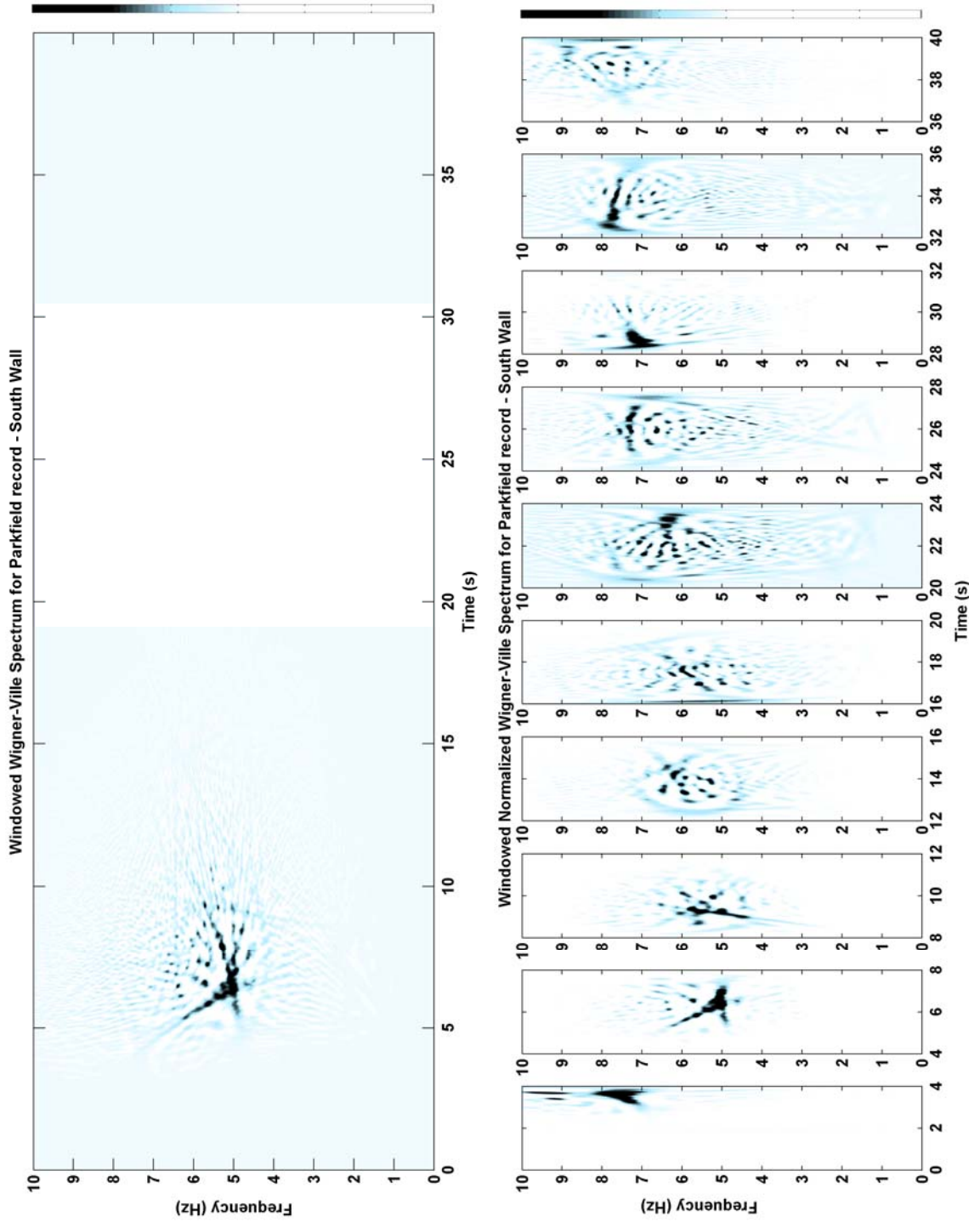
Figure 5.21: Wigner-Ville spectrums of the south wall.

The time and frequency analyses demonstrated that linear modal parameters must compensate for the nonlinear responses. Nonlinearity is introduced by the hysteretic characteristics of the structure. Observations of the hysteresis loops offer several insights to the high damping as well. It is well known that the area inside the hysteresis curve has a direct relationship with the damping estimate (e.g. Uang and Bertero 1986). A formula for calculating the value is available for the linear viscous damper (Paz 1997). An empirical formula for estimating the damping value for nonlinear responses depends on the overall shape of the hysteresis. Even without an exact measurement, the variation in the area enclosed by the hysteresis curve supports the amplitude dependence in damping estimates. Typically, with larger ground motions, the structure yields and higher deformations extend the outer excursions of the hysteresis curve. This inherently increases the area enclosed by the curve and suggests greater energy dissipation. Time-segmented hysteresis loops show the enclosed area as a function of the amplitude of ground motion. The variations support the variations of damping estimates seen in windowed analysis. Therefore, the higher degree of nonlinearity seen in hysteresis loops, the higher the energy dissipation. High linear viscous damping estimates are compensating for hysteretic damping. The procedure here also depends on the extraction of meaningful hysteresis loops. Double-integration errors can hamper this process.

5.4.2 *Inconsistencies in Reported Damping Estimates*

5.4.2.1. *CUREE Task 1.3.3 – Forced Vibration Tests*

There are several confirmations of high linear viscous damping estimations as a result of hysteretic damping compensation. However, recent experimentations on full-scale wood-frame structures reported significantly lower damping values. The discrepancies have supported theories that the damping estimates calculated from the MODE-ID method are overcompensating for the hysteretic behaviors in wood-frame structures. The wide range of reported damping values makes it difficult for engineers to determine the appropriate amount of viscous damping to be employed in modeling. Since the choice of damping estimates depends on the type of model being used (linear or nonlinear), it is imperative that scholars emphasize the methods used to calculate the value and describe what the damping estimate represents. Some engineers proclaim that damping estimates over 10% is unreasonable. These statements could cloud the judgment in determining an appropriate damping estimate. One must first recognize that there is no single correct value for damping estimate, as it depends on type of model being used. To further resolve these uncertainties on damping estimates, the hysteretic extraction procedures mentioned in the previous section can help provide insights to this issue.

Forced vibration tests (Camelo, Beck and Hall 2002) reported damping estimates in the range of 2.5% to 8%. The damping estimates were calculated through a regression analysis on the forced vibration measurements. Figure 5.22 and Figure 5.23 show the forced vibration results from the test on a three-story wood-frame apartment complex.

Damping estimates reported are between 4.6% and 5.1%. With the increasing force generated from the shaker, the fundamental frequency is shifted 0.5 Hz. This shift, however, is fairly small compared to the ones observed from the Parkfield school building. This small frequency change suggests that the nonlinear response may not be significant at all. Figure 5.24 to Figure 5.26 are hysteresis loops extracted from the measured accelerations for the apartment complex. Damping estimates are also calculated based on the enclosed area. The hysteresis loops exhibit no signs of pinching and behave like a linear viscous damping element. The cyclic nature of the forces generated from the shaker produce well-defined hysteresis loops in complete cycles.
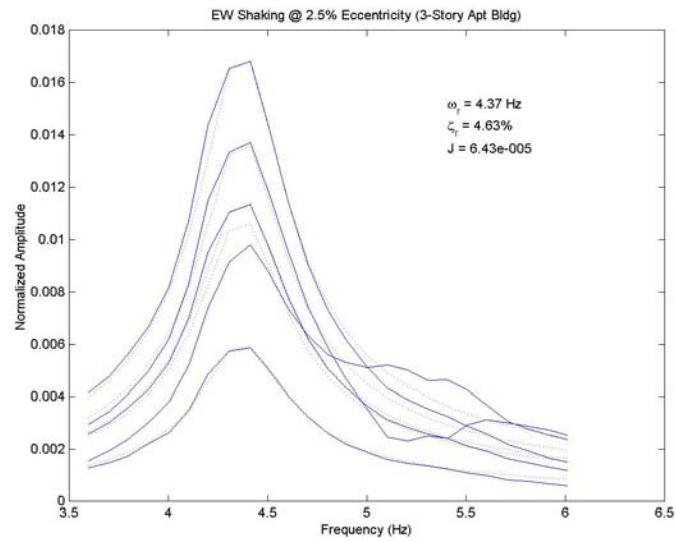
Figure 5.22: Forced vibration results with low level shaking force on the three-Story Del Mar apartment (Camelo 2003).
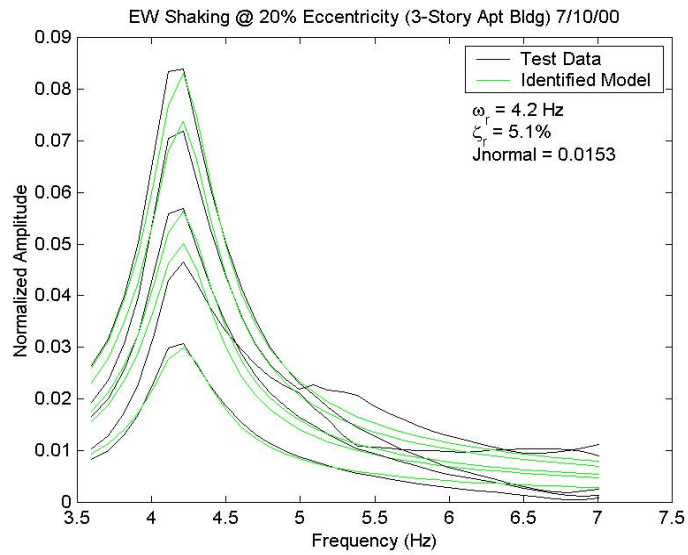
Figure 5.23: Forced vibration results with low level shaking force on the three-Story Del Mar apartment (Camelo 2003).

98
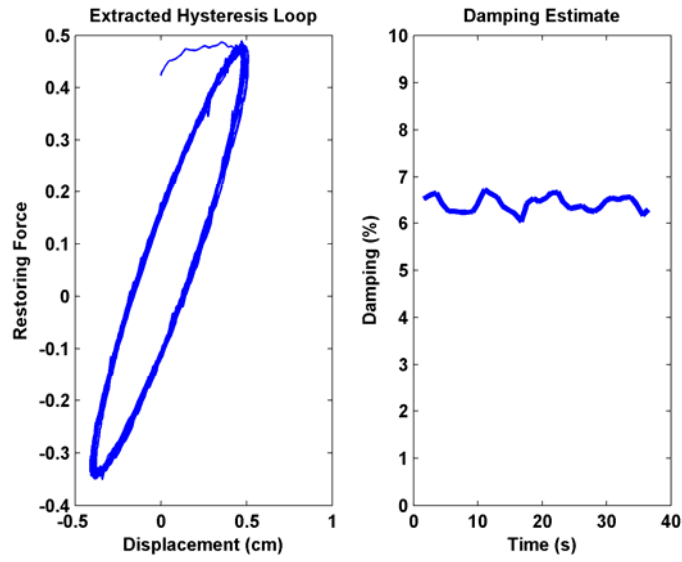
Figure 5.24: Hysteresis loop and damping estimate of the three-story Del Mar apartment building at low level shaking forces.
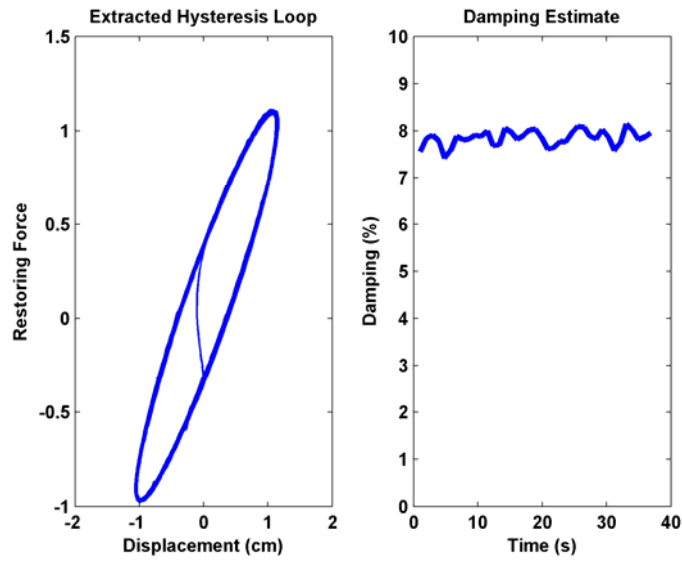
Figure 5.25: Hysteresis loop and damping estimate of the three-story Del Mar apartment building at middle level shaking forces.
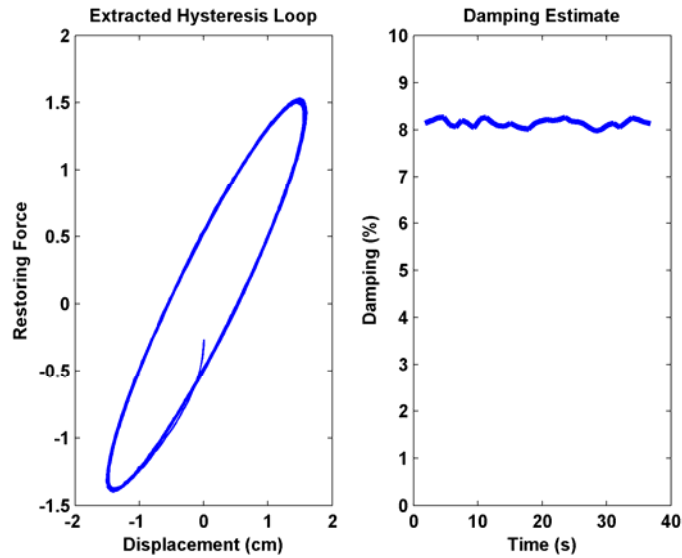
Figure 5.26: Hysteresis loop of the three-story Del Mar apartment building at high level shaking forces.

Since the hysteresis loops has an elliptical shape, we can assume it behaves like a Kelvin solid viscoelastic element. The formula is described in Paz (1997) and Fischer et al. (2001). Calculating the area inside the curve can be done in most numerical packages. The maximum restoring force and relative displacement are also needed for the final damping estimate. The calculations show that the system exhibited 6%-8% damping across increasing forces, which is higher than the 4.5%-5.5% damping estimated by Camelo from fitting resonant peaks. These discrepancies are sensitive to the phase delay and the filter used in the extraction process.

The damping estimation can be applied at multiple time intervals. This may be an alternative way to estimate damping variations with time. Since the shapes of the hysteresis loops suggest little or no nonlinear responses, the method should provide an accurate estimate. However, these forced vibration tests indicated the building's motion exceeded

100

couple centimeters of vibration. Typically at these amplitudes, the building would show signs of hysteresis. A possible explanation is that forced vibration tests usually record the measurements only during steady state motion. To reach steady state motion, the building experiences shaking levels at constant amplitude for several seconds. At steady state, the building connections may have already softened and measurements may only show the nailed connections traversing the gap created by the initial cycles of the shaking. Therefore, it should be further investigated on the differences of experimental procedures and the impact I has on the results such as showed here for forced vibration experiments.

5.4.2.2. CUREE Task 1.1.1 – Shake Table Tests

The analysis on the series of shake table tests from CUREE Task 1.1.1 report an average damping estimate of 7.6%. Most of the damping values are within one standard deviation (5.3% to 10%). Figure 5.27 compares the modal parameters obtained from the UCSD and MODE-ID analysis. The test specimen is a complete wood-frame structure without sheathing and nonstructural finishes. The ground motions for the seismic tests were scaled versions of the Northridge earthquake, with seismic level 1 having 0.05g peak ground acceleration and level 5 having 0.9g.

The fundamental frequencies match well at lower levels of ground motion, possibly when the structure has not yet reached nonlinear behavior. Amplitude dependence can be seen as these frequency estimates shifted lower during larger seismic motions. The frequencies reported by UCSD were calculated by finding the maximum resonant peak in spectral densities. At higher levels of ground motion where a nonlinear response is

expected, spectral densities are multi-peaked as shown in earlier frequency spectrums. Simply picking the maximum peak in the frequency response will lead to a bias, as seen in the frequency estimates at larger seismic levels.
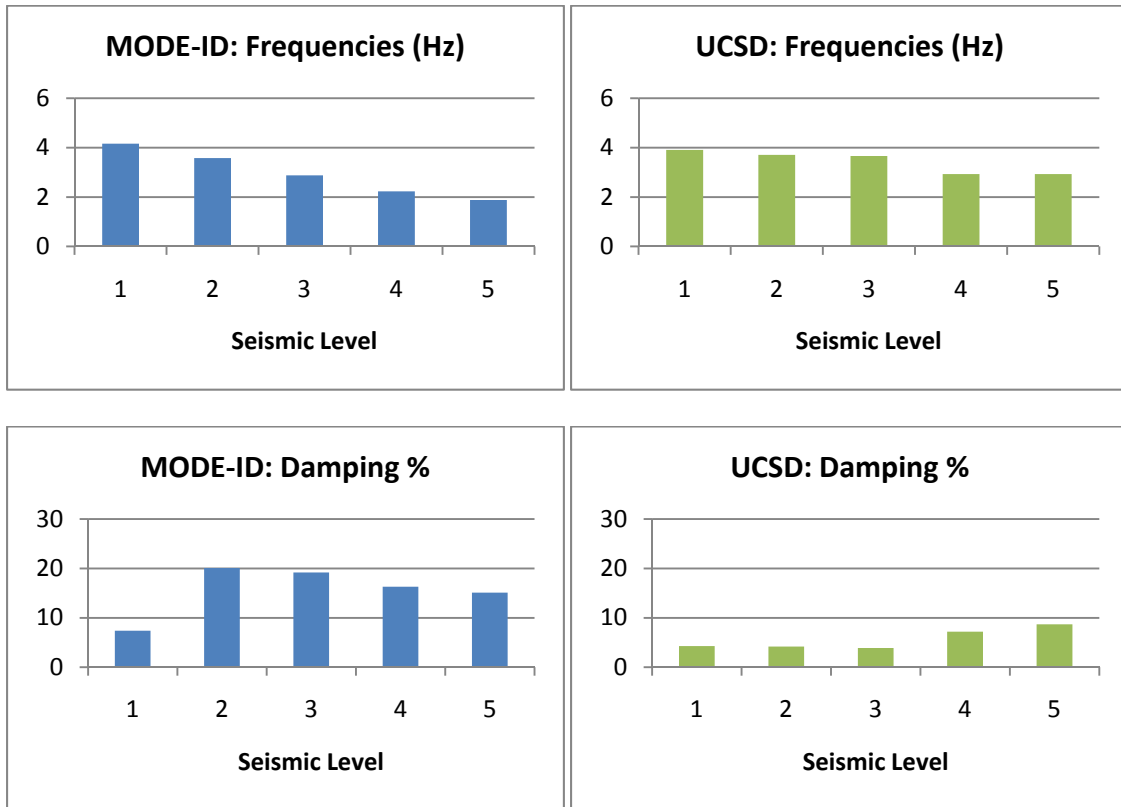
Figure 5.27: Comparison of modal parameter estimates from UCSD and MODE-ID analyses on the same test structure.

By obtaining both the UCSD and MODE-ID analyses and then directly comparing them can lead to very misleading conclusions. One may think that since the fundamental frequencies are similar, comparing the damping estimates can be justified. From Figure

5.27, one might conclude that MODE-ID analysis is inferior, because it reports a 20% damping which can be unreasonable to many structural engineers. However, when comparing these results it is important to understand the methods used to calculate it. MODE-ID analysis uses data fitting based on a linear dynamic model and the modal parameters are the estimates reported in Figure 5.27. The data used were the responses recorded on the test structure during the increasing seismic levels of shaking. On the other hand, the UCSD analysis uses the maximum peaks in frequency domain to conclude these correspond to modal frequencies of a linear dynamic model. The identified frequencies are used to excite the test structure at resonance. The shake table was then brought to a complete stop after the structure had been in resonance for 30 seconds. A logarithmic decrement procedure was used to determine the viscous damping (Fischer, et al. 2001). Although both analyses invoke a linear dynamic model, the MODE-ID calculates an equivalent linear model to strong ground motions and nonlinear responses, while UCSD characterizes the linear behavior of the building after it has experience strong seismic motions. Without properly considering all the differences, reported results of modal parameters can be misleading.

It is true that the UCSD analysis does incorporate the effects of hysteretic damping (Camelo 2003), however, the peak structural acceleration at the roof level for the majority of the tests was only around 0.05g. It is unlikely that nonlinear responses were reached even though the structure was under resonance. Furthermore, most hysteretic behaviors are caused by large deformations and low frequency motions. Shaking the structure at 4 to 6

103

Hz with a peak structure acceleration of 0.05g typically does not yield the same deformations by large transients as seen in seismic motion.

Additionally, the damping trend for MODE-ID can be supported by understanding the experimental procedures. The same test structure was used for all of the seismic levels. Therefore, if any damage occurred in a previous test, the current test structure is not the same system unless the in-between structural repairs were perfect. If most of the connections were soften during seismic level 2, it is realistic that MODE-ID will report the highest damping value. Later seismic values may have higher amplitudes, but the initial crushing of wood fibers at the connections already happened. .

The damping estimates reported by MODE-ID can be further supported by estimating them from the hysteretic loops obtained from the UCSD building. One way is to first calculate the area inside the pinching hysteresis loop and formulate an ellipse with an equivalent area. The ellipse must have the restoring force and displacement extrema on its perimeter. The damping estimate can then be calculated as previously mentioned.
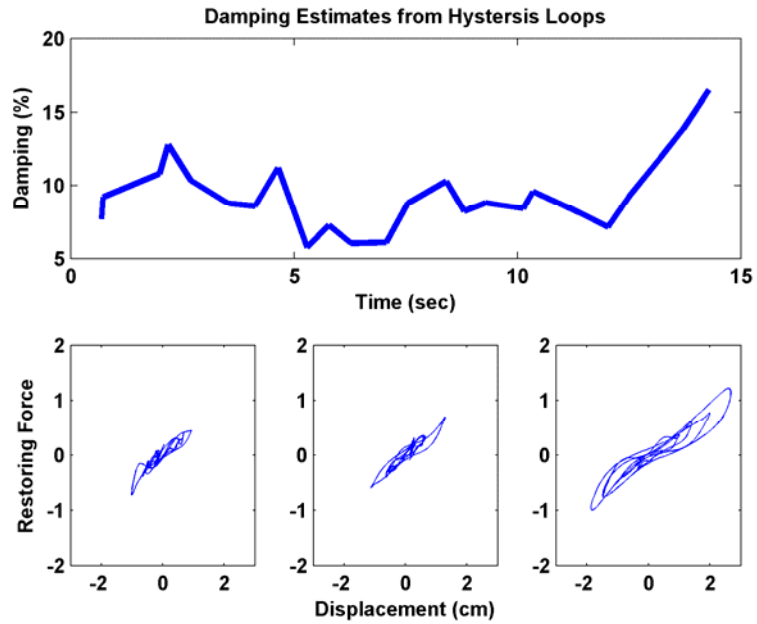
Figure 5.28: Variations in the damping estimate through time. Hysteresis curves are from Test Phase 9 at seismic level 4.
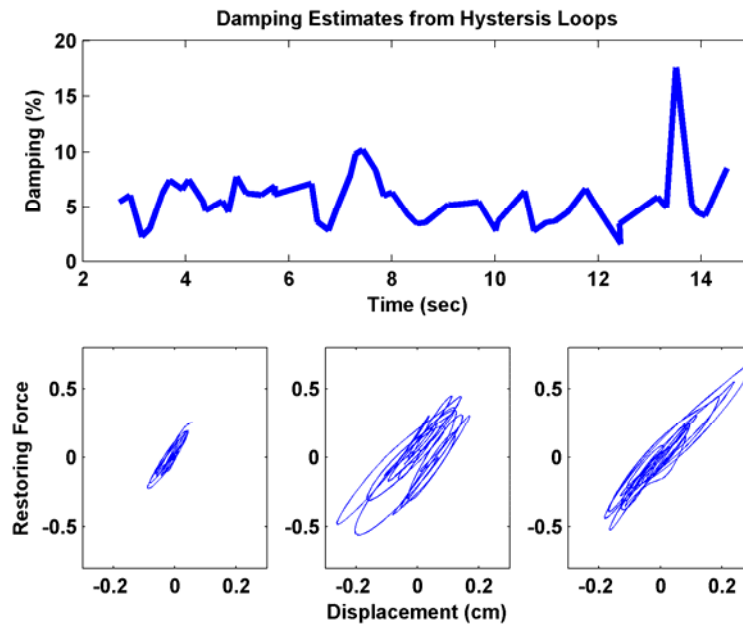
Figure 5.29: Variations in the damping estimate through time. Hysteresis curves are from Test Phase 10 at seismic level 4.

105
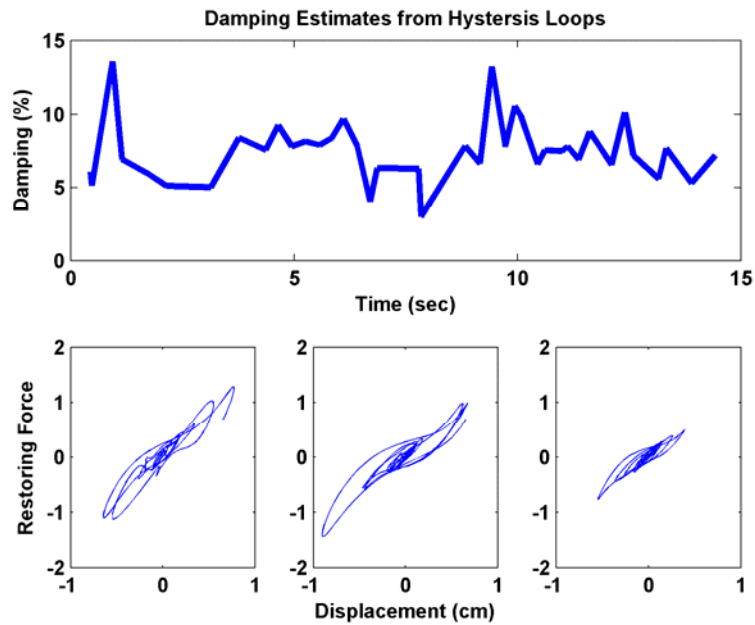
Figure 5.30: Variations in the damping estimate through time. Hysteresis curves are from Test Phase 10 at seismic level 5.

The estimated damping values are consistent with physical intuition. When the pinching hysteresis is more pronounced, the damping estimate is larger. Since the shape of the hysteresis loops changes over time, variations in the damping can occur. Estimating the damping variations through time would require calculating ellipses for each cycle of the hysteresis loop. Figure 5.28 through Figure 5.30 demonstrate how this method can effectively capture the changes in energy dissipation throughout the record. Each figure also provides the hysteresis loops corresponding to the time interval above it. Again, 15% damping are seen when the pinching hysteresis is more prominent.

106

5.5 Conclusions

Discrepancies seen in the data fitting and reported modal parameters are a result of the hysteretic responses. This chapter has shown that most of the damping estimates reported from MODE-ID are not over-compensating for nonlinear effects. Many of the discrepancies found from experimental results are due to unfair comparisons between linear and nonlinear responses. If a linear model is used to characterize the response, a 12-20% modal damping estimate can be expected for large seismic motion. Nonlinear models with custom hysteresis models should use a 5-10% viscous damping estimate to avoid over-compensating for the dissipation of energy.

This chapter showed that by observing hysteresis loops, one can infer the degree of nonlinearity and the amount of energy dissipated by wood-frame structures. Time-segmented hysteresis curves can yield more accurate estimates in damping fluctuations during seismic motion. These benefits rely on the development of a more robust procedure in extracting hysteresis loops from acceleration measurements. Current procedures are still hampered by double-integration errors and measurement noise. An alternative approach could be to use measured accelerations to identify models with hysteretic elements. This eliminates an intermediate step and avoids double-integration errors.

CHAPTER 6

Hysteretic Finite Element Model Updating

Analyzing the seismic responses measured on the Parkfield school building using MODE-ID and hysteresis curves has provided several important insights into the characteristics of wood-frame structures. However, to accurately simulate the nonlinear behavior of the structure, a more extensive analysis is needed. The finite element method is a powerful numerical analysis that has been widely applied in various engineering fields. This chapter presents the finite element procedure and models used to characterize the Parkfield school building. Model updating procedures will be applied based on recorded response and various updating routines.

Creating representative models serve several purposes. First, it serves as a validation tool to assess the hysteretic extraction process as mentioned in Chapter 5. Second, the model can simulate and predict responses from various earthquakes. This can decrease the number of expensive experimental tests that need to be conducted. Furthermore, the predicted responses can be used to update building codes. Lastly, the development of accurate models will attest to the value of the instrumentation program. A

database of seismic records that is continually updated serves as a perfect complement to the updating of models.

The challenge in creating these models from data is that this inverse problem is ill-conditioned because not all data records provide information on the nonlinear behavior. Furthermore, the process is complicated by the number of parameters needed to characterize the hysteretic restoring force of the building. Without sufficient data, tradeoffs are seen among the parameters, making the system unidentifiable. This chapter will discuss the different model updating techniques used to find an appropriate model. The chosen model will simulate the Parkfield records and provide information in the physical behavior of the structure during the earthquake.

6.1 Finite Element Procedure

A simple mathematical model of a wood-frame building during an earthquake response uses plane stress elements for the walls and diaphragm. The finite element program was written specifically to model tilt-up buildings. A modified version was used to model wood-frame structures.

In this model, a node can contain six degrees of freedom: translations u_i, v_i and w_i in the global X, Y and Z directions and rotations θ_i, γ_i, and α_i about these axes, where i denotes node i. Element matrices and vectors are first created in a local coordinate system x', y', z'. They are then rotated to the global reference frame for assembly.

Degrees of freedom:

u'_i, v'_i, w'_i ; $i = 1, 4$
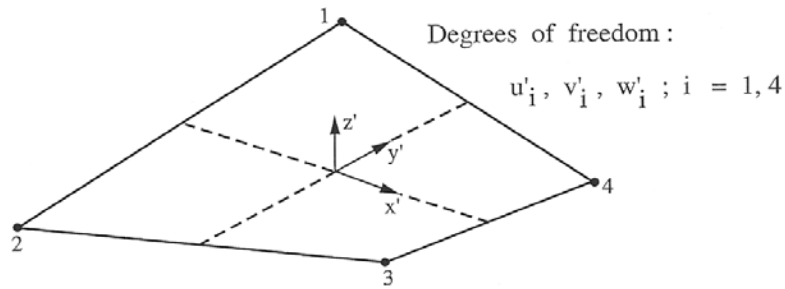
Figure 6.1: Geometry of the plane stress element.

6.1.1 Elements

Plane stress elements are standard 4-node quadrilaterals whose local coordinate system in shown Figure 6.1. Evaluation of the elements is done through 2-by-2 Gauss integration. For linear behavior in the element, the stresses and strains are related in the conventional way by defining Young's modulus, Poisson's ratio and shear modulus. For nonlinear behavior, the relation between the shear force and shear strain are dictated by the hysteretic behavior shown in Figure 6.2. No stiffness degradation is implemented at the moment. When nonlinearity is present for shear, the linear relation is still used for the normal stresses and strains. Material parameters can be specified either for the actual thickness or a unit thickness. The program uses a constant average acceleration time integration scheme to solve the matrix equation of motion. The tangent stiffness matrix and diagonal mass matrix are assembled from each of the individual elements, while the damping matrix is constructed through Rayleigh damping.

The main reason for choosing plane stress elements is the fewer number of parameters used to compare to a plate element. Although some of the moment and bending

110

parameters can be inferred from a detailed structural plan, the aim here is to develop

models directly from the amount of information provided online. Highly detailed models

through a study of structural plans can be useful, but the current instrumentation would not

be able to fully support this procedure. Another reason for choosing plane stress elements is

that the expected response from a one-story building would predominantly be shearing

motions as opposed to bending motions.
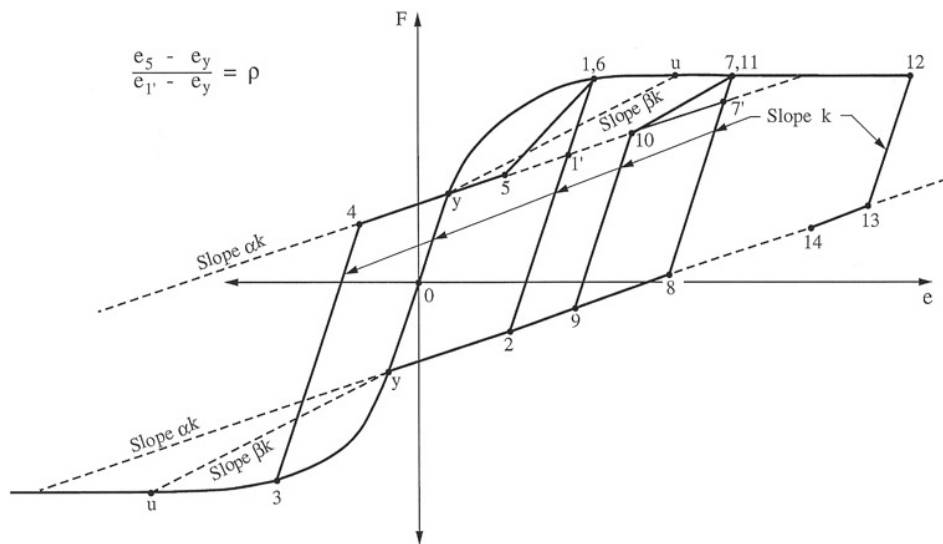
Figure 6.2: Hysteresis behavior with pinching. F is a generalized action and e is a generalized deflection. Required parameters are F_y, F_u, k, α, β, and ρ where y = yield and u = ultimate. An illustrative history follows the path 0-1-2-3-4-5-6-7-8-10-11-12-13-14.

111

6.1.2 Models

The numerical modeling procedure uses the results from MODE-ID as a basis. The ratio of the mass and stiffness of the elements are adjusted accordingly so that the fundamental frequencies of the Parkfield school building model match the fundamental modes identified through MODE-ID. Acceleration records from the numerical model and recorded data from the building will be compared at corresponding locations. It is important that the relative acceleration is used for comparison, as the total acceleration is largely dominated by the ground motion. The extracted hysteresis curves are also useful in correcting the model. As shown previously, the extraction method should provide insights into the hysteretic behaviors that the model needs to mimic. Therefore, attempts to model the relative acceleration are also largely dependent on implementing similar hysteretic characteristics.

A variety of finite-element models were considered in the process. Figure 6.3 shows the different types of discretizations used. All the ground nodes are constrained in all six degrees of freedom while the roof nodes can move in the transverse and longitudinal directions. Depending on the nonlinearity and the model resolution, each simulation can take 30 seconds to a minute.

The model on the left in Figure 6.3 consists of 42 nodes and 29 elements. Each roof element is 10' × 8', the north and south wall element are 8' × 12', and the east and west wall element are 10' × 12'. This discretization does not take advantage of the acceleration time history on top of the south shear wall since the height of the model is one element. The middle model in Figure 6.3 provides multiple elements along the height of the model.

78 nodes and 58 elements were used. Each of these models served as a basis for deriving

models with openings shown in Figure 6.4.
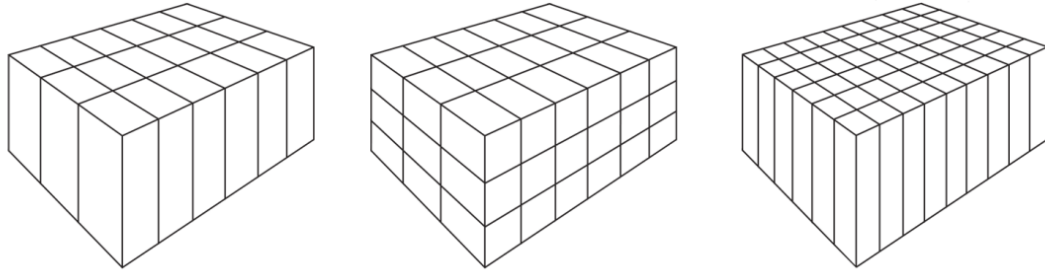
Figure 6.3: Sample of the different types of model discretizations used (south-west point of view).
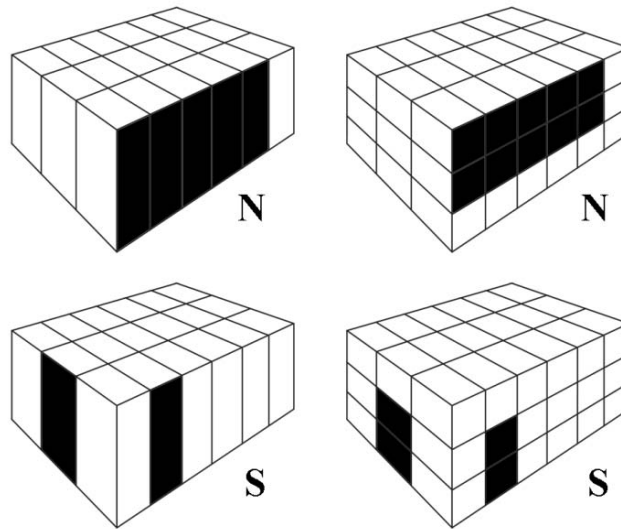
Figure 6.4: Black elements show the windows and door openings in the structure. The procedure models these as openings.

Based on physical intuition, including these openings should improve the data fit of the model. However, results showed poor data fit and lack of convergence. It is possible that in this finite element model framework, better fit can be achieved by not modeling these openings. Furthermore, complications occur with the use of plane stress elements along the height discretization of the building. Additional constraints are needed at these nodes to keep the problem numerically stable. The restraints are not representative of the building's behavior.

Instead of incorporating the openings, each face of the building is modeled as one equivalent wall. The model on the right in Figure 6.3 consists of 80 nodes and 66 elements. Each roof element is 6' × 6' and each wall element is 6' × 12'. This discretization does not take advantage of the acceleration time history on top of the south shear wall since the height of the model is one element. Figure 6.5 shows the 80-node model with three different configurations. The different shades of gray indicate a different set of parameters is used to characterize the structural component. A list of parameters in each set is shown in Table 6-1.
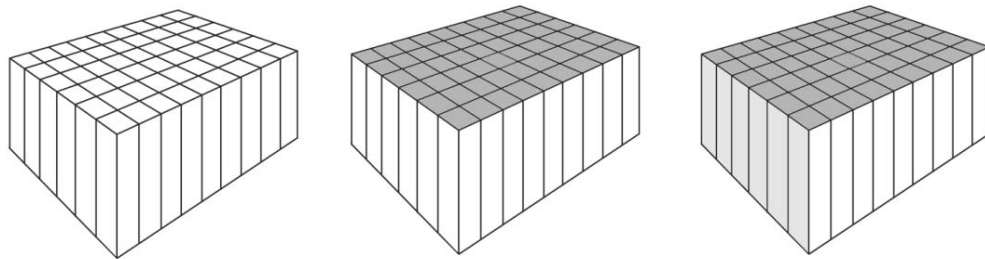
Figure 6.5: (From left to right) Model 1. Walls and diaphragm have same set of parameters. Model 2. Walls and diaphragm have different set of parameters. Model 3. East-West walls, North-South walls, and diaphragm have different set of parameters.

Table 6-1: List of parameters used to characterize a structural component.

Parameter	Description	Parameter	Description
POI	Poisson's Ratio	**GG**	Shear Modulus
BET	Hysteretic Parameter: Slope 1	**ALP**	Hysteretic Parameter: Slope 2
RP	Hysteretic Parameter: Return Path	**SXY1**	Shear Yielding Strength
SXYU	Shear Ultimate Strength	**K**	Young's Modulus
DAMP	Rayleigh Damping (one value per model)		

Aside from geometric information and the parameters listed above, other variable inputs include the mass and thickness of the elements. These values are kept constant to help narrow the inverse problem. When the Parkfield earthquake is added as ground motions, the model performs a dynamic analysis to calculate the acceleration and displacement time histories.

6.2 Validating the Hysteretic Extraction Process

Prior to searching optimal parameters for the model, an index wood-frame structure having the same dimensions as the Parkfield school building was assembled in the finite element program. The purpose is to provide insights into the effects of ground motion perpendicular to the sensors. As described in Chapter 5, the hysteresis extraction process worked well for the uni-axial shake table tests, but the results for field records were less conclusive. This validation process simply involves different ground motion inputs, the number of

acceleration channels used, the presence of viscous damping forces, and the degree of nonlinearity in the elements. The following hysteresis curves in Figures 6.6 and 6.7 represent the behavior on the east wall of the building.

Figure 6.6 presents a scenario where a structure behaves linearly under earthquake loading. The calculated and extracted hysteresis curves are expected to be straight lines without viscous damping. However, in Figure 6.6a, even without the presence of the East-West horizontal ground motion, some discrepancies may be seen. The sway in the middle portion of the hysteresis curve comes from the error in the doubly integrated acceleration records. With proper treatment through filtering or removing linear trends in the displacement record, the expected hysteresis curve in Figure 6.6b can be obtained. Figures 6.6c and 6.6d depict the hysteresis curves with the addition of the East-West horizontal ground motion. The only difference is that Figure 6.6d is obtained from the two acceleration records corresponding to Parkfield sensor locations 1 and 2, whereas 6.6c is solely from the acceleration record from location 1. Figures 6e and 6f plot the same curves presented in Figures 6c and 6d but with the addition of viscous damping in the structure. It appears that the extraction process appears to be in good agreement with the calculations of the model despite changing certain factors.
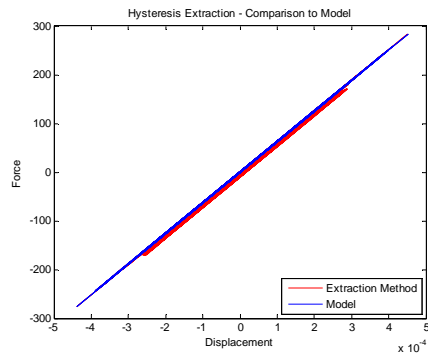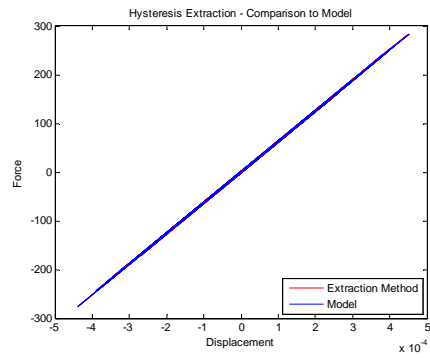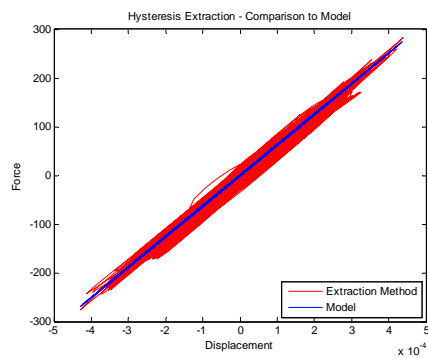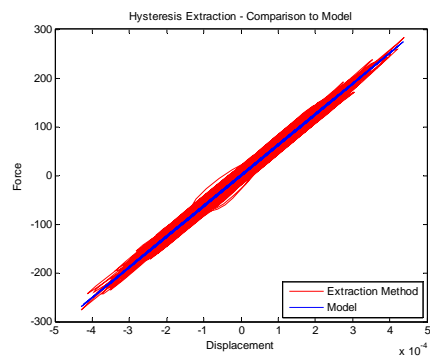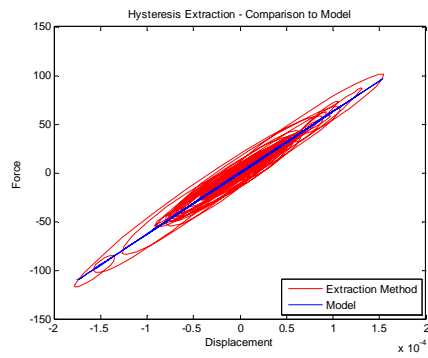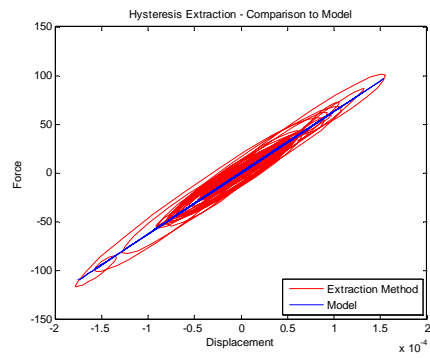
Figure 6.6: Parkfield Earthquake Input – Linear Model a) No horizontal ground motion b) No horizontal ground motion but with adjusted displacement time c) With horizontal ground motion and obtained from an east wall sensor location d) With horizontal ground motion and obtained from Parkfield sensor locations e) Add viscous damping in the model and obtained from an east wall sensor location f) Add viscous damping in the model and obtained from Parkfield sensor locations.

Figure 6.7 presents a different scenario where a structure behaves nonlinearly under earthquake loading. Again, Figure 6.7a demonstrates that, without viscous damping, the extraction method can perfectly retrieve the hysteresis curve from acceleration records. However, with the presence of East-West horizontal ground motion and limitations on the number of sensors, the extraction of the hysteresis curve becomes less accurate, as shown in Figure 6.7.
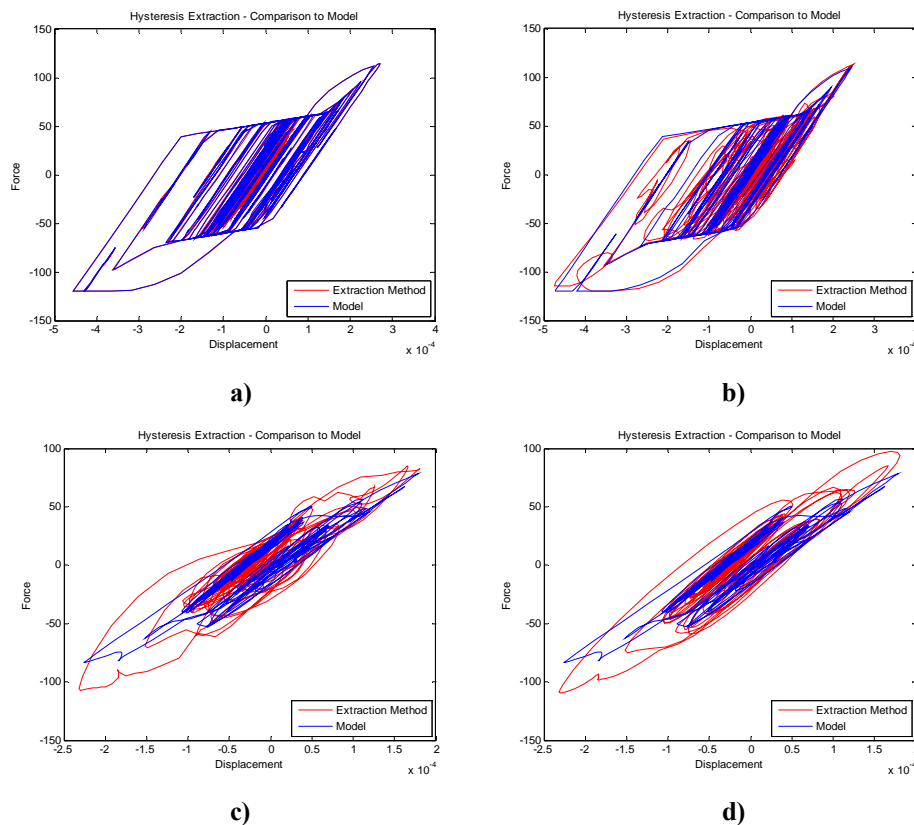
Figure 6.7: Earthquake Ground Motion Input – Nonlinear Model. a) No horizontal ground motion b) With horizontal ground motion c) Add 10% viscous damping in the model and obtained from an east wall sensor location f) Add viscous damping in the model and obtained from Parkfield sensor locations.

This behavior is consistent with the observations in Chapter 5, where hysteretic curves derived from uni-axial ground motions yielded near-perfect extraction, while bidirectional ground motions tampered with the fidelity of the extraction due to the nonlinear forces applied on the walls from the shearing of diaphragm.

By including viscous damping the discrepancies are further magnified, as shown in Figure 6.7c. Figure 6.7d presents the hysteresis curve when Parkfield acceleration records from two sensor locations are used in the FBD approach as described in section 5.2.1. It is clear that simply integrating the acceleration record – which is common practice – on top of the east wall (Figure 6.7c) does not perform as well as the FBD approach (Figure 6.7d). More importantly, this highlights the importance of sensor placement, the types of measurements to be recorded, and the number of sensors needed for each instrumented station.

6.3 Model Optimization

Aside from being a validation tool, the predicted responses from the model can be used for building code design. However, this requires the model to reflect accurately both linear and nonlinear behaviors of the structure. The metric for evaluating the model's fidelity would rely on comparing recorded and simulated seismic responses. In the search for an "optimal" set of parameters, finite element model updating techniques must be used. Finite element model updating is a process of searching for a model that better reflects the measured data than the initial starting model. There are several approaches in implementing least-squares

updating process (Parker 1977; Sambridge 2002; and Tarantola 2005). This section will discuss some routines from both direct and gradient search methods.

6.3.1 Direct Search Methods

Direct search methods are a class of techniques that do not involve finding extrema of the objective function with calculating derivatives. Instead, results generated from several thousand samples are collectively used to determine a better model. Advanced direct search methods include simulated annealing, which is based on mimicking a natural thermodynamic optimization process that occurs in cooling of a crystal and genetic algorithms that follow a biological analogy that occurs in natural selection. At the most rudimentary level of direct search methods is the uniform search. Uniform search discretizes the parameter space into grids of pre-determined sample points. Each point is simulated and the least-square-error is recorded. Variations of the uniform search include uniform random search, where sample points are not predetermined, and nested uniform search, where the discretization level is finer in areas of lower least-square-error.

The main advantage of uniform search is its ease of implementation. The structure of the routine fits perfectly in parallel computing as none of the simulations depend on any other samples. Uniform search was used as a first measure to understand the data misfit across several combinations of parameters. Each of the uniform searches conducted for the Parkfield school building model involved 3 parameters. The discretization level is 50 samples across each dimension for a total of 125,000 samples for each uniform search. The sample size spanned the range of values that seem probable. The uniform search makes it

easy to analyze the tradeoffs between parameters, as a data misfit surface can be plotted. Figures 6.8 and 6.9 show two of the 150 surfaces that were generated for the Parkfield school building. The model only used one set of parameters.
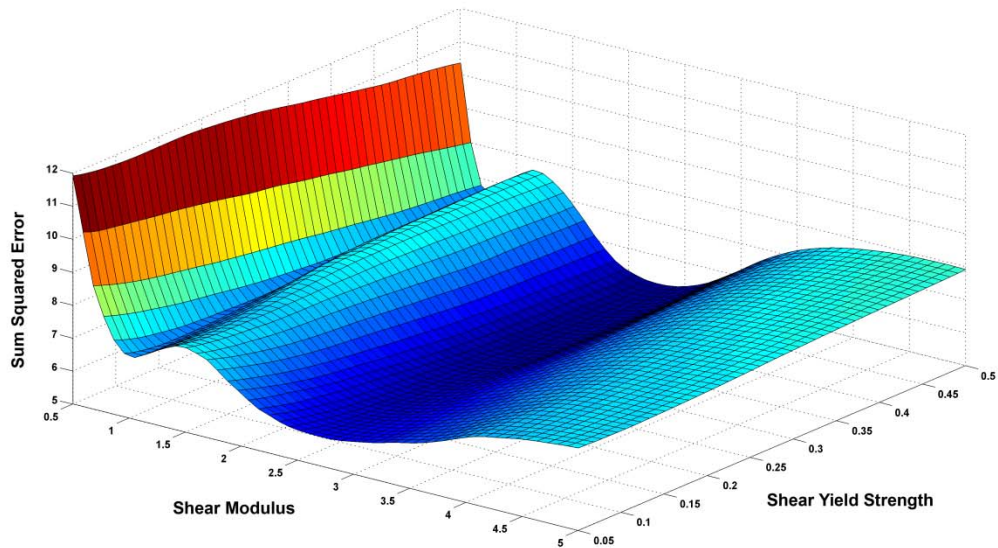
Figure 6.8: Data misfit surface between shear modulus and shear yield strength. Axes values are relative to the nominal values of the parameters.
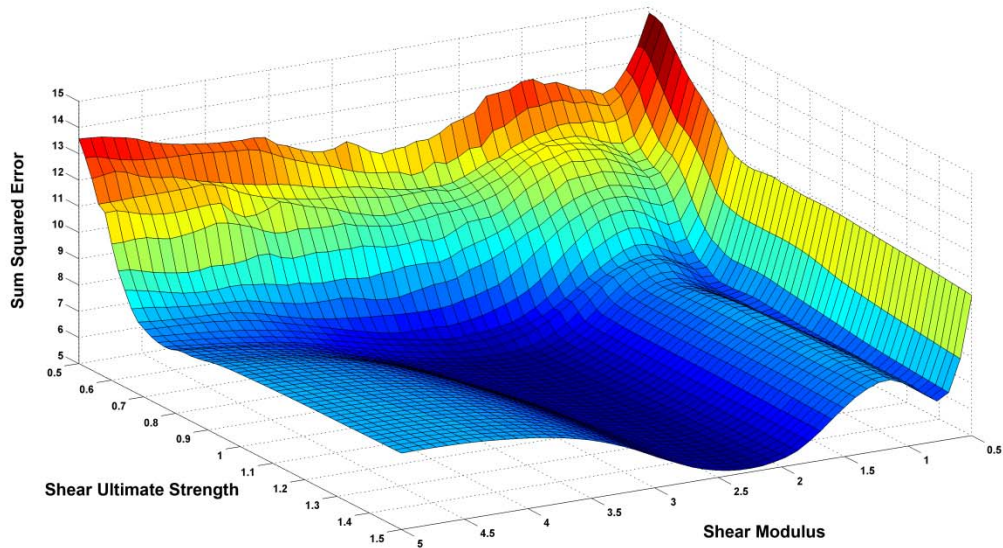
Figure 6.9: Data misfit surface between shear modulus and shear ultimate strength.
Axes values are relative to the nominal values of the parameters.

The data misfit surface in Figure 6.8 shows how the error topology changes with different shear modulus and shear yielding strength. The shear ultimate strength and other parameters are fixed for this surface. The figure shows that the nominal value of the shear modulus performs better than values below it and up to 1.5 times above it. However, at 2.5 times the shear modulus value, a new valley of local minima can be seen. The lowest point appears to be when the shear yielding strength is half its nominal value. The physical interpretation behind this is that the nominal shear modulus may have fit one of the measurements well which matches a particular fundamental mode. However, by increasing the overall shear stiffness of the building, the data fit for all channels have increased and the model matches more than a single fundamental mode. For Figure 6.9, the shear yielding

122

strength of the structure is unlikely to be less than half of its nominal value. The valley of minima can be seen again where the shear modulus is at 2.5 times its nominal value. The shear ultimate strength does not seem to play a factor in the topology until it is 0.6 times its nominal value. This threshold occurs probably when the numerical model has exceeded its shear ultimate strength. Since the error reported in that region is high, it is unlikely the building surpassed its ultimate strength.

The uniform search was also performed on models with multiple sets of parameters. Figure 6.10 shows the comparison of shear modulus among the east-west walls, north-south walls, and the diaphragm. Without going into full detail, multiple minima and tradeoffs between the parameters are evident. The topologies suggest that the diaphragm shear modulus should be half of its nominal value.
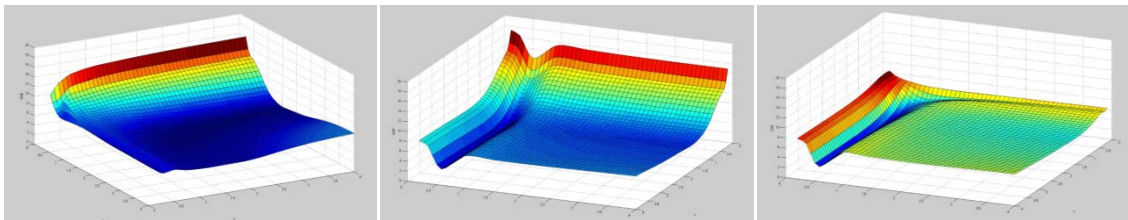
Figure 6.10: Data misfit surfaces of the shear modulus from all three subcomponents of the building.

Although uniform search is easy to implement and data misfit surfaces are simple to understand, the method is inefficient and impractical for problems with high dimensions, as there are issues in choosing discretization levels and number of samples. The method also makes it difficult to present the results in a collective manner. Since the Parkfield school

building model can have up to 26 parameters, the uniform search is only useful in studies on specific parameters.

6.3.2 *Gradient Search Methods*

Gradient search methods, as the name implies, utilize the gradients of the parameters to determine the minimum of an objective function. The objective function usually takes the form of the data residual term plus some regularization terms (Aster 2004). Gradient methods often incorporate least squares or damped least square solutions in minimizing the objective function. A common feature of the objective function is that not all parameters are constrained by the data. A regularization term is often included in the objective function to provide additional constraints and thus reduce the non-uniqueness of the problem. A main assumption for gradient methods is that the objective function is smooth enough to make use of the derivatives.

Instead of pre-selecting all simulation points in a uniform search, gradient methods use iterative steps and select a new simulation point for each successive approximation to the solution. This approach eliminates unnecessary simulations that do not contribute directly to the optimization of the problem. However, calculations for the gradient vector can become costly as well. For example, the finite central difference method would require performing twice the number of parameters of simulations at the initial guess to estimate the gradient vector. The computational efficiency diminishes if several iterations are needed for optimization.

The simultaneous perturbation stochastic approximation (SPSA) optimization algorithm overcomes the computational hurdle by only requiring two simulations to estimate the gradient vector. This improvement relies on generating the two simulation points from random perturbations of all the parameters of the initial guess. The optimization algorithm follows a recursive equation (Equation 6-1), starting with an initial guess $\boldsymbol{\theta}_0$:

$$\boldsymbol{\theta}_{k+1} = \boldsymbol{\theta}_k - a_k g_k(\boldsymbol{\theta}_k) \tag{6-1}$$

$$g_k(\boldsymbol{\theta}_k) = \frac{V(\boldsymbol{\theta}_k + c_k \Delta_k) - V(\boldsymbol{\theta}_k - c_k \Delta_k)}{2c_k D_k} \tag{6-2}$$

V : Numerical model
$g_k(\boldsymbol{\theta}_k)$: Estimate of the gradient of V evaluated at $\boldsymbol{\theta}_k$
Δ_k: Perturbation vector $[\Delta_{k1}, \Delta_{k2}, \ldots, \Delta_{kD}]$
D: Perturbation distribution (symmetric Bernoulli distribution
$P(D_i = 1) = P(D_i = -1) = 0.5, \text{for } i = 1,2, \ldots, D$) (Spall 1998).
$a_k = \frac{a}{(A+k+1)^\alpha}$: Gain sequences with A and α as user selected coefficients
$c_k = \frac{c}{(k+1)^\gamma}$: Gain sequences with c and γ as user selected coefficients

The optimization algorithm requires the parameters to be normalized for numerical stability purposes. Further information regarding the SPSA can be found in Spall (1998) and Cheung and Beck (2008).

The SPSA algorithm was implemented in the optimization of all numerical models. Conclusions regarding inadequate modeling of openings stem from the lack of convergence seen in the SPSA routine. Each SPSA search had a minimum of 500 iterations and stopped when a convergence criteria was met. Each configuration was repeated at least 48 times to incorporate both the same and different initial guesses. A configuration involves selecting

the gain sequences, the number of measurement channels for data fit, and the number of parameters to be perturbed. It was necessary to confine some of these factors to obtain a better initial guess.

Results from SPSA demonstrated the lack of convergence to a single set of parameters. This is expected as the nature of system identification hysteretic structures is ill-conditioned. It is inevitable that there will be tradeoffs between the parameters that can produce similar results. The parameter set that yielded the least data fit error was chosen from the SPSA result. The predicted responses are shown in Figure 6.10. The overall data fit is satisfactory, with slightly more discrepancies in channel 1. However, the hysteresis curves obtained from the fit (Figure 6.11) showed behaviors that are not physically representative of wood-frame buildings. Therefore, even with the lowest data fit error, the presented model may not be non-characteristic of real structures.
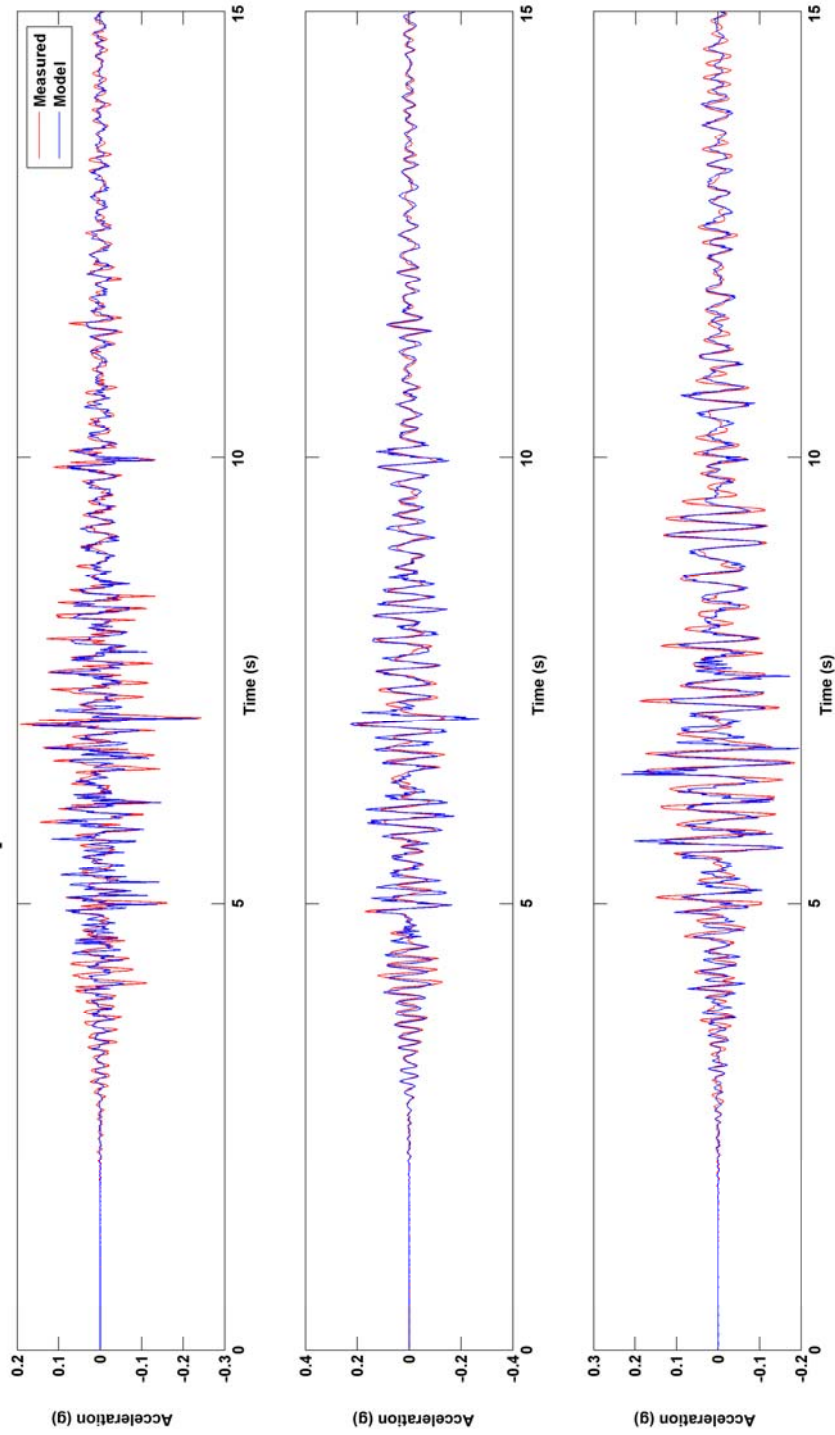
Figure 6.10: Data fit of the Parkfield school record from SPSA identified parameters.

127
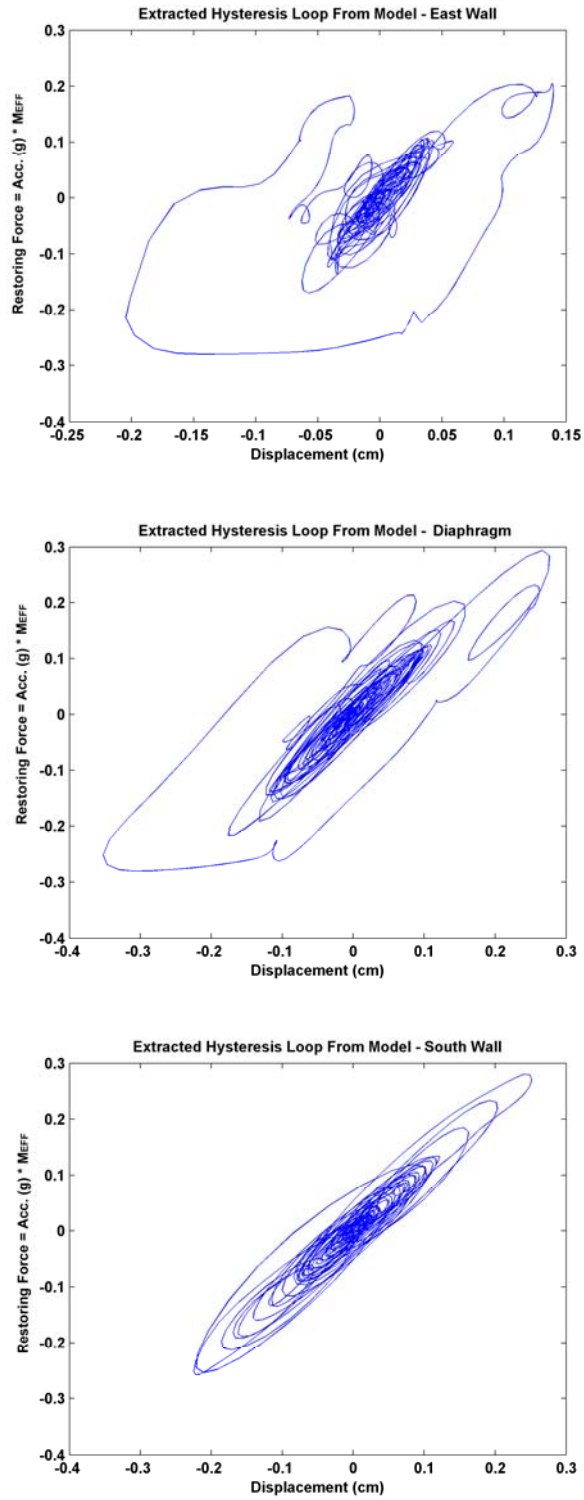
Figure 6.11: Hysteresis curves obtained from the SPSA identified numerical model.

The SPSA and other gradient methods have the advantage of relating the minimization problem to an inversion problem. However, it is necessary to regularize the problem to reduce the non-uniqueness of the problem. In a nonlinear problem that solves for the hysteretic behavior of wood-frame structures, the models are almost always unidentifiable based on the available data. Regularizing a problem will lead to a tradeoff between data fit and model resolution. Also, formulating an initial guess for a gradient method is very important as a problem can converge to one of several local minima as it attempts to find the global minimum. This can be seen when the SPSA algorithm converges to multiple final parameter values during different runs. Since the SPSA routine only provides one solution even though multiple solutions occur in hysteretic structures, the reliability and consistency is a concern when the models are designed for updating building codes.

6.3.3 Bayesian Updating and Model Selection

The Bayesian updating and model class selection approach (Beck and Yuen 2004, Muto and Beck 2008, Beck and Cheung 2009) is similar to direct search methods in simulating several thousand samples, but its ability to deal with ill-conditioned identification problems merits its own section. Given a set of candidate models for a system, the method calculates the probability of each model given a data set. In this Bayesian approach, the probability of a model should not be interpreted as the frequency of an event given similar conditions, but a value quantifying how plausibly each candidate model is based on the data and prior information (Jaynes 2003; Beck and Cheung 2009). Bayesian updating and model selection

is a process where uncertainties in the model are quantified by a probability density functions (PDF). Even uncertainties of an ill-conditioned identification problem such as identifying hysteretic models of structures can be incorporated (Muto and Beck 2006).

The use of a PDF occurs both at the parameter and model selection stage. Since there are always uncertainties in the parameter values, Bayesian updating analyzes the relative likelihood of each combination of parameter values; one can, for example, present only the most probable one. Similarly, out of a collection of candidate models, Bayesian model selection can be used to check which candidate model class is the most probable. By using Bayes' Theorem which states:

$$Posterior\ PDF\ \alpha\ (prior\ PDF)(likelihood\ function) \tag{6-3}$$

$$p(\theta|D,M)\ \alpha\ p(\theta|M)\,p(D|\theta,M) \tag{6-4}$$

$$p(\theta|D,M)\ \alpha\ p(\theta|M)\prod_{i=1}^{N}p(y_i\mid x_i,\theta,M) \tag{6-5}$$

Posterior PDF: Uses available information to update prior information about the uncertain parameter values.

Prior PDF: Contains prior knowledge of the parameter values.

Likelihood function: Quantifies the probability of the parameter combination to resemble the current data set.

θ: Set of uncertain parameters.

D: Set of N data points representing input x_i, output y_i.

M: Candidate Model.

α: Denotes "proportional"

The most probable model in a model class can be found by maximizing the posterior PDF for the model class. The uncertainties associated with the most probable parameters depend on the shape of the PDF. Typically, given a larger amount of data, the posterior PDF becomes narrower.

The model class selection takes a step further by utilizing the *evidence* (normalizing constant of the posterior PDF) to quantify the information gain and data fit of the model. Beck and Yuen (2004) and Muto and Beck (2008) provide a detailed discussion on this topic. The calculation of the probability of M_i is based on Bayes' Theorem and proceeds as follows:

$$Posterior\ PDF\ = \frac{(prior\ PDF)(likelihood\ function)}{evidence} \tag{6-6}$$

$$p(\theta_i|D, M_i)\ = \frac{p(\theta_i|M_i)\ p(D|\theta_i, M_i)}{EV_i} \tag{6-7}$$

$$p(M_i|D) = \frac{EV_i}{\sum_i EV_i} \tag{6-8}$$

$$evidence =\ EV_i = \int (prior\ PDF)(likelihood\ function) \tag{6-9}$$

$$= \int_\theta\ p(\theta_i|M_i)\ p(D|\theta_i, M_i)\ d\theta_i$$

$$= p(D|M_i)$$

To generate samples which are distributed according to the PDF, stochastic simulation methods are needed when dealing with a large number of uncertain parameters.

The Transitional Markov Chain Monte Carlo (TMCMC) method developed by Ching and Chen (2006) is selected for the Bayesian updating of the Parkfield school numerical models. The TMCMC algorithm for generating posterior samples of the modal parameters is a variation of the multiple-stage model updating procedure proposed by Beck and Au (2000, 2002) which uses the Metropolis-Hastings algorithm at each stage. The difference is the Beck-Au method accomplishes the gradual updating by using an increasing fraction of the data while TMCMC does it by introducing a *tempering* exponent on the likelihood function. This exponent works similarly to that of simulated annealing. TMCMC is implemented in a transformed parameter space as proposed by Cheung and Beck (2008) to enhance the efficiency of simulations by reducing the rejection rate in the Metropolis-Hastings algorithm, that is, reducing the number of repeated samples.

This analysis extends the work done by Muto and Beck (2008) by using real data involving hysteretic models of structures. All three 80-node models were considered as candidate models for the Parkfield records. Each level had 1000 samples simulated for the proposal PDF. Models 1 and 2 required 31 levels for the prior PDF to converge to the posterior PDF. Model 3 needed 49 levels. The parameters chosen for updating are the same as those listed in Table 6-1 with the addition of a variance factor. Figure 6.12 shows the samples from the prior PDF (black) compared to the samples from posterior PDF (green) for Model 1. Figure 6.13 shows posterior samples for different pairs of uncertain parameters. From the shape of the correlation plots, it is evident that the hysteretic model is unidentifiable based on the seismic records.
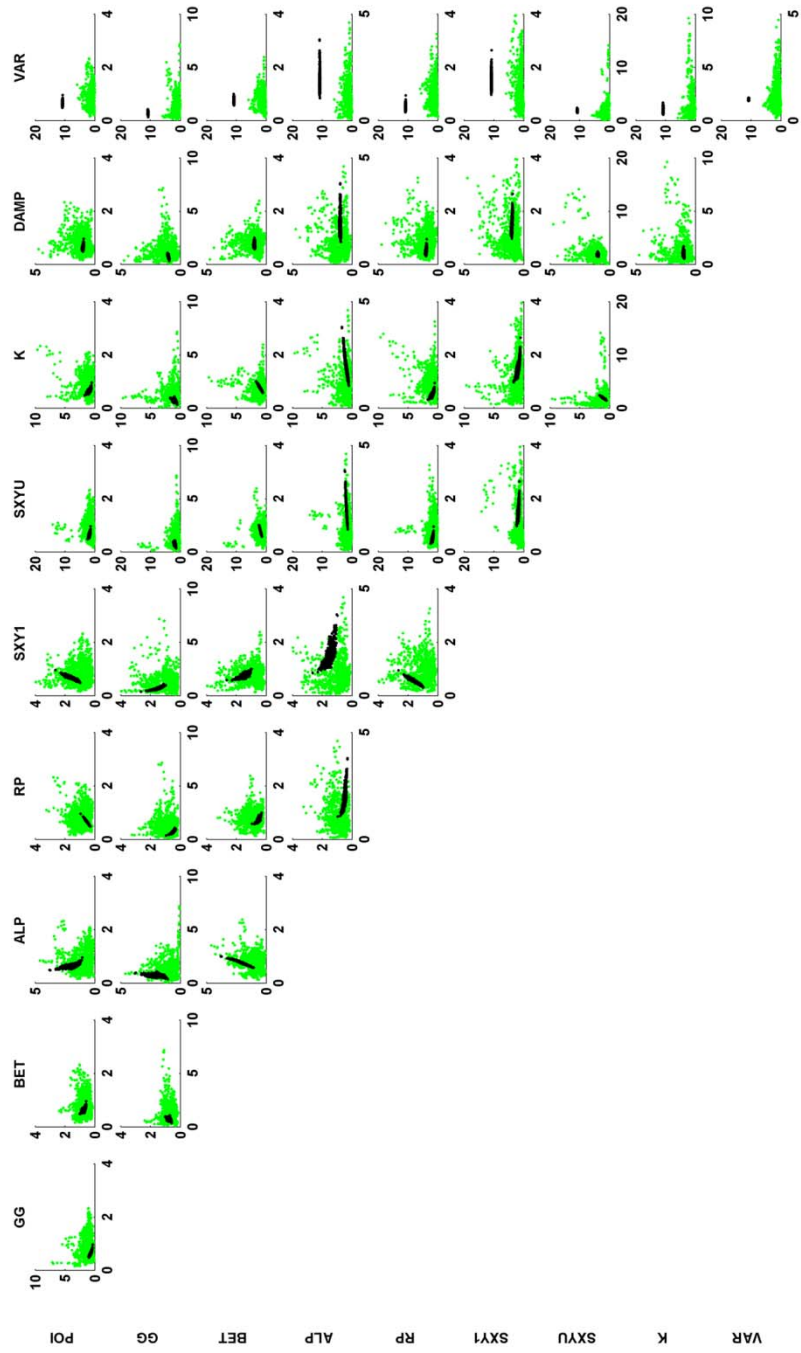
Figure 6.12: Samples from both prior (green) and posterior (black) PDF.
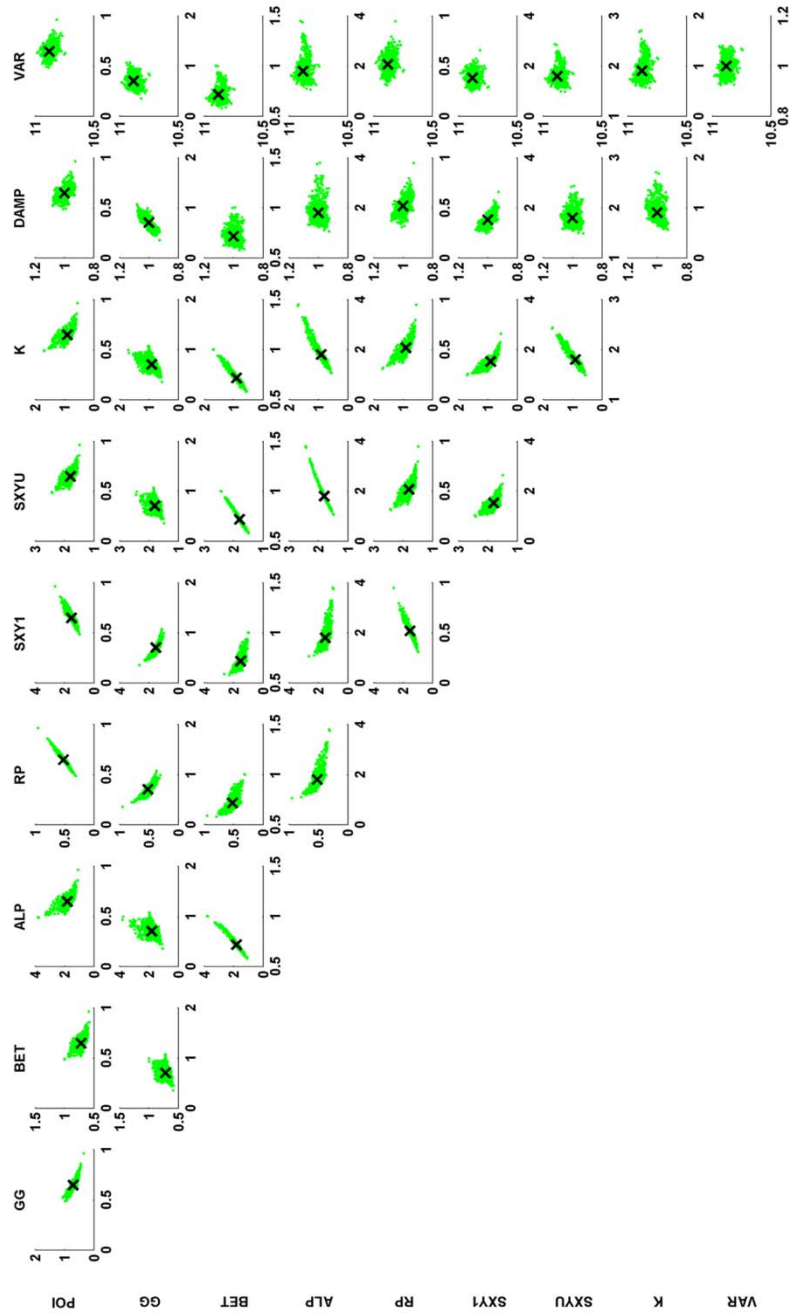
Figure 6.13: Posterior samples for different pairs of uncertain parameters in Model 1. X marks the mean of the posterior PDF. This illustrates the difficulty in identifying hysteretic structures.

134

Table 6-2 displays the mean and variance of the parameters in each of the models. The high variance demonstrates the challenges present in identifying hysteretic systems. Future runs can have tighter constraints on the parameters to reduce the variance of the parameters. Model 2 and Model 3 showed significantly lower shear yielding strength than Model 1 at the east and west wall parameters. This suggests that the model potentially uses hysteretic behavior of the plane element for the data fit. Shear yielding strength for the other subcomponents remain relatively higher. Shear moduli across all models and subcomponents have similar values, but reported hysteretic parameters have a very wide range in relation to their nominal values. Another interesting note is that the damping had little fluctuation. The nominal value was 10% and therefore the Bayesian updating suggests a value close to 8% which is consistent with estimates from experimental tests.

Table 6-3 shows the result of the model class selection. Model 3, with a 100% probability, is the most plausible model among the three candidate models, given the Parkfield data. It is not always the case that the most complex model will yield the highest probability since there are penalties involving the value of the "information gain," which describes how much information (in the sense of C. Shannon) is extracted from the data by the model class (Muto and Beck 2008). The higher the information gain from the data, the more the model class is penalized in calculating its posterior probability. However, in this particular case, the larger information gain is countered by the higher value of the data fit. Figures 6.14 show the final data fit from Model 3.

Table 6-2: Mean and standard deviation of the posterior PDF from all candidate models. Note: - indicates values constrained to be same as above parameters.

	Parameter	Model 1 Mean	Model 1 σ	Model 2 Mean	Model 2 σ	Model 3 Mean	Model 3 σ
East and West Walls	POI	0.6489	0.0610	0.7017	0.0113	0.2572	0.0075
	GG	0.7078	0.1168	0.6024	0.0170	0.8206	0.0108
	BET	0.7179	0.0644	0.2842	0.0087	0.3358	0.0034
	ALP	1.8088	0.3700	0.3189	0.0103	0.3390	0.0201
	PR	0.5188	0.0792	0.0479	0.0024	0.0882	0.0180
	SXY1	1.5322	0.2338	0.1862	0.0076	0.1802	0.0182
	SXYU	1.8008	0.1381	0.2559	0.0129	0.2258	0.0344
	K	0.9069	0.1726	1.2778	0.0653	1.1914	0.0023
Diaphragm	POI	-	-	0.8205	0.0102	0.5058	0.0076
	GG	-	-	0.9482	0.0333	0.7026	0.0107
	BET	-	-	0.8416	0.0225	0.6840	0.0149
	ALP	-	-	0.0832	0.0036	0.5792	0.0193
	PR	-	-	1.9319	0.0153	0.6142	0.0046
	SXY1	-	-	0.8155	0.0203	0.4471	0.0099
	SXYU	-	-	0.4389	0.0320	3.2640	0.0528
	K	-	-	1.3879	0.0334	2.4600	0.0571
North and South Walls	POI	-	-	-	-	1.2873	0.0158
	GG	-	-	-	-	0.6507	0.0118
	BET	-	-	-	-	0.7644	0.0133
	ALP	-	-	-	-	1.5509	0.0502
	PR	-	-	-	-	0.6242	0.0064
	SXY1	-	-	-	-	1.8261	0.0422
	SXYU	-	-	-	-	1.0314	0.0166
	K	-	-	-	-	1.2139	0.0059
	DAMP	1.0000	0.0321	0.8141	0.0512	0.8445	0.0254
	Var	10.8797	0.0321	10.7768	0.0604	20.64110	0.6545

Table 6-3: Bayesian Model Selection with calculated probability of the model.

	Data fit (10^3)	Information Gain	Log Evidence (10^3)	Probability
Model 1	8.70	68.17	8.64	0.0
Model 2	7.93	121.51	7.80	0.0
Model 3	13.49	1000.70	12.48	1.00
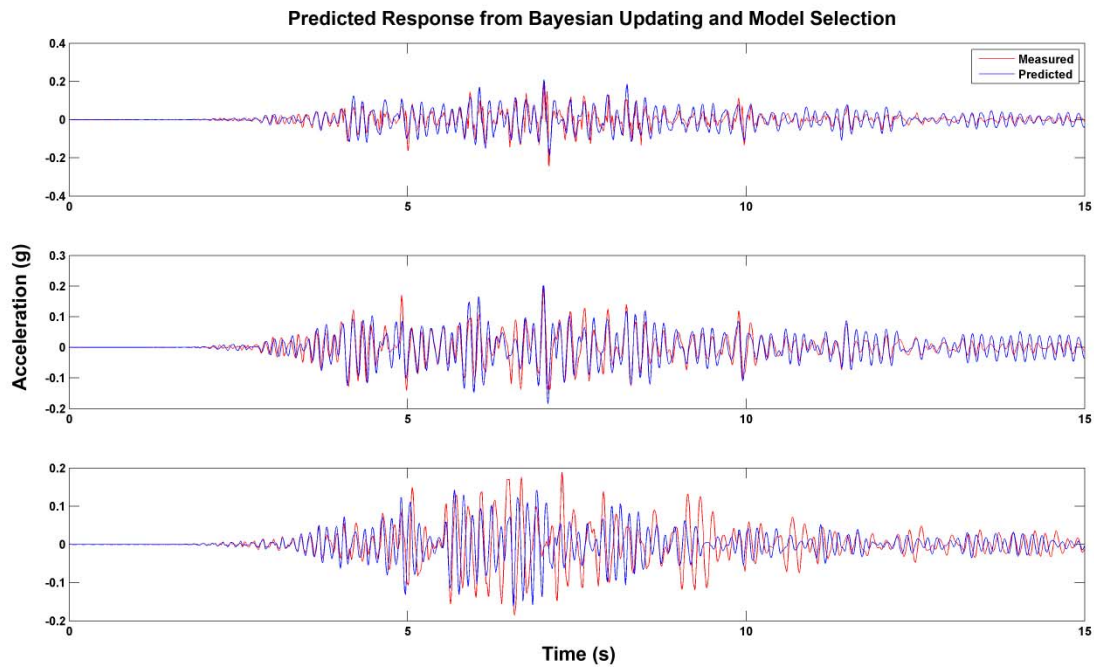
Figure 6.14: Data fit of Model 3 predicted by the most probable model from Bayesian updating and model selection.

The Bayesian updating and model selection method was able to provide an appropriate candidate model for the analysis in next section. By dealing with the uncertainties of the model parameters in a probability framework, this method surpasses other routines in

dealing with ill-conditioned problems. Furthermore, the Bayesian framework can be a great method to analyze a strong seismic motion database. The posterior PDFs from past earthquakes can be used to produce prior PDFs for new earthquakes and aftershocks by continual updating of current models. The potential integration is promising in monitoring and enhancing the value of the instrumentation program.

6.4 Model Results

With the use of model updating techniques, sets of model parameters were chosen to simulate the Parkfield response. This section uses the model and parameters selected from the Bayesian framework. Aside from fitting the seismic records, constructing the model provides insights into the physical behavior of the wood-frame structure.

6.4.1 Hysteretic Behavior

The hysteresis extraction process is performed on the acceleration time histories for comparison purposes. In Chapter 5, it was uncertain if the east wall and diaphragm exhibited pinching behavior, while the south wall demonstrated mostly linear behavior. The hysteresis curves from the model are shown in Figures 6.15 through 6.17. Figure 6.15 shows a clear sign of pinching at the east wall, while Figure 6.16 shows a mostly linear response with slight yielding at the extremes. The south wall exhibited a linear response as shown in Figure 6.17. Unlike the hysteresis curves generated from an updated model calculated from the SPSA approach, these hysteresis curves are more consistent with current knowledge of wood-frame structures. The results here also demonstrate why

MODE-ID was able to fit the channels at the diaphragm and south wall with a better accuracy compared to the nonlinear behavior seen at the east wall.
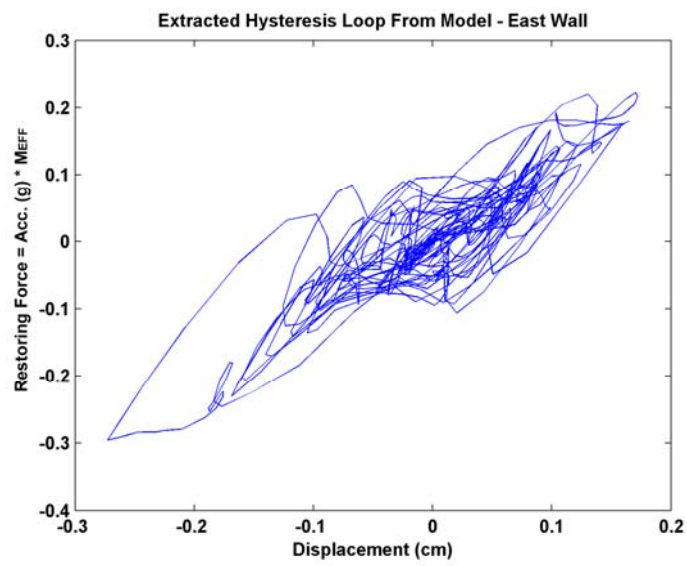
Figure 6.15: Extracted hysteresis loop from east wall. Model chosen by Bayesian model selection.
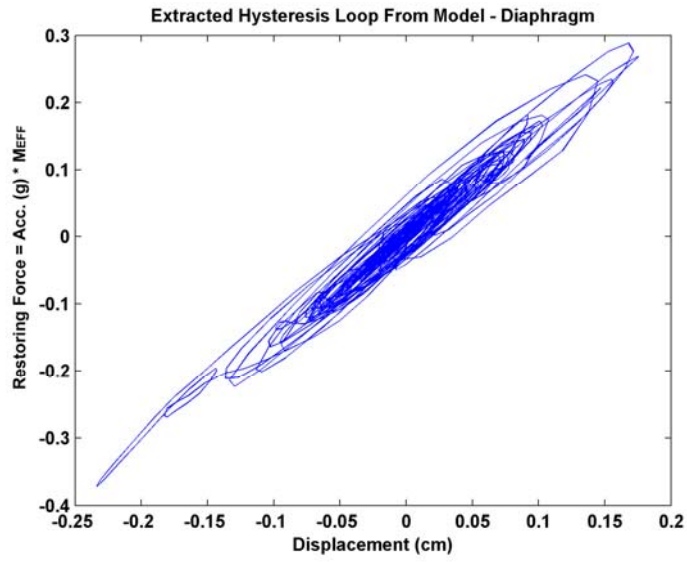
Figure 6.16: Extracted hysteresis loop from diaphragm. Model chosen by Bayesian model selection.
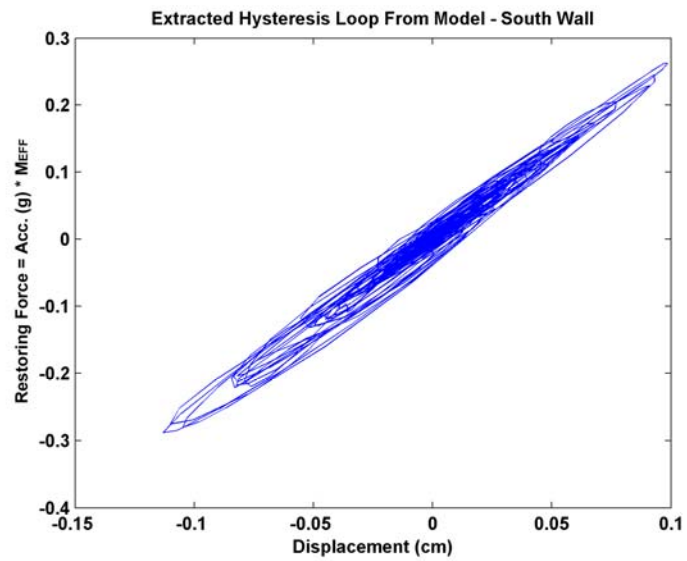
Figure 6.17: Extracted hysteresis loop from south wall. Model chosen by Bayesian model selection.

6.4.2 Model Response

The calculated displacement time histories from the model can be used to plot the instantaneous deformations in the wood-frame structure during the Parkfield Earthquake. Figures 6.18 through 6.20 display the progression of the structure's deformation during the seismic motions. Each figure displays a top view of the building with the open circles representing roof nodes. A blue trail for each node marks the relative displacements to the ground at selected time intervals. The displacements are magnified for visual purposes. The largest displacements seen in the figures are at most 0.5 cm.

The diaphragm appears to be flexible and no substantial torsion was observed. The largest deformations can be seen in the plane from the west portion of south wall to the east portion of the north wall. One reason is that the Parkfield Earthquake had strong fault-normal motions toward the northeast and the Parkfield school building was located northeast of the fault. Figure 6.21 displays a close-up version of the displacement particle motions seen in Chapter 3 to demonstrate the strong northeast motion produced from the earthquake. Another reason for the large deformations was the structure's stiffness; in the process of achieving a better fit, the model updating process found that the structure needed to be more flexible. These observations are consistent with the structural drawings in Chapter 3, where a major portion of the right north wall consisted of windows, and the south wall had two doors located near the south-west portion of the wall. These structural openings lower the structural stiffness and allow greater deformations to be exhibited in these local areas.
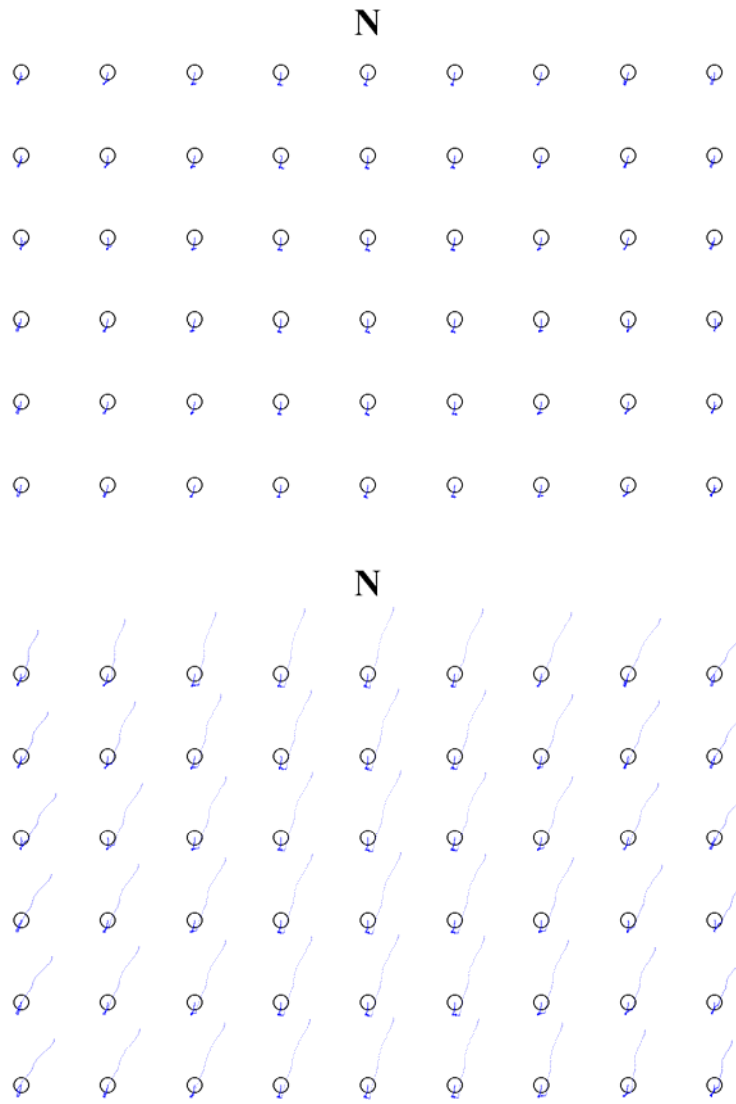
Figure 6.18: (Top) Structural deformations up to the first 2 seconds of seismic record. (Bottom) Structural deformations up to the first 3 seconds of the seismic record.
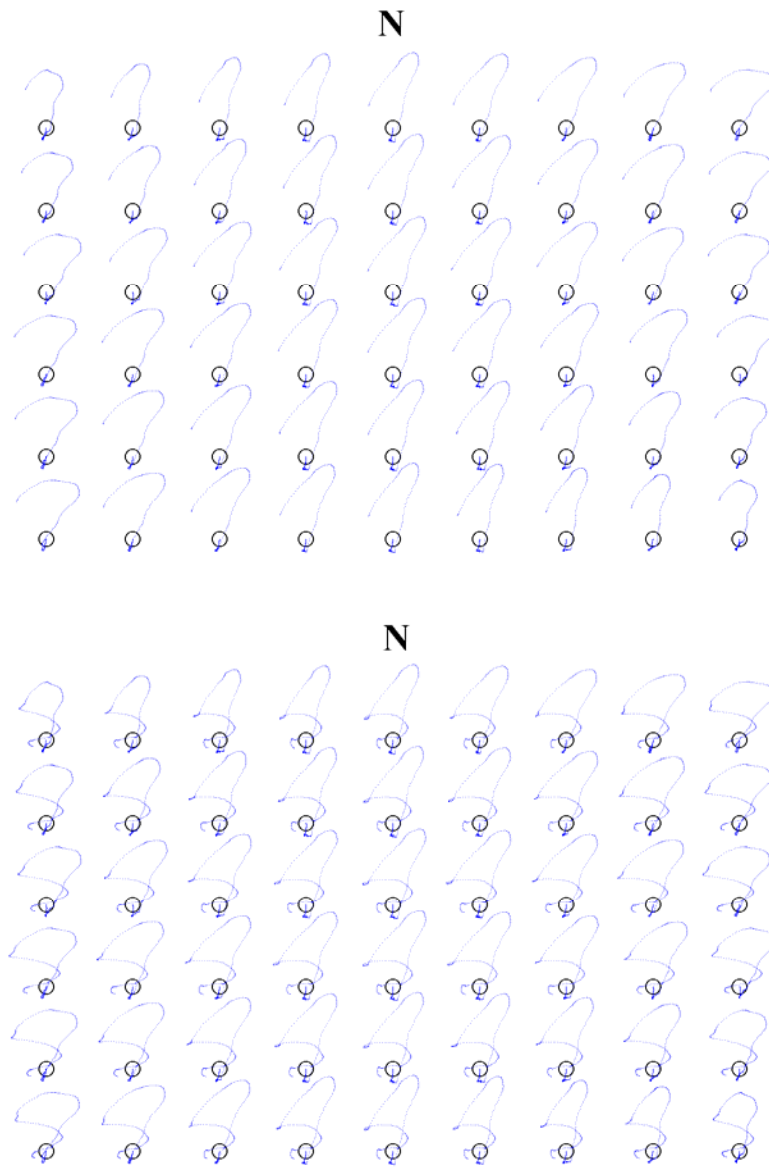
Figure 6.19: (Top) Structural deformations up to the first 5 seconds of seismic record. (Bottom) Structural deformations up to the first 6 seconds of the seismic record.

143
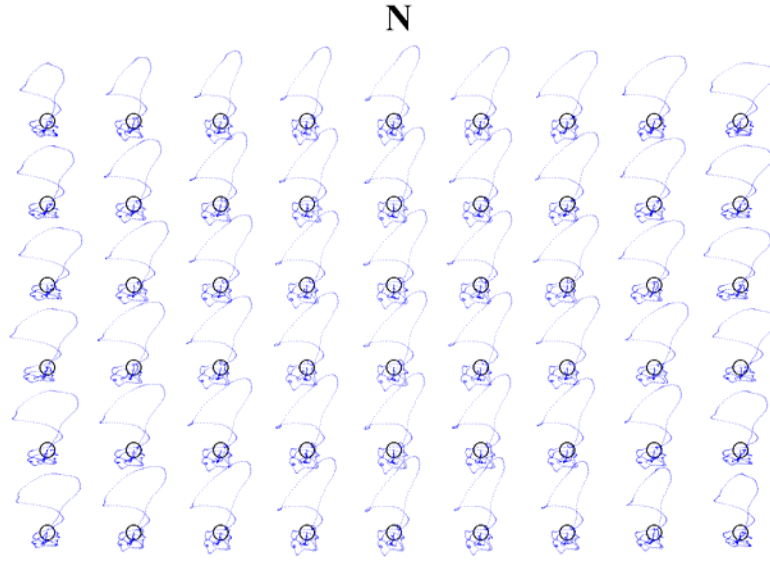
Figure 6.20: Structural deformations up to the first 8 seconds of the seismic record.
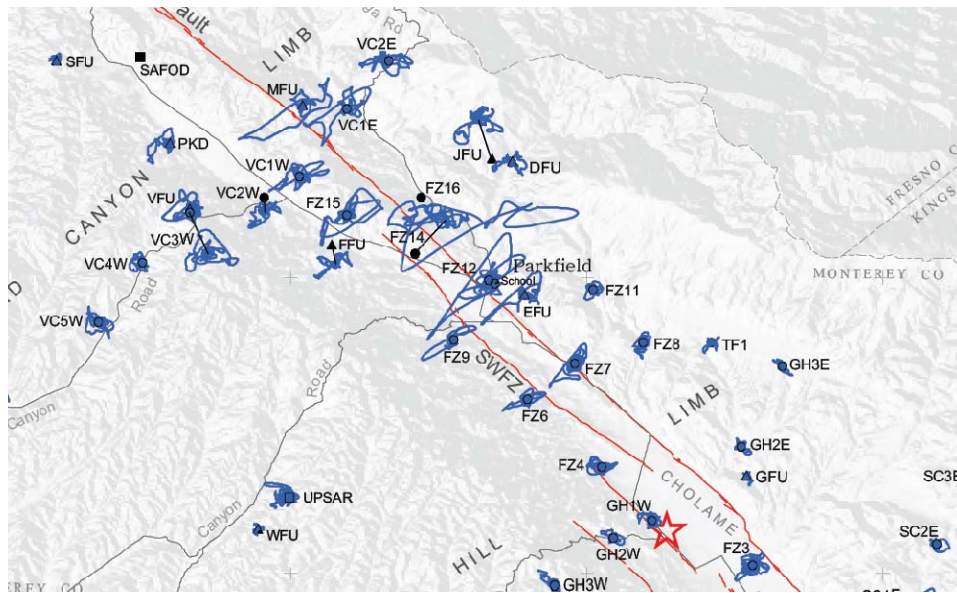
Figure 6.21: Displacement particle motion of instrumented stations during the Parkfield Earthquake. The Parkfield school building is located in the middle of the figure (CSMIP 2006).

144

6.4.3 Energy Dissipation

Model deformations provide an understanding of the structure's behavior during the earthquake, but it is unclear where and how most of the energy dissipation takes place. Using the hysteresis extraction method described in Chapter 5, instantaneous damping estimates can be obtained at various locations of the structure. Figures 6.22 and 6.23 present the energy dissipation of structure based on hysteresis curves. Figure 6.22 analyzes the hysteresis curves obtained from the east-west motion. The shear wall located on the southeast corner of the wall exhibited the highest damping at 10%. Since the model is symmetric, 10% damping can be observed at the northwest corner. However, it is important to note that the northwest corner is much stiffer than the rest of the north wall, which consists mostly of window openings. The rest of the walls and diaphragm exhibited 5% - 8% damping which is expected in a wood-frame structure. Figure 6.23 shows much more energy dissipation with the maximum being more than 20% damping. Most of the dissipation comes from the east and west walls. The flexing motion of the diaphragm in the north-south direction also contributes to the dissipation of energy.

Damping estimates (%) of the building (aerial view) in the East West motion
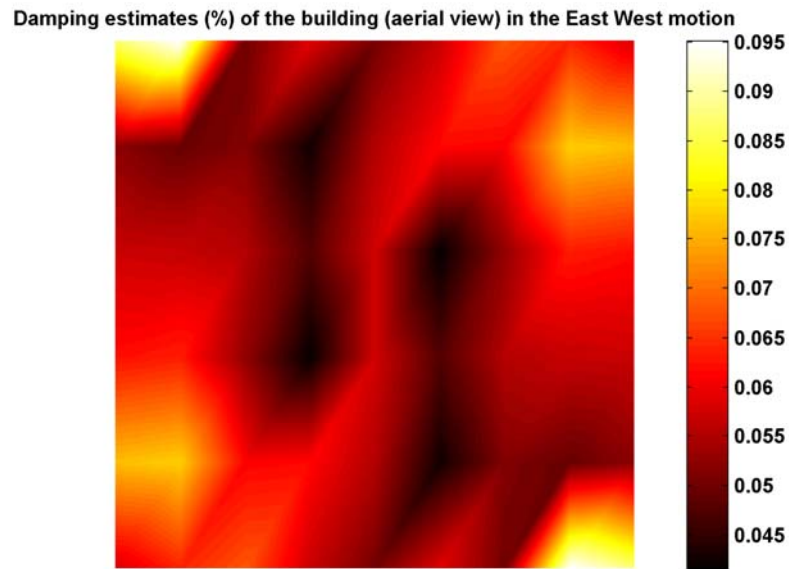
Figure 6.22: Energy dissipation in the east-west motion. 10% damping can be seen at the top left and bottom right corners.

Damping estimates (%) of the building (aerial view) in the North South motion
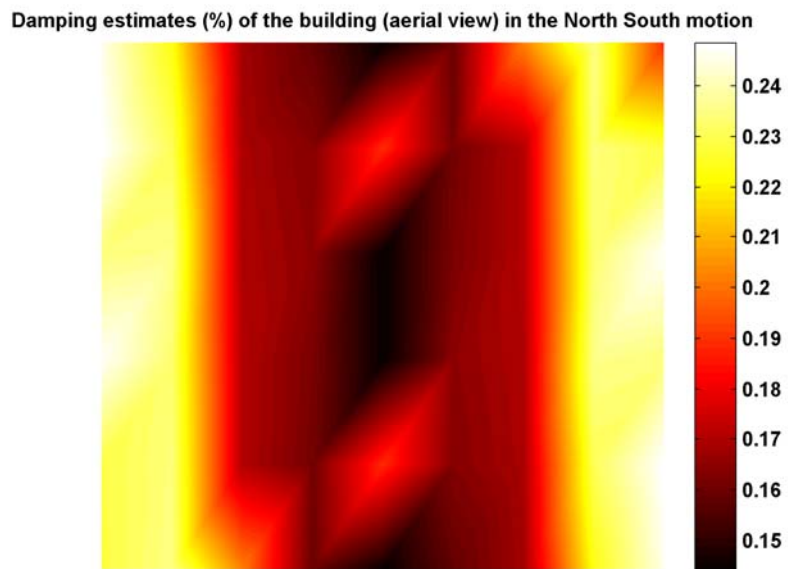
Figure 6.23: Energy dissipation in the north-south motion. More than 20% damping can be seen at east and west walls.

146

6.5 Conclusions

This chapter presented the finite element modeling and updating procedure and the various models that were considered. The numerical model can be used as a validation tool for the hysteresis extraction process. Paired with finite element model updating routines, the model can also lead to better simulation of seismic records. Different routines were implemented and their advantages and drawbacks were mentioned. Bayesian updating and model class selection stand out for their robustness and quantification of uncertainty. A model can be used to predict based on prior PDFs alone, but using posterior PDFs greatly improves predictions. A Bayesian framework integrated with the CSMIP seismic database can certainly enhance the value of the current instrumentation program by making better use of all earthquake data.

The numerical model achieved a representative data fit and offered insights into the physical behavior of the structure by displaying hysteresis curves and deformation shapes. The model showed signs of pinching hysteresis at the east wall and mostly linear behavior at the other two Parkfield sensor locations. Deformation shapes were consistent with the propagation of the earthquake motion and structural drawings of the building. By using hysteresis curves to calculate damping estimates, the model can also offer insights into the locations of largest energy dissipation.

CHAPTER 7

Conclusions and Future Work

The overall goal of the research presented in this dissertation is to extract as much information from seismic records as possible. The aim is to extend the understanding of wood-frame structures without relying solely on full-scale experimental tests. With new knowledge and data, necessary updates to wood-frame building codes can take place to reduce the severe damage and losses seen in the 1994 Northridge Earthquake. Successes and failures in the extraction of information can help evaluate the value of the California Strong Motion Instrumentation Program, and also helps prioritize the necessary upgrades to the program.

Chapter 2 summarized the various full-scale wood-frame tests that have taken place in the past. The case studies collectively demonstrated amplitude dependence of the fundamental frequency and the substantial role of nonstructural elements in providing lateral stiffness. Unresolved issues include the role of the diaphragm and the wide range of reported damping estimates.

Chapter 3 introduced the seismic records and experimental data used for analysis. The seismic records were significant because they displayed some of the highest peak structural accelerations recorded for wood-frame structures. However, due to the limited locations of the instrumentation, utilizing the data to analyze the full structure can be challenging. Recent experimental data from CUREE Tasks 1.1.1 and 1.3.3 were used to validate the extraction process.

Chapter 4 employed a modal identification routine MODE-ID to study significant amplitude dependence of the modal frequencies (which decrease for higher amplitude of shaking) and damping values (which increase for stronger motion) from the seismic response of wood-frame buildings. A 25% to 50% drop in frequency during the stronger earthquakes examined in this dissertation was common. A damping ratio at about 15% to 20% was also typical. Nonlinear behavior of the structure can be inferred from the frequency drop and increased damping.

Chapter 5 outlined a process to retrieve the hysteretic characteristics of wall and diaphragm components. The extraction process worked well for experimental data, but was less successful for field data. Error inherent in the process was the double integration of acceleration records. The chapter listed several measures to resolve this issue and also found that hysteresis loops in wood-frame structures were very susceptible to errors introduced in tilting of sensors and phase delays from filtering. Additionally, the nonlinear behavior of the diaphragm due to the shearing from bidirectional ground motions was also a factor in tampering the integrity of the extracted curves when insufficient instrumentation is available.

By obtaining more accurate hysteresis curves, damping estimates can be calculated from an equivalent elliptical area. The results have shown that low damping estimates inferred from experimental tests are due to structures never reaching or only momentarily exhibiting significant nonlinear behavior. Instantaneous damping estimates can also be obtained with this method. With the presence of energy dissipation from hysteretic behavior, equivalent viscous damping estimates can be as high as 15%-20%, which reaffirms the estimates from MODE-ID. Without the presence of nonlinear behavior, 5% - 10% damping can still be expected in wood-frame structures. The damping estimates should be carefully chosen base on the type of model being used. Furthermore, reports on damping estimates should always be supplemented with the methodologies used, since these values can be easily misrepresented without proper context.

In Chapter 6, different nonlinear models were created to simulate the relative accelerations at the Parkfield school building. Model updating techniques were used to obtain representative parameter values. Bayesian updating and model selection provides an excellent framework for dealing with ill-conditioned problems like the system identification of hysteretic structures. The framework also complements the strong motion database, as both old and new data are available to provide continual updates to the model. Furthermore, the presentation of posterior samples of parameter values and model selection aids human interpretation.

The calculated response of the selected numerical model resembled the recorded data. Displacement time histories from the model were consistent with the anticipated response of the building and suggest that the diaphragm was flexible. By using the damping

estimation technique in Chapter 5, the model showed that most of the energy dissipation is from the east and west walls. The diaphragm also contributed by showing flexible behavior.

Goals for future work should focus on the application to building code design and a seamless integration of the Bayesian framework with the CSMIP database. Other objectives include adding a hysteresis degradation parameter in the current numerical model, studying the effects of openings and eccentricity, and refining the hysteresis extraction process.

In conclusion, without significant changes in the current instrumentation program, a substantial amount of new information can be obtained by using the methodology covered in this dissertation. By accurately extracting hysteresis curves, structural deformations and dissipation of energy in wood-frame structures can be inferred. The extraction process can certainly benefit from upgrading to multi-axial sensors and placing sensors strategically. These improvements help account for tilting and bias in sensors, study the nonlinear effects of diaphragm induced from multi-directional ground motions, and characterize the full structure with sufficient amount of records. Furthermore, an integration of the database with a Bayesian updating framework can increase the overall value of the CSMIP program by making better use of each seismic record.

References

Aster, R., B. Borchers, C. Thurber. *Parameter Estimation and Inverse Problems*. London, UK: Elsevier Academic Press, 2005.

Bakun, W. H., J. O. Langbein, A. G. Lindh, and E. R. Roeloffs. *History of the Parkfield Prediction Experiment.* Fall Meeting 2004, Menlo Park, CA: American Geophysical Union, 2004.

Beck, J. L. *Determining Models of Structures from Earthquake Records.* EERL REport No. 78-01, Pasadena, California: California Institute of Technology, 1978.

Beck, J. L. "Statistical System Identification of Structures." *Structural Safety and Reliability* (ASCE), 1990: 1395-1402.

Beck, J. L., and J. Mitrani. "MODE-ID Program for Time-Domain Modal Identification." *COMET - Caltech Online Monitoring and Evaluation Testbeds.* November 04, 2003. http://comet.caltech.edu/sn_theory_eq3.asp (accessed December 31, 2008).

Beck, J. L., and K. V. Yuen. "Model selection using response measurements: Bayesian probabilistic approach." *Journal of Engineering Mechanics* 130 (February 2004): 192-203.

Beck, J. L., and M. Dowling. "Quick Algorithms for Computing either Displacement, Velocity or Acceleration of an Oscillator." *Earthquake Engineering and Structural Dynamics*, 1988: 245-253.

Beck, J. L., and P. C. Jennings. "Structural Identification Using Linear Models and Earthquake Records." *Earthquake Engineering and Structural Dynamics*, 1980: 145-160.

Beck, J. L., and S. H. Cheung. "Probability logic, model uncertainty and robust predictive system analysis." *Proc. 10th International Conference on Structural Safety and Reliability (ICOSSAR09).* Osaka, Japan, 2009.

Beck, J. L., and S. K. Au. "Bayesian updating of structural models and reliability using Markov Chain Monte Carlo Simulation." *Journal of Engineering Mechanics* 128 (2002): 380-391.

Beck, J. L., and S. K. Au. "Updating robust reliability using Markov Chain simulation." *Proceedings of the International Conference on Monte Carlo Simulation.* Monte Carlo, Monaco, 2000.

Beck, R. T., and J. L. Beck. *Comparison Between Transfer Function and Modal Minimization Methods for System Identification.* EERL Report No. 85-06, Pasadena, California: California Institute of Technology, 1985.

Boore, David M. *Long-Period Ground Motions from Digital Acceleration Recordings: A New Era in Engineering Seismology.* Vol. 58, in *Directions in Strong Motion Instrumentation*, by Polat Gulkan and John G. Anderson, 41-54. Springer Netherlands, 2005.

Bradford, Samuel C. *Time-Frequency Analysis of Systems with Changing Dynamic Properties.* Ph.D. Thesis, Pasadena, California: California Institute of Technology, 2006.

Brigham, E. *Fast Fourier Transform and its Applications.* New York: Prentice-Hall, 1988.

Camelo, Vanessa. *Dynamic Characteristics of Wood-frame Buildings.* Ph.D. Thesis, Pasadena, California: California Institute of Technology, 2003.

Camelo, Vanessa, James Beck, and John Hall. *Dynamic Characteristics of Wood-frame Structures.* CUREE-Caltech Woodframe Project, Richmond, CA: CUREE W-11, 2002.

Carr, Athol J. "RUAUMOKO." Christchurch, New Zealand: University of Canterbury, 1998.

Carydis, P. G., and E. A. Vougioukas. "1.1.1 Full-Scale Dynamic Test of a Two-Storied Timber Frame Construction House using a 6-DOF Earthquake Simulator." *European Earthquake Engineering*, February no. 2, 1989: 17-21.

CESMD, Center for Engineering Strong Motion Data -. *Information for Strong-Motion Station Templeton - 1 story hospital.* 2006. http://www.strongmotioncenter.org/cgi-

bin/ncesmd/stationhtml.pl?stationID=C36695&network=CGS (accessed December 31, 2008).

Chen, Kun-Yu. *System Identification Theory of Torsionally Couple Multistory Buildings.* Thesis, Taoyuan, Taiwan: Nactional Central University, 2003.

Chen, Xiaodong. *Near-Field Ground Motion from the Landers Earthquake.* EERL 95-02, Pasadena, California: California Institute of Technology, 1995.

Cheung, S. H., and J. L. Beck. "Calculating the posterior probability for Bayesian model class selection and averaging by using posterior samples based on dynamic system data." *Computer-Aided Civil and Infrastructure Engineering*, under review, 2009.

Cheung, S. H., and J. L. Beck. "On using posterior samples for model selection for structural identification." *Proc. Asian-Pacific Symposium on Structural Reliability and its Applications 2008.* Hong Kong, China: Hong Kong University of Science and Technology, 2008.

Ching, J., and Y. J. Chen. "Transitional Markov Chain Monte Carlo method for Bayesian model updating, model class selection and model averaging." *Journal of Engineering Mechanics*, 2007.

Chopra, A. K. *Dynamics of Structures: Theory and Applications to Earthquake Engineering.* Prentice Hall, 2001.

Cifuentes, A. O., and W. D. Iwan. "Nonlinear System Identification Based on Modeling of Restoring Force Behavior." *Soil Dynamics and Earthquake Engineering* 8, no. 1 (1989): 2-8.

Cifuentes, Arturo O. *System Identification of Hysteretic Structures.* EERL 84-04, Pasadena, California: California Institute of Technology, 1984.

CISN, California Integrated Seismic Network. *Parkfield - 1-story School Building.* September 1, 2006. http://www.quake.ca.gov/cisn-edc//buildingpages/BLD36531.HTM (accessed December 31, 2008).

Clinton, J. F., and T. H. Heaton. "Lab and field performance of the VSE-355G2/3 strong motion velocity instrument." *Seism. Soc. Am. Ann. Meet. Abstracts.* Palm Springs, CA: Seism. Soc. Am., 2004.

Clinton, John F., and Thomas H. Heaton. "Potential Advantages of a Strong-motion Velocity Meter over a Strong-motion Accelerometer." *Seismological Research Letters* 73, no. 3 (2002): 332-342.

Cobeen, Kelly, James Russel, and J. Daniel Dolan. *Recommendations for Earthquake Resistance in the Design and Construction of Wood-frame Buildings.* CUREE-Caltech Woodframe Project, Richmond, CA: CUREE W-30b, 2004.

CSMIP. *California Geological Survey - About CSMIP.* May 15, 2006. http://www.conservation.ca.gov/cgs/smip/Pages/about.aspx (accessed January 18, 2007).

CSMIP. "Displacement Particle Motions of Parkfield Earthquake of 28 Sep 2004." *Displacement Particle Motions of Parkfield Earthquake of 28 Sep 2004.* 2006. http://www.quake.ca.gov/cisn-edc/IQR/Parkfield_28Sep2004/parkfield_displacement.pdf.

CUREE. *CUREE-Caltech Woodframe Project.* November 11, 2008. http://www.curee.org/projects/woodframe/index.html (accessed December 31, 2008).

Diekmann, Edward F. "Design and Code Issues in the Design of Diaphragms and Shearwalls." Edited by Greg C. Foliente. *Analysis, Design and Testing of Timber Structures Under Seismic Loads.* Richmond, CA: Forest Products Laboratory, 1994. 9-20.

Eykhoff, P. "System Identification: Parameter and State Estimation." *Wiley*, 1974.

Filiatrault, Andre. *Wood-frame Project Testing and Analysis Literature Review.* CUREE-Caltech Woodframe Project, Richmond, CA: CUREE W-03, 2001.

Fischer, David, Andre Filiatrault, Bryan Folz, Chia-Ming Uang, and Frieder Seible. *Shake Table Tests of a Two-Story Wood-frame House.* CUREE-Caltech Woodframe Project, Richmond, CA: CUREE W-06, 2001.

Foliente, Greg C. "Modeling and Analysis of Timber Structures Under Seismic Loads." *Analysis, Design and Testing of Timber Structures Under Seismic Loads.* Richmond, CA: Forest Products Laboratory, 1994. 87-104.

Folz, B., and A. Filiatrault. *CASHEW - Version 1.0 A Computer Program for Cyclic Analysis of Wood Shear Walls.* SSRP, San Diego, CA: University of California, San Deigo, CA, 2000.

Gang, Jin, M. K. Sain, and B. F. Jr. Spencer. "Frequency Domain system identification for controlled civil engineering structures." *Control Systems Technology* (Control Systems Technology) 13, no. 6 (Nov. 2005): 1055-1062.

Graizer, V. M. "Determination of the true displacement of the ground from strong-motion recordings." *Acad Sci Phys Solid Earth*, 1979: 875-885.

Graizer, V. M. "Effect of tilt on strong motion data processing." *Soil Dynamics and Earthquake Engineering* 25 (2005): 197-204.

Graves, Robert W. "Processing Issues for Near Source Strong Motion Records." *Strong-Motion Instrumentation of Buildings.* Richmond, CA: Consortium of Organizations for Strong Motion Observation Systems (COSMOS), 2004.

He, X., B. Moaveni, J. P. Conte, and A. Elgamal. "System Identification of New Carquinez Bridge Using Ambient Vibration Data." *Experimental Vibration Analysis for Civil Engineering Structures.* Bordeaux, France, 2005.

Hirashima, Y. "Analysis of Observed Earthquake Response of Post-and-Beam Wood Structure." *Proceedings from the International Conference on Timber Engineering.* Seattle, Washington: ICTE, 1988.

Iwan, W. D., and A. O. Cifuentes. "A Model for System Identification of Degrading Structures." *Journal of Earthquake Engineering and Structural Dynamics*, 1986: 877-890.

Iwan, W. D., and C.-Y. Peng. "Identification of Hysteretic Behavior from Strong-Motion Accelerograms." *Proceedings 9th World Conference on Earthquake Engineering.* Tokyo, Japan, 1988.

Iwan, Wilfred D., Micahel A. Moser, and Chia-Yen Peng. *Strong-Motion Earthquake Measurement Using a Digital Accelerograph.* EERL 84-02, Pasadena, California: California Institute of Technology, 1984.

Iwan, Wilfred D., Michael A. Moser, and Chia-Yen Peng. "Some Observations of Strong-Motion Earthquake Measurement Using a Digial Accelerograph." *Bulletin of the Seismological Society of America* 75, no. 5 (1985).

James, George H., Thomas Carne, and James P. Lauffer. *The Natural Excitation Technique (NExT) for Modal Parameter Extraction From Operating Wind Turbines.* Distribution, Sandia National Labs, 1993.

Jayakumar, P. *Modeling and identification in structural dynamics.* EERL 87-01, Pasadena, California: California Institute of Technology, 1987.

Jayakumar, P., and J. L. Beck. "System identification using nonlinear structural models." *Structural safety evaluation based on system identification approaches,.* Vieweg and Sons, 1988.

Jaynes, E. T. *Probability Theory: the Logic of Science.* Cambridge and New York: Cambridge University Press, 2003.

Jovanovie, Olivera. "Identification of Dynamic System Using Neural Network." *Facta Universitatis - Architecture and Civil Engineering*, 1997: 525-532.

Judd, Johnn. "Analytical Modeling of Wood-Frame Shear Walls and Diaphragms" M.S. Thesis, Provo, Utah: Brigham Young University, 2005.

Kijewski, T., and A. Kareem. "Wavelet Transforms for System Identification in Civil Engineering." *Computer-Aided Civil and Infrastructure Engineering*, 2003: 339-355.

Kohara, K., and K. Miyazawa. "Full-Scale Shaking Table Test of Two-Story Wooden Dwelling Houses." *Proceedings of the International Conference on Timber Engineering.* Montreux, Switzerland, 1998. 548-555.

Ma, Fai. *Analysis of the equations of motion of linearized controlled structures.* Academy Proceedings in Engineering Sciences, Springer India, 1995.

Malhotra, Praveen K. "Response spectrum of incompatible acceleration, velocity and displacement histories." *Earthquake Engineering and Structural Dynamics*, 2001: 279-286.

Malik, Ajay. "Estimating Building Stocks for Earthquake Mitigation and Recovery Planning." Cornell Institute for Social and Economic Research, 1995.

Michael, Andy. "The Parkfield 2004 Earthquake." *USGS.* October 26, 2006. http://online.wr.usgs.gov/calendar/2006/oct06.html (accessed July 15, 2008).

Muto, M., and J. L. Beck. "Bayesian Updating and Model Class Selection for Hysteretic Structural Models Using Stochastic Simulation." *Journal of Vibration & Control*, Janurary 2008.

Parker, R. "Understanding Inverse Theory." *Ann. Review Earth Planet Science*, Vol. 5:35-64, 1977.

Paz, M. *Structural Dynamics: Theory and Computation.* Springer, 1997.

Peng, C.-Y., and W. D. Iwan. "An Identification Methodology for a Class of Hysteretic Structures." *Earthquake Engineering & Structural Dynamics*, 1992: 695-712.

Peng, Chia-Yen. *Generalized Modal Identification of Linear and Nonlinear Dynamic Systems.* EERL 87-05, Pasadena, California: California Institute of Technology, 1987.

Phillips, T. L., R. Y. Itani, and and D. I. McLean. "Lateral Load Sharing by Diaphragms in Wood-Framed Buildings." *Journal of Structural Engineering* 119, no. 5 (1993): 1156-1571.

Polensek, A, and B. D. Schimel. "Dynamic Properties of Light-Frame Wood Subsystems." *Journal of Structural Engineering* (ASCE), no. 117 (1991): 1079-1095.

Reitherman, Robert. "Overview of the Northridge Earthquake." *Proceedings of the NEHRP Conference and Workshop on Research on the Northridge, California Earthquake of January 17, 1994, Vol. I.* Richmond, CA: California Universities for Research in Earthquake Engineering, 1998. I-1.

Ribeiro, J. G. T., J. L. F. Freire, and J. T. P. De Castro. "Problems in analogue double integration to determine displacements from acceleration data." *International Society for Optical Engineering.* Bellingham, Washington: Society of Photo-Optical Instrumentation Engineers, 1997. 930-934.

Sambridge, M. and K. Mosegaard. "Monte Carlo Methods in Geophysical Inverse Problems." *Reviews of Geophysics, 40, 3,* September 2002.

Seo, J. M., I. K. Choi, and J. R. Lee. "Static and Cyclic Behavior of Wooden Frames with Tenon Joints under Later Load." *Jounral of Structural Engineering* (ASCE), no. 125 (1999): 344-349.

Seo, J. M., I. K. Choi, and J. R. Lee. "Experimental Study on the Aseismic Capacity of a Wooden House Using Shaking Table." *Earthquake Engineering and Structural Dynamics*, 1999: 1143-1162.

Shakal, Anthony, Vladimir Graizer, Mo Huang, Hamid Haddadi, and Lin Kuo-wan. "Strong-Motion Data From the M6.0 Parkfield Earthquake September 28, 2004." *SMIP05 Seminar Proceedings.* Sacramento, CA: California Geological Survey, 2005.

Shi, Z. Y. "Identification of Linear Time-Varying Dynamical Systems Using Hilbert Transform and Empirical Mode Decomposition Method." *Journal of Applied Mechanics* 74, no. 2 (March 2007): 223-230.

Spall, J. C. *An overview of the simultaneous perturbation method for efficient optimization.* APL Technical Digest 19: 482-492: John Hopkins, 1998.

Spall, J. C. "Implementation of the simultaneous perturbation algorithm for stochastic optimization." *IEEE Transactions on Aerospace and Electronic Systems*, 1998: 34: 817-823.

Sugiyama, Hideo, Naoto Andoh, Shigeru Hirano, Takayuki Uchisako, and and Noboru Nakamura. "Full-Scale Test on a Japanese Type of Two-Story Wooden Frame House Subjected to Lateral Load." *Proceedings of the International Conference on Timber Engineering.* Madison, Wisconsin: Forest Products Res. Soc., 1988. 55-61.

Sutoyo, D. and J. Hall. "Study of Wood-frame Building Records from the Parkfield and San Simeon Earthquakes." *SMIP06 Seminar Proceedings.* Oakland, CA: CSMIP, 2006. 81-101.

Tarantola, A. *Inverse Problem Theory*. Philadelphia, PA: Society for Industrial and Applied Mathematics, 2005.

Tanaka, Yuki, Yoshimitsu Ohasi, and Isao Sakamoto. "Shaking Table Test of Full-Scale Wood-Framed House." *Proceedings of the 10th Earthquake Engineering Symposium.* Yokohama, Japan, 1998. 2487-2492.

Thong, Y. K., M. S. Woolfson, J. A. Crowe, B. R. Hayes-Gill, and D. A. Jones. "Numerical double integration of acceleration measurements in noise." *Measurement* 36, no. 1 (2004): 73-92.

Trifunac, M. D., and V. Lee. *Routine Computer Processing of Strong-Motion Accelerograms.* EERL 73-03, Pasadena, California: California Institute of Technology, 1973.

Uang, Chia-Ming, and Vitelmo V. Bertero. *Earthquake simulation tests and associated studies of a 0.3-scale model of a six-story concentrically braced steel structure.* UCB/EERC-86/10, Berkeley, California: University of California, Berkeley, 1986.

USGS. *Earthquake Facts and Statistics.* December 31, 2008. http://neic.usgs.gov/neis/eqlists/eqstats.html (accessed December 31, 2008).

USGS. *The Parkfield, California, Earthquake Experiment.* November 11, 2008. http://earthquake.usgs.gov/research/parkfield/index.php (accessed December 31, 2008).

Wang, Luo-Jia. *Processing of Near-Field Earthquake Accelerograms.* EERL 96-04, Pasadena, CA: California Institute of Technology, 1996.

Werner, S. D., A. Nisar, and J. L. Beck. *Assessment of UBC Seismic Design Provisions Using System Identification of Recorded Earthquake Motions in Buildings.* Report to NSF, National Science Foundation, 1992.

Werner, S. D., J. L. Beck, and M. B. Levine. "Seismic Response Evaluation of Meloland Road Overpass Using 1979 Imperial Valley Earthquake Records." *Earthquake Engineering and Structural Dynamics* 15 (1987): 249-274.

Yamaguchi, Nobuyoshi, and Chikahiro Minowa. "Dynamic Performance of Wooden Bearing Walls by Shaking Table." *Proceedings of the International Conference on Timber Engineering.* Montreux, Switzerland, 1998. 26-33.

Yang, J., J. B. Li, and G. Lin. "A simple approach to integration of acceleration data for dynamic soil-structure interaction analysis." *Soil Dynamics and Earthquake Engineering* 26, no. 8 (2006): 725-734.

Yasamura, Motoi, Isao Nishiyama, TatuoMurota, and and Nobuyoshi Yamaguchi. "Experiments on a Three-Storied Wooden Frame Building Subjected to Horizontal

Load." *Proceedings of the International Conference on Timber Engineering.* Madison, Wisconsin: Forest Products Res. Soc., 1988. 262-275.

Yokel, F. Y., G. Hsi, and N. F. Somes. *Full scale test on a two-story house subjected to lateral load.* pp. 1-26, Washington, D.C.: U.S. National Bureau of Standards, 1973.